



**Università
degli Studi
di Palermo**

AREA QUALITÀ, PROGRAMMAZIONE E SUPPORTO STRATEGICO
SETTORE STRATEGIA PER LA RICERCA
U. O. DOTTORATI

Corso di Dottorato in Ingegneria dell'Innovazione Tecnologica.
Dipartimento di Ingegneria.
ING-IND/16 Tecnologie e Sistemi di Lavorazione.

RESHAPING AS NOVEL CIRCULAR ECONOMY STRATEGY FOR SHEET METAL BASED END-OF-LIFE COMPONENTS

IL DOTTORE
ING. OMER ZAHEER

IL COORDINATORE
CHIA.MO PROF. SALVATORE GAGLIO

IL TUTOR
CHIA.MO PROF. LIVAN FRATINI

IL CO TUTOR
CHIA.MO PROF. GIUSEPPE INGARAO

CICLO XXXIV
ANNO CONSEGUIMENTO TITOLO 2020-2021.

TABLE OF CONTENTS

Table of Contents.....	2
Acknowledgements.....	5
Abstract and Dissertation Structure.....	6
Graphical Abstract.....	11
List of Abbreviations.....	12
1. Introduction.....	14
1.1 Circular Economy.....	18
1.2 Metal Reuse Framework.....	21
1.3 Single Point Incremental Forming.....	27
1.4 Proposed Approach.....	31
2. SPIF Used as Reshaper: Technical Feasibility.....	33
2.1 Deep Drawing.....	33
2.2 Technical Feasibility Analysis.....	34
2.2.1 The Adapted Approach.....	34
2.2.2 Case study 1: SPIF operations away from highly thinned areas.....	36
2.2.3 Case study 2: SPIF operations close to highly thinned areas.....	38

2.3 Effectiveness of Reshaping Using Conventional Forming Process.....	43
2.3.1 The Adapted Approach.....	43
2.3.2 Analysis of Alternative Reshaping Solutions.....	45
2.4 Discussions	49
3. Formability and Geometrical Accuracy Performances.....	52
3.1 Geometrical Accuracy of EoL Component.....	53
3.1.1 The Adapted Approach.....	53
3.1.2 Results Analysis.....	57
3.2 Formability Variation And Geometrical Accuracy of SPIF Process.....	67
3.2.1 The Adapted Approach.....	67
3.2.2 Methodology for α max calculation.....	69
3.2.3 Methodology for Geometrical Accuracy Analysis.....	71
3.2.4 Results.....	74
3.3 Discussions.....	82
4. Energy Efficiency Analysis.....	84
4.1 The comparative CED and CO ₂ -eq analysis.....	85
4.2 System Boundary and Major Assumptions.....	86
4.3 Life Cycle Inventory.....	87

4.4 Results.....	93
4.5 Discussions	97
5. Reshaping by Hydroforming: Feasibility Analysis.....	100
5.1 Experimental Setup.....	101
5.1.1 Deep Drawing Setup.....	101
5.1.2 Hydroforming Setup.....	102
5.1.3 Geometric Acquisition Setup.....	104
5.2 Results.....	106
6. Conclusions.....	113
6.1 Summary.....	113
6.2 Future Developments.....	117
Bibliography.....	120
Publications List.....	136

Acknowledgements

This dissertation is the outcome of my research carried out during the last three years at the Department of Engineering of the University of Palermo. Firstly, I would like to thank my supervisors, Prof. Livan Fratini and Prof. Giuseppe Ingarao, who supported me through my doctoral studies with their mentoring and guidance. I also gratefully thank my colleague from MTG research group Ing. Davide Campanella, who helped me during the course of my doctoral course and accompanied me in this journey. Lastly, I'd like to thank my family and friends who've always supported and encouraged me during this important period of my academic life.

Abstract and Dissertation Structure

Abstract

Making materials consumes about 21% of the global energy demand and specifically metals production, it accounts for about 8% of total global energy consumption. In fact, in the past few decades, the use of lightweight alloys has become increasingly widespread in many major industrial sectors thanks to the weight reduction associated with their applications. Most lightweight materials like aluminum alloys are characterized by high-energy demands primary production cycles that are responsible for a relevant share of the global CO₂ emissions. Circular economy strategies such as longer life, more intense use, repair, product upgrades, modularity, remanufacturing, component re-use and open/closed loop recycling are strategies to put in place urgently to reduce the environmental impact. Although recycling of metals is the most used strategy and is being improved in terms of efficiency, it is mandatory moving towards more virtuous circular economy strategies, such as product/component reuse. A potentially effective strategy would be the incorporation of metal reuse techniques that would enable material recuperation at low environmental costs and in consequence, reducing the environmental impact of material production. Several researchers have brought forward strategies in response to the metal reuse question. In this dissertation, a novel reuse strategy for sheet

metal-based End-of-life components is proposed. Specifically, a proposal towards the use of Single Point Incremental Forming for the Reshaping of End-of-Life sheet metal components has been presented. In particular, the suitability of this strategy as a circular economy enabler, has been studied with a particular focus on the technical feasibility of the SPIF process for the function of Reshaping, the quality of the end products of Reshaping and the energy efficiency along with the equivalent CO₂ emissions of this strategy has been focused upon.

Dissertation Structure

Chapter 1, titled “Introduction”, deals with the general introduction to the metal recycling issues and capabilities, with particular focus on the lightweight alloys. The first subsection 1.1 introduces the concept of circular economy, followed by the metal reuse framework (section 1.2) which discusses the existing state of art on the various approaches proposed and studied in the past. Section 1.3 provides an introduction to the Single point Incremental forming process and it’s mechanics, followed by the proposed approach explained in section 1.4.

Chapter 2, titled “SPIF used as a Reshaper: Technical Feasibility”, contains the analysis of the technical feasibility of the proposed Reshaping strategy. Section 2.1 provides an introduction to the Deep Drawing process and technical aspects of the same. Section 2.2 details the procedure adopted, in terms of the experimental campaigns, and the results of analysis conducted. The discourse is then shifted towards the study of the effectiveness of

Reshaping using conventional forming processes (section 2.3). The final sub-section of this chapter is a discussion of the overall outcome of the technical feasibility analysis and the direction towards which the research would focus after having obtained the said results (Section 2.4). The work presented in this chapter was published as:

1) Ingarao G, Zaheer O, Campanella D, Fratini L (2020) Re-forming end-of-life components through single point incremental forming. *Manufacturing Letters*, 24:132-135.

2) Zaheer O, Ingarao G, Di Lorenzo R, Fratini L (2021) On the effectiveness of SPIF process to re-form End-of-Life components as compared to conventional forming approach. *SHEMET* 2021.

Chapter 3, namely “Formability and Geometrical Accuracy Performances”, focuses on the analysis of the geometrical accuracy of the Reshaping technique. The first section 3.1 deals with the analysis of the geometrical accuracy of the End-of-Life component, in terms of the non-worked zones of the component during the Reshaping process. This research work was also focused on analyzing the effects of different process parameters (those of the original forming process, as well as, those of the Reshaping process) on the geometrical accuracy of the End-of-Life component. Section 3.2 was rather focused on the variation of the SPIF process formability when used as a Reshaper for different kinds of End-of-Life parts (Sheet metal components having different types of pre-strainings). Consequently, the geometrical accuracy of Reshaping pertaining to the different types of

End-of-Life components was also analyzed in order to better understand the correlation between the pre-straining type/level and the obtainable geometry by SPIF. Finally, in section 3.3 the key findings of this chapter are summarized. The work presented in this chapter was published as:

1) Zaheer O, Ingarao G, Pirrotta A, Fratini L (2021) Geometrical deviation of end-of-life parts as a consequence of reshaping by single point incremental forming. *International Journal of Advanced Manufacturing Technology*, 115:1579-1588.

2) Zaheer O, Ingarao G, Di Lorenzo R, Fratini L (2021) Understanding formability and geometrical accuracy of SPIF process used as Reshaping approach. *ESAFORM 2021*.

Chapter 4, titled, “Energy Efficiency Analysis”, covers the performance of the Reshaping strategy in comparison to two other recycling techniques (Conventional and solid state recycling). This study was carried out in light of the overall energy consumption and the CO₂ emissions relative to the entire process cycles. Section 4.1 covers the cumulative energy demand and CO₂-emission analysis followed by the system boundary identification and assumptions. The energy demands and CO₂ emissions of the three routes are compared to using experimental measurements of necessary data and LCI techniques in section 4.3. The results of these analysis and their relative discussions are elaborated in sections 4.4 and 4.5. This work presented in this chapter was published as:

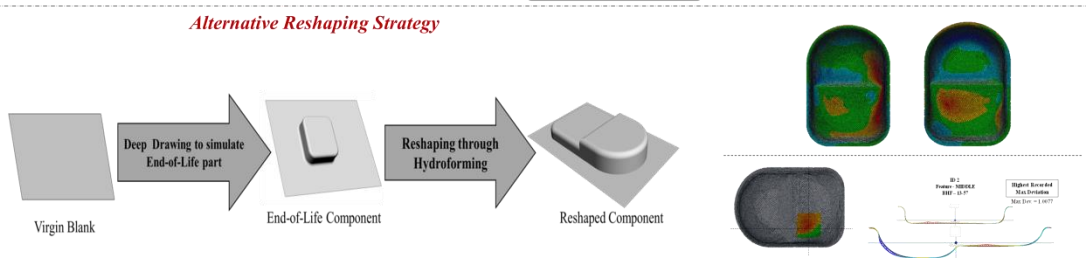
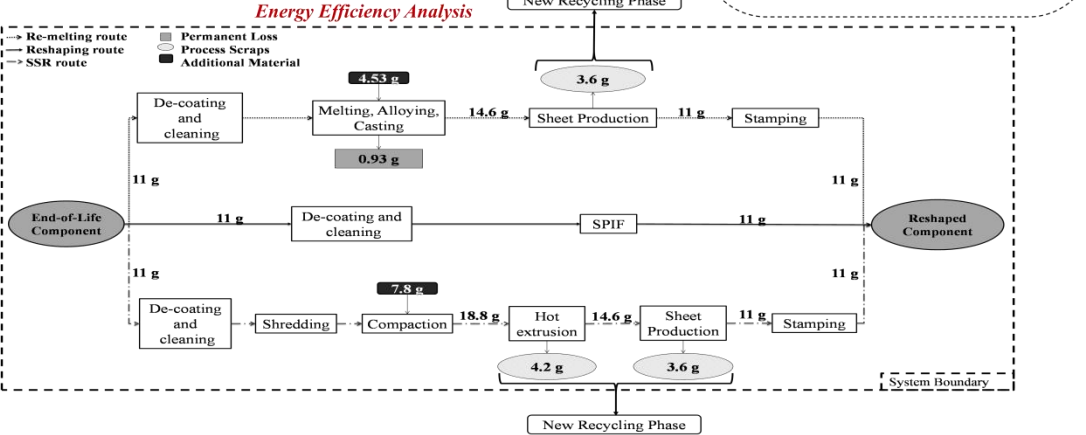
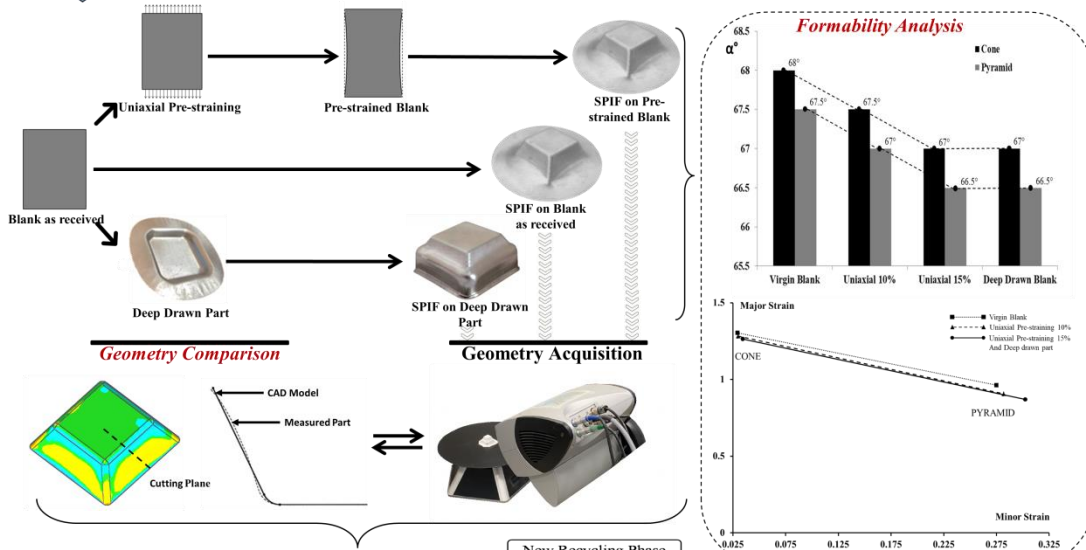
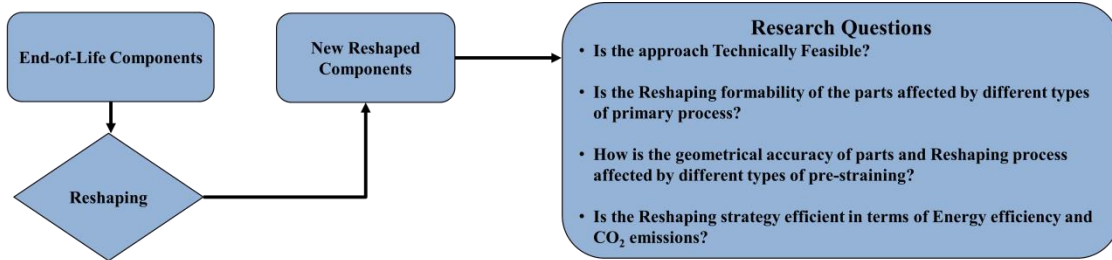
1) Ingarao G, Zaheer O, Campanella D, Di Lorenzo R, Fratini L (2020) An energy efficiency analysis of single point incremental forming as an approach for sheet metal based component reuse. *Procedia CIRP*, 90:540-545.

2) Ingarao G, Zaheer O, Fratini L (2021) Manufacturing processes as material and energy efficiency strategies enablers: The case of Single Point Incremental Forming to reshape end-of-life metal components. *CIRP Journal of Manufacturing Science and Technology*, 32:145-153.

Chapter 5, titled “Reshaping by Hydroforming: Feasibility Analysis”, focuses on the studying the potential of carrying out the Reshaping strategy using an alternative forming process, i.e. Hydroforming. Section 5.1 cover the description of the designed experimental campaign and the technical parameters utilized. The results of this research (section 5.2) detail the key findings of the study and the influence of the process parameters on the process efficiency and quality of the obtained Reshaped components.

Chapter 6, titled “Conclusion”, provides a summary of the general results obtained for the entire research scope, highlighting the advances of the state of the art enabled by the research presented in this dissertation (section 5.1). Section 5.2 finally provides a general outlook of the investigated process, the milestones yet to be studied and a focus on the possible future developments of this work.

Graphical Abstract



List of Abbreviations

SSR Solid State Recycling

CE Circular economy

SPIF Single Point Incremental Forming

FLC Forming Limit Curve

EoL End-of-Life

TIG Tungsten Inert Gas

DED Direct Energy Deposition

HAZ Heat Affected Zone

AA Aluminum Alloy

CS Cold Spray

DD Deep Drawing

CNC Computerized Numerically Controlled

BHF Blank Holder Force

O-CONE Outwards Cone

I-CONE Inwards Cone

O-PYRAMID Outwards Pyramid

I-PYRAMID Inwards Pyramid

FLD Forming Limit Diagram

H Deep Drawn Part Height

A SPIF Angle

B SPIF Base

FFL Fracture Forming Limit

CED Cumulative Energy Demand

CO₂-eq Carbon Dioxide Equivalent Emission

ECAP Equal Channel Angular Pressing

LCI Life Cycle Inventory

UTS Ultimate Tensile Strength

HFR High Feed Rate

LFR Low Feed Rate

BP Break-even Point

HF Hydroforming

PLC Programmable Logic Control

1. Introduction

Reducing anthropogenic environmental impact is an urgent issue to deal with. Technological innovation is needed in all the economic sectors in order to replace current practices with environmentally friendly alternatives. One of the main contributors to yearly CO₂ emissions is materials production, accounting for about 25% of the global CO₂ emissions [1]. Production processes account for about 8% of total global energy demands, which is expected to rise in the upcoming years due to decreasing ore grade [2]. Looking at the energy breakdown analysis it is possible to notice that such an environmental burden is dominated by only five materials: steel (25%), cement (19%), plastics (5%), paper (4%) and aluminum alloys (3%) [3]. Global demand for key materials has grown considerably over past decades and is predicted to rise furthermore in the upcoming years (Figure 1).

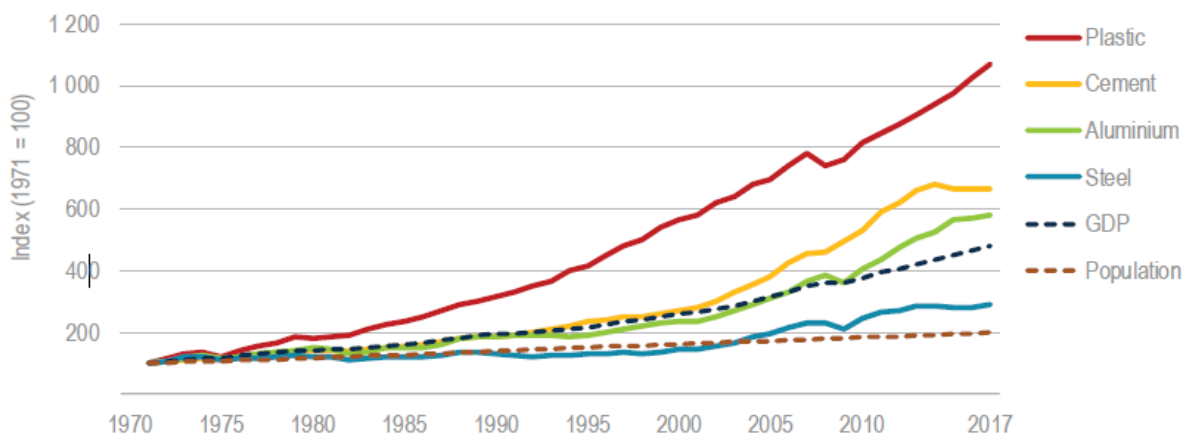


Fig. 1. Demand growth for key materials, GDP and population (Source [4])

Besides the rise in material demand, energy consumption and emission effects from materials production have grown substantially, by more than one and a half times over the last 25 years. Industry accounted for nearly 40% of total final energy consumption and nearly one-quarter of direct CO₂ emissions in 2017 [4] as illustrated in Figure 2.

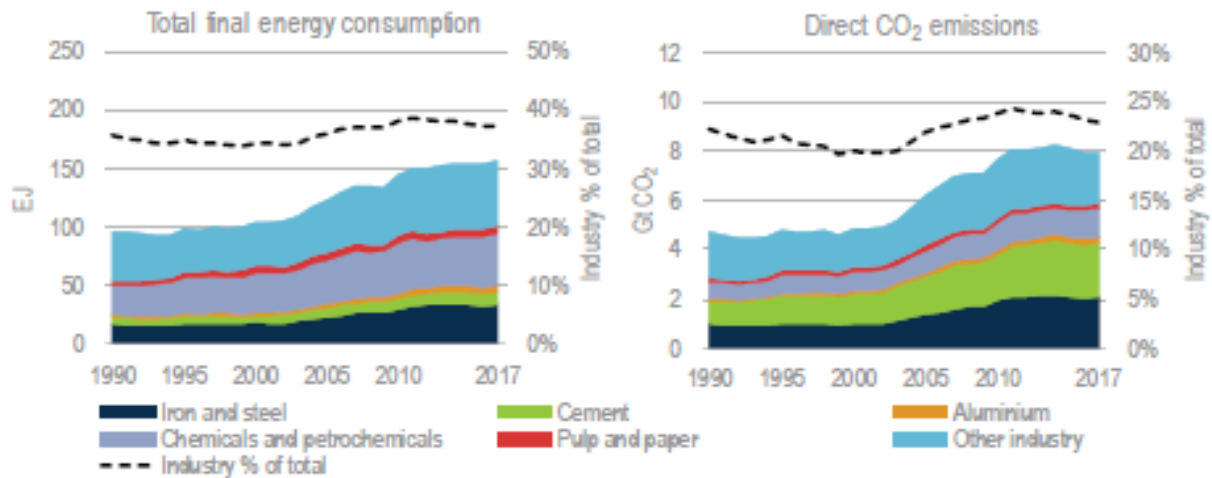


Fig. 2. Global industry final energy consumption and direct CO₂ emissions (Source [4])

Regarding metals, recycling is one of the most applied strategies. Metal reusing options have a double advantage; in fact, contribute not only to a reduction in the demand for virgin ores, but also have a positive effect on energy requirements.

Specifically, for metals all of the strategies can be successfully implemented; in fact, metallic material can undergo direct reuse, non-destructive recycling and conventional recycling. In fact, many metals can be recycled at high rates over and over again [5]. Light weight alloys (such as aluminum, magnesium, and titanium alloys) have been of particular interest over the last few years, thanks to their capability of permitting weight reduction whilst improving mechanical performance of the components [6]. In fact,

Recycling of these lightweight alloys, results in a substantial energy savings in comparison to primary production. A study showed a reduction up to 90% was achievable [7]. As it can be observed from Figure 3, recycling enables a significant energy saving with respect the primary production.

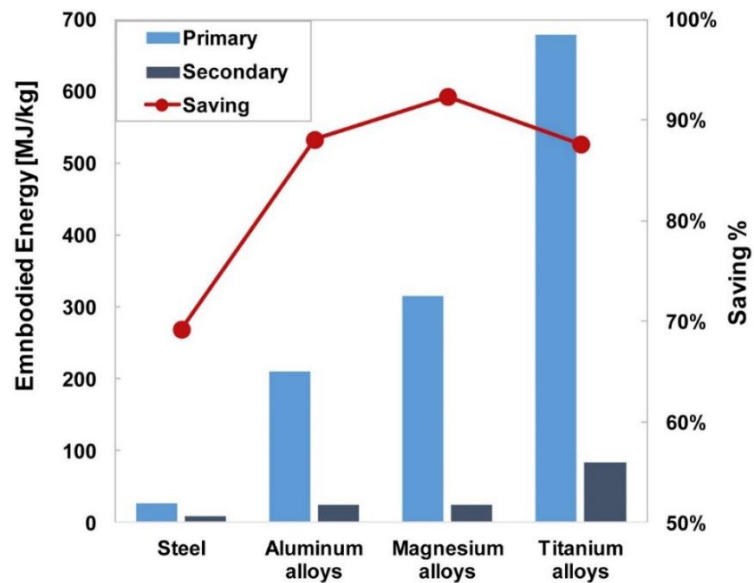


Fig. 3. Embodied energy comparison for primary and secondary production of different metals alloys, savings scale on the right (Source [8])

Recycling of lightweight alloys thus has significant ecological and economic implications that most countries cannot confront due the limited domestic primary productions, especially when the growing demands of these light-weight materials is taken into consideration. Commonly lightweight alloys are recycled using the conventional remelting-based recycling routes, these unfortunately have been proven to be still very energy-intensive. Besides being inefficient in terms of energy demand, permanent material losses occur tend to occur a lot as well. In the cases of aluminum alloys, the high affinity of aluminum to oxygen leads to permanent material losses during remelting due

to its oxidation. These losses were found to be almost 15-20% of the total recycled material, in the case of light-gauge scraps recycling [9].

With the aim for overcoming these issues, the scientific community turned to Solid State Recycling (SSR) strategies [10]. Due to the solid-state nature of such recycling processes material losses due to oxidation can be avoided. Solid state consolidation depends on pressure, temperature and contact time among surfaces to be joined. These conditions can be activated by different manufacturing processes mainly relying either on severe plastic deformation or on sintering processes. This process depends on pressure, temperature and contact time among surfaces to be joined and several strategies have been already successfully applied. Many different approaches have been made for performing SSR. Haasse et al. [11] used the Equal Channel Angular Pressing (ECAP) integrated extrusion processes to consolidate aluminum chips into a billet. Widerøe et al. [12] presented a variation of this process where the authors applied a direct screw extrusion method, to compact scraps and extrude profiles in one single step. Kamilah et al. [13] utilized a hot forging process as an alternate sustainable direct recycling technique of aluminum. Friction Stir Extrusion (FSE) was used to fully consolidated wires from aluminum alloys chips by other researchers [14]. Recycling processes can be still improved, though; solid state recycling processes have been developed for light alloys recycling [15] and have proved (for the case of aluminum alloys) to lower the environmental impact of recycling [9, 16, 17]. Although these works took different processes and materials into

consideration, both concluded that the best performance of SSR processes is mainly due to the material losses avoided during the process, as well as the reduction of processes steps required to obtain the end product.

Even though the recycling of aluminum is improved in terms of efficiency using the above strategy. There still is room for the overall improvement of the process, making it mandatory to move towards the adaptation of a more virtuous circular economy strategy.

1.1 Circular Economy

Recent studies have found that the reduction of the environmental impact of material production could be achieved by the implementation of a Circular Economy (CE) paradigm. CE is an economic system aimed at eliminating waste and the continual use of resources. This regenerative approach is in contrast to the traditional linear economy, which has a 'take, make, dispose' model of production. Circular economy aims to redefine growth, focusing on positive society-wide benefits. It entails gradually decoupling economic activity from the consumption of finite resources and designing waste out of the system [18]. The Circular Economy concept finds its root roughly from the theory of “Regenerative Design” by Lyle introduced in the late 70s links sustainable development to the concept of resource regeneration [19]. This idea has begun gathering a very fast pace, and there is a global need to move towards a closed-loop society [20]. Stahel and Reday in a study [21] presented an initial an idea for a transition of a regenerative design to a non-linear industrial model. This idea was further refined with

the concept of “Cradle-to-Cradle” design by McDonough and Braungart [22]. The “Cradle-to-Cradle” design is an economic, industrial, and social framework that focuses on the creation of systems that are not only efficient but waste free as well. The study of material and energy flows through industrial systems also termed as “Industrial Ecology” [23], has close links to the CE concept as well. Similar to Industrial Ecology, CE also has a systemic point of view, i.e., designing production processes in line with local ecological constraints, while taking their global impact from the outset into consideration.

The theory of CE emphasizes on the promotion of a sustainable lifestyle, where resources are used in an efficient manner so as to retain them in the economy for as long as possible. This can be achieved by maintaining a loop flow that feeds the resources back into the system for the same utility or with a newer functionality [24].

MacArthur Foundation [25] can be accredited for the modern concept of Circular Economy. Four different mechanisms for value creation in CE were introduced that present opportunities in comparison with linear usage:

- The power of inner circle: the closer the product gets to direct reuse, i.e., serving the same purpose as its original function, the higher the cost savings will be in terms of material, labor, energy, capital, and the associated externalities.
- The value of circling longer: A value created by keeping the products, components, and materials in use longer within the CE. This can be achieved by

enabling more cycles of product use or by its spending more time within a single cycle.

- The power of cascaded use: a value created by employing the use of discarded materials from one value chain as by-products hence, replacing virgin material in another.
- The power of pure circles: uncontaminated material streams increase collection and redistribution efficiency while maintaining quality.

In practice, the following Circular Economy options are implemented in the industrial practice:

Closed-loop recycling: recycling of a material can be done indefinitely, without properties degradation (upcycling). In closed-loop recycling, the inherent properties of the recycled material are not considerably different from those of the virgin material, thus making substitution possible [26].

Open-loop recycling: the conversion of material from one or more products into a new product, involving degradation in the intrinsic properties of the material (downcycling). In open-loop recycling, the inherent properties of the recycled material differ from those of the virgin material in such a way that it is only usable for other product applications, consequently substituting other materials [26].

These options call for different value and material preservation levels. Intense usage, product repair and upgradation, remanufacturing, component re-use are some of the strategies that if implemented, keeping the existing material in the circle, would therefore contribute towards reducing the environmental impact of raw material production [27]. The main principle focuses on turning an End-of-Life (EoL) product/component directly either into a reusable material or, better yet, into new products/components. As far as metals are concerned, recycling is still the most applied strategy as it provides environmental, technological, and economic benefits. Besides material itself, reuse strategies would also allow functions recovery from EoL components. Functions recovery would result in also avoiding the environmental impact of manufacturing processes already embodied in the EoL Component/Product.

1.2 Metal Reuse Framework

In the metal reuse framework proposed by Cooper and Allwood [28] four main strategies are identified:

1. Remanufacture/Repair: Remanufacturing typically entails further disassembly, metallic spraying, and thermal techniques to recover worn and fatigued surfaces. A remanufactured product fulfils a function similar to the original part. It is remanufactured using a standardized industrial process, in line with technical specifications [29]. Typical applications for metallic materials concerning automotive engines and die re-manufacturing. Repair refers to actions performed

in order to return a product or component purely to a functioning condition after a failure has been detected, either in service or after discard [30].

2. Relocate: Relocating focuses on recovering components and reconditioning them, by cleaning and simple repairs/ adjustments in order to be reused in the same type of products.
3. Cascade: Recovering component and using it for a different and less demanding function (downgrading).
4. Reshape: Application of manufacturing approaches (additive, subtractive, mass conserving) are applied to obtain a new, more useful, geometry reprocessing the returned EoL component changing its shape.

Of these four main strategies, Remanufacturing/Repair and Reshaping have been two of the most revisited strategies. Remanufacturing in particular has been widely analyzed by researchers in the past [27, 31]. In the Remanufacturing sector, many different strategies such like, fusion welding which has been used for repairing surface cracks and more in general damaged aerospace and automotive components Tungsten Inert Gas (TIG) welding, plasma arc welding and laser welding have proved their suitability for metal component repairs (tools, dies, mold, mechanical compotes, etc.) [32]. These technologies have been successfully applied also on aluminum alloys [33].

The welding process is often very manual and tedious and, in the meantime, additive manufacturing technologies have shown great potential for the automation of the repair

process with a significant increase in the accuracy of the final repair [34]. Within Additive manufacturing process category, Direct Energy Deposition (DED) processes have proved their suitability for component repair [35]. Such process category provides minimal distortion of the workpiece, reduced heat affected zones (HAZs) and better surface quality with respect conventional coating and repairing techniques such as arc welding and plasma spraying. Their suitability for metal components repair was also proved in terms of environmental impact reduction with respect to conventional repairing [36].

Some applications of laser-based powder deposition processes have been successfully applied for aluminum components repairing. Caiazza et al. [37], applied laser direct deposition to prove the suitability of this process for repairing AA-2024 aluminum plates. Liu et. al. [38] found that it is possible to use direct laser deposition as a repair technology to improve structural integrity in aluminum alloy aircraft structures in terms of corrosion reduction and geometrical restoration. Specifically, they used AA7075-T651 alloy plate with a thickness of 6.25mm as substrate and Al-12%Si and 7075 Aluminum powder was used as coatings. Results concerning performance of metallurgical bonding, resistance to corrosion and hardness were quite positive making the repairing process very promising. Recently, Guepner et al. [39], applied direct metal laser deposition to repair EN AC-43000 aluminum alloys, this material family are characterizing by a restricted weldability. A powder of the same material was used as filler material.

Hascoët et al. [40], focused more on the process automation improvements and they presented a method to automate the repair process of aluminum castings, by using a machine vision system and direct laser metal deposition.

To further improve the mechanical properties of the repaired component, scientists have lately turned to Cold Spray (CS) technology. This process category is gathering momentum as repairing strategies for metal parts [41]. In such process, propulsive gas is used to accelerate powder feedstock to a high velocity and to induce deposition when the powders impact onto a substrate. In contrast to conventional high-temperature deposition processes, the formation of a cold spray deposit relies largely on the particle kinetic energy prior to impact rather than the thermal energy. Also, the powder used remains solid state during the entire deposition process. The solid-state status of the process allows avoiding defects normally occurring in high-temperature deposition processes, such as oxidation, residual thermal stress, and phase transformation. The advantages of using CS as repair tool are clearly listed in a recent review paper on Cold Spray technologies provided by Li et al. [42]. The authors identified the following advantages with respect existing repairing technologies such as traditional welding, electroplating, and 3D printing: (1) high repairing efficiency; (2) in-site repairing; (3) the powders employed can be of the same material as the worn metal parts; (4) cold spray can be used for precision processing; and (5) Cold Spray can result in residual compressive stresses, avoiding crack initiation and propagation, therefore improving the fatigue properties of

base metals. Reshaping has been overlooked by the scientific community so far. In general, most of the research are concerned with Additive Manufacturing application, often coupled with machining processes, either to repair or to change the EoL geometry [43, 44]. Among repairing technologies of aluminum-based components composite patch repairs are worth mentioning, being a technique that has been mainly applied on aircraft component/structures [45]. The development of composite materials led to the creation of a new method for the repair of metallic structures, based on the adhesive bonding of composite patches on cracked panels. Bonded patch repair is mechanically efficient and is a cost-effective method for maintaining both military and civil aircraft. In fact, most of the available studies are applied on the aluminum alloys normally used in aircraft components. Some advantages of repairing the cracked structures by the composite patches (normally, Carbon/epoxy, Boron/epoxy; systems are used as composites) are high stiffness, high fatigue life, low weight, and low cost and time of repairing process [46]. Specifically, several authors focused on the analysis of composite patch repairing of AA 2024 aluminum alloys [47, 48, 49, 50] others analyzed the performance of such technique on AA-7075 aluminum alloy [51, 52, 53, 54, 55]. Other researchers proved the suitability of their repairing techniques also on the 6061-T6 alloy [56] and on AA-5083 [57].

Forming processes applied specifically as Reuse strategy are covered in very few scientific papers published so far. Tilwankar et al. [58] proposed to reroll steel recovered from vessels into semi-finished products (plates, bars and rods used). Brosius et al. [59]

in a review paper describe how a demounted automotive engine-hood can be Reshaped into a rectangular sheet metal component by sheet hydroforming process. Takano et al. [60] applied Single Point Incremental Forming (SPIF) on a flattened sheet. In fact, the Reshaping they propose includes the flattening of a previously bent sheet and a subsequent incremental forming step. Abu-Farha and Khraisheh [61] proposed the application of super plastic forming for applying Reshaping strategies on magnesium-based sheet components. The aforementioned research provides the innovative ideas of using forming process as Circular Economy enablers. However, these studies are preliminary and the potential of forming process in this new domain is not explored yet. It is worth mentioning that there is a lack of process mechanics analysis; for the proposed processes neither process windows nor process parameters influence have been analyzed so far. This doctoral thesis focuses on the application of Single Point Incremental Forming (SPIF) as a novel approach to Reshape sheet metal based EoL components. It is worth remarking that returned EoL components are normally characterized by high heterogeneity as there are localized thinning areas (caused by the original forming processes) while large part of the component underwent limited deformation. The thinned zones might be characterized by a limited formability while, in the less deformed zones it is still possible to take advantage of almost the entire original formability. Ideal manufacturing processes for reforming sheet metal based components should be

characterized by higher formability as well as by a local action. In this respect, Single Point Incremental Forming meets the aforementioned requirements perfectly

1.3 Single Point Incremental Forming

Current advances in the utilization of computers in sheet metal manufacturing processes paved the way towards the development of many novel flexible forming processes evolving from commonly used manufacturing processes. Of these flexible processes is SPIF, a sheet metal component manufacturing process, where incremental stepwise forming is performed by a CNC controlled hemispherical tool, [62], in Figure 4 a schematic representation of the process is shown.

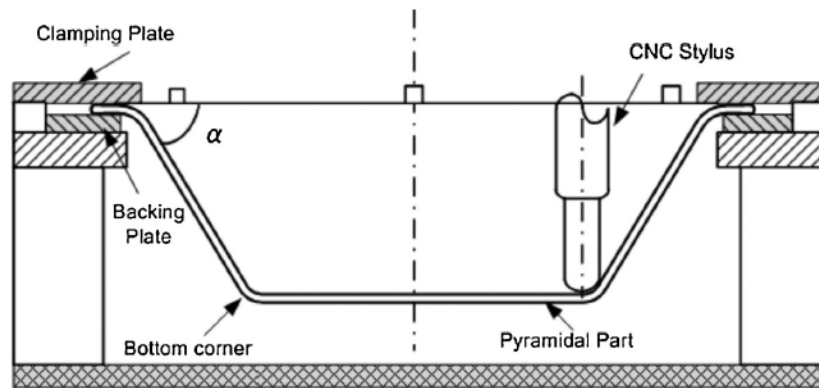


Fig. 4. Schematic representation of a Single Point Incremental Forming Setup (Source [63])

The SPIF process provides considerably high degree of flexibility in comparison to conventional forming processes due to its independence from the requirement of a dedicated die. This results in the reduction of tooling costs as well as the lead-time. Consequently, the process performs as a relatively cost effective and efficient

manufacturing process in the production of small batches of sheet metal parts. [63]. The formability of SPIF has been found to be higher than that of conventional forming processes such as stamping [64]. The forming limit curve (FLC) of SPIF lies on the right-hand side of the forming limit diagram forming a negative slope, as illustrated in Figure 5. In this study the authors also identified the maximum wall angle (before failure) for characterizing the forming limits. This maximum angle is influenced mainly by the material type, thickness of the sheets worked upon and the process parameters such as, the process feed-rate, sheet temperature, tool radius, step down etc. [65].

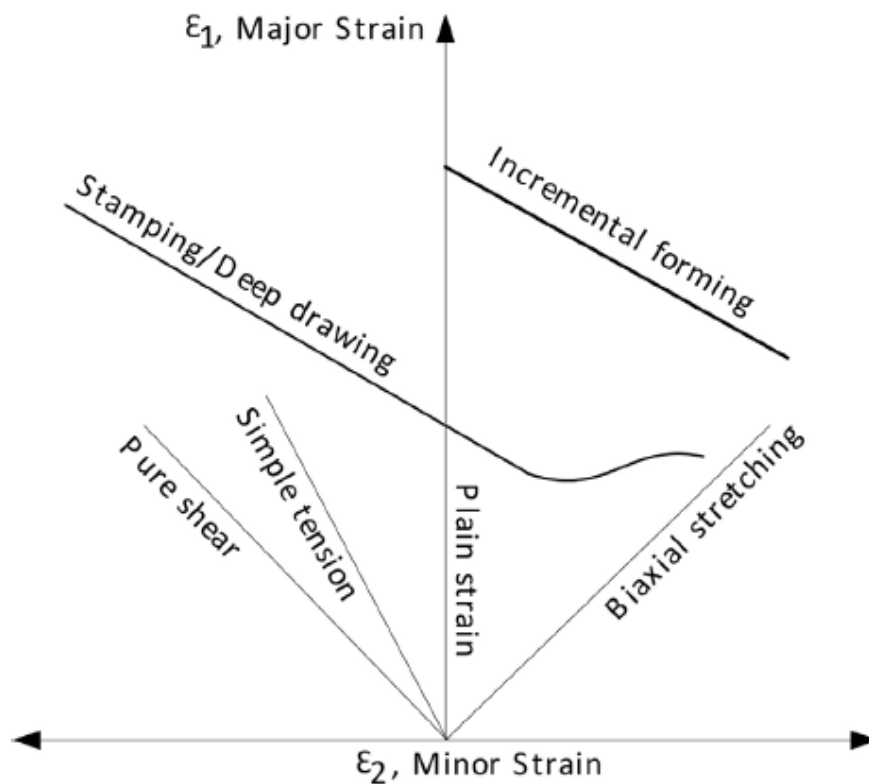


Fig. 5. Schematic representation of FLC in SPIF compared with conventional forming (Source [63])

Typically, two types of geometries are used to determine this angle on forming by SPIF: (i) constant wall angle parts such as a cone and pyramid or (ii) variable wall angle parts such as a hyperboloid cup.

Hussain et al. [66] observed that in cases of parts with varying wall angles, the failure wall angle is dependent on the geometry being formed and tends to be almost 4° higher than that obtainable by a constant wall angle geometry. Filice et al. [67] designed an experimental technique to understand whether an online monitoring of the tool force could be utilized for predicting part failure. Through this technique, the authors successfully avoided failure in a conical part, through the observation of the force trend and changing the process parameters (tool diameter and step down). Aerenset al. [68] presented force models in support of the selection of the same process parameters, where the axial force was proportional to the step down and tool diameter. Szekeres et al. [69] in research illustrated that though an online monitoring was useful for conical parts, it wasn't as applicable for pyramidal parts due to the fact that the edges separating the planar faces acted as reinforcements. These reinforcements hindered any potential increase in the force right before failure of the component. Hussain et al. [70] used the reduction in cross-sectional area at the point of tensile failure as a factor for the determination of failures in SPIF, thus deriving an empirical FLD for the same. Eyckens [71] presented a theory on the failure of conventional FLDs SPIF where the authors motivated their assertion as the conventional FLCs being valid only under the

assumptions of linear strain path, while being negligible through thickness shear, plane stress and deformations arising mainly by the membrane forces with no bending. These conditions do not occur in SPIF. Centeno et al. [72] observed that a postponed necking followed by ductile fracture was the reason in governing the failure limits in the case of AISI 304, this was particularly the case for high tool diameters which gave a low ratio (t_0/R) of the initial sheet thickness (t_0) to the radius of the tool (R). It was observed that the failure limits depended on the tool diameter and the reduction of the tool diameter improved formability. With respect to stretch bending, the fracture strains were located close to the fracture forming line, which in the case of SPIF were much higher. So far, several experimental campaigns and numerical models have been used to study formability in SPIF. Emmens and Van den Boogaard et. al. [73] initially attempted examining if in incremental forming, the forming by shear could be used for explaining the forming mechanics. A deeper analysis by the same authors, a detailed study on the mechanisms of explaining the improved formability in SPIF as a localization of plastic deformation [74]. In this study the authors summarized the different explanations as six different phenomena: contact stress; bending-under-tension; shear; cyclic straining; geometrical inability to grow and hydrostatic stress. Of these, hydrostatic stress fails to explain the higher location of the FLC. Martins et al. [75] analyzed the enhanced formability of SPIF by the combination of ductile damage mechanics with membrane analysis. In this article the authors presented an explanation through the use of Fracture

Forming Limits (FFL), which relies on the onset of fracture rather than on the onset of necking, as in the case of conventional FLDs.

From a literature review analysis Trzepieciński concluded that the use of conventional forming is found to be counterproductive and time-consuming when applied in the production of parts in small batches. This conclusion pointed towards the need of alternate processes for the reduction of manufacturing costs and time in the forming of individual parts. Incremental sheet forming has been seen to be a promising option as it nullifies the requirement of manufacturing of dies for operation and at the same time has the ability to shape elements on a conventional CNC milling machines [76]. In fact, SPIF has been proven to be a flexible process, characterized by a local forming action. Its local action along with its enhanced formability has been widely proved [77]. Such advantages are the result of the unique process mechanics of SPIF [78, 79].

1.4 Proposed research

The overall scope of this research relies on the studying of possibility to implement the Reshaping strategy, through the use of a flexible forming process, as a successful metal reuse alternative. The concept implies the safe extraction by disassembly of large sheet metal components from End of Life products, such as car/bus/truck body, washing machines, etc. and directly reform the components by means of SPIF processes (Figure 6).

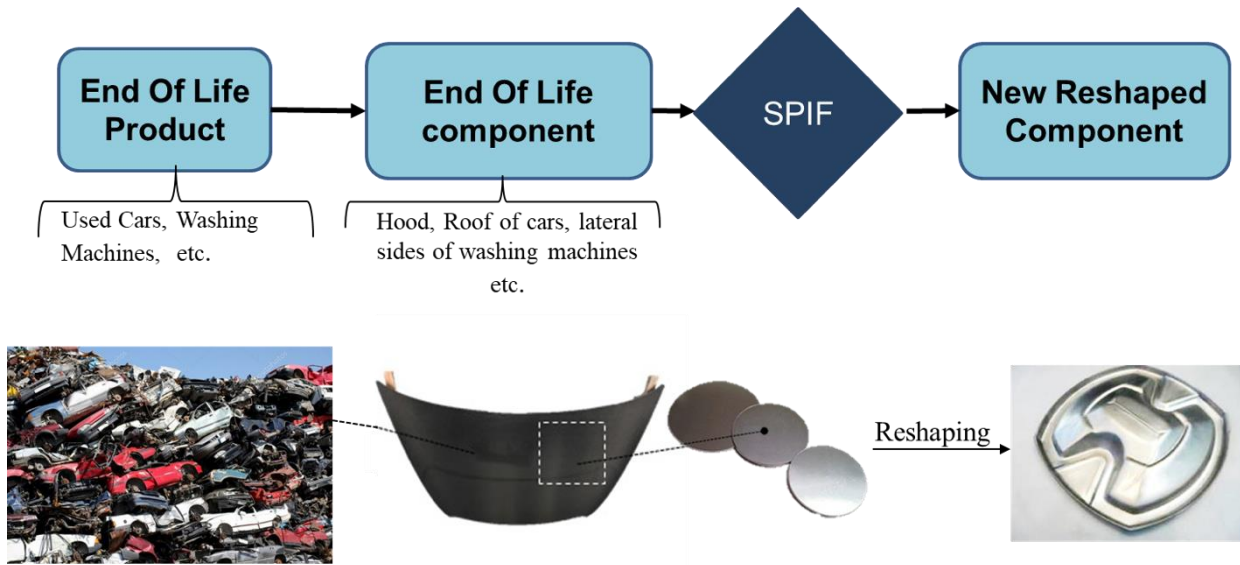


Fig. 6. Proposed Research Approach

In order to simulate this metal reuse approach, the material selected was a series 5 aluminum AA5754 alloy sheets 0.5mm thick in diameter. These AA5754 sheets were characterized as H22, work hardened by rolling then annealed to quarter hard. The research procedure as reported in Figure 7 was adopted. In particular, after cutting a circular virgin blanks out of the aluminum sheet, pre-straining of the sheets was performed, as Deep Drawing (DD) or Uniaxial pre-straining, for simulating EoL component. The then obtained EoL component was then Reshaped using the SPIF process for the studying of the various process/product properties.



Fig. 7. Research Procedure,

2. SPIF used as Reshaper: Technical Feasibility

Reprocessing sheet metal based EoL components poses new technological issues. In fact, returned components are normally characterized by high heterogeneity as there are localized thinning areas (caused by the original forming processes) while large part of the component underwent limited deformation. The thinned zones might be characterized by a limited residual formability while, in the less deformed zones it is still possible to take advantage of almost the entire original formability. The ideal manufacturing process for reforming sheet metal-based components should be a flexible one and characterized by local forming action. SPIF seems to perfectly meet these requirements. Its local action along with its enhanced formability has been widely proved [80]. Such advantages are provided by the unique process mechanics of SPIF process [81, 82].

2.1 Deep Drawing

Deep Drawing (DD) process is used for the manufacturing of cup or box shaped parts where a flat sheet is pressed through a die using a punch while the blank is held in place using a blank holder. Figure 8 illustrates a schematic representation of the DD system. The blank holder force (BHF) and horizontal clearance between punch and die plays an important role in the process performance.

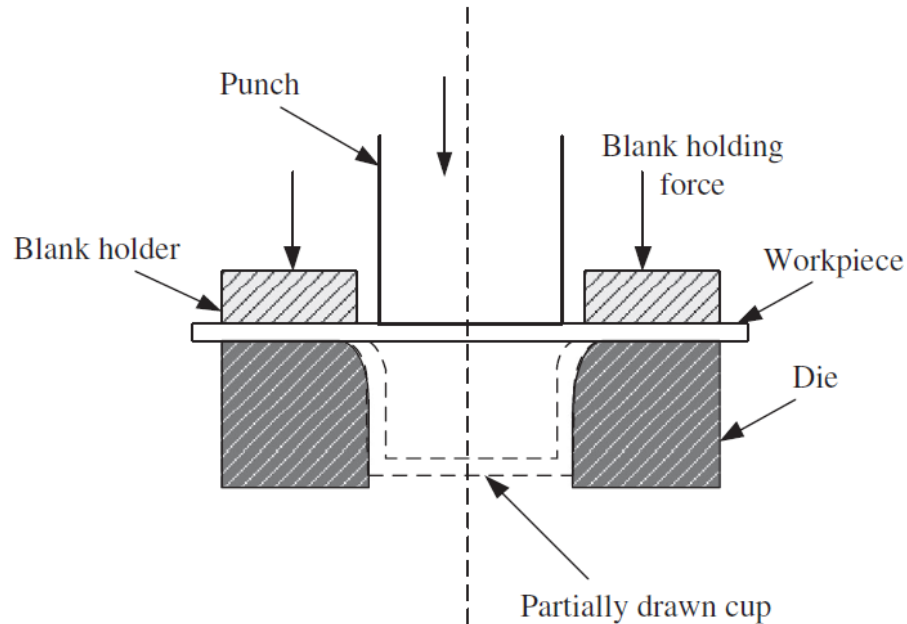


Fig. 8. Schematic representation of the Deep Drawing setup. (Source [83])

Excessive BHF causes tearing, and too less BHF causes wrinkling [84]. Similarly, regarding the clearance between the punch and the die, Too less clearance tends to cause ironing of the sheet. The minimum clearance necessary is usually calculated ranging as between 7% to 15% of the sheet thickness [83].

2.2 Technical Feasibility Analysis

2.2.1 The Adapted Approach

The approach adapted to prove the technical feasibility of SPIF based Reshaping strategy proceeded with the forming of a square cup using the DD process, with the geometrical details presented in Figure 9. On The base of the obtained square cup SPIF process was applied. Both truncated cones and truncated pyramids were obtained by

SPIF. For each selected shape SPIF was performed along two different directions as depicted in Figure 9. The two variants were referred to as inwards and outwards. The left over flange from the deep drawing process was intentionally left and used as a flat sheet portion to apply the clamping system on. SPIF was performed following a helical tool path with a 0.1 mm descent for all the experimental tests.

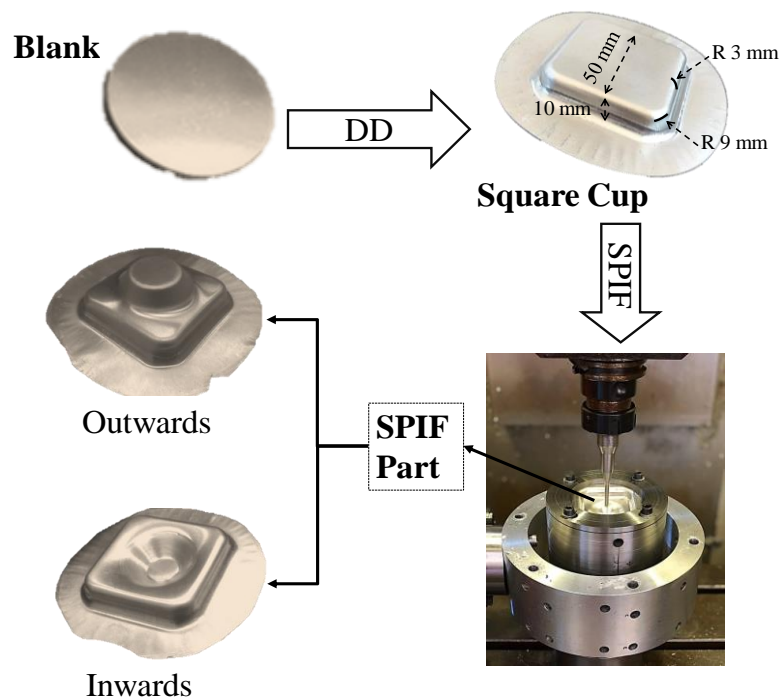


Fig. 9. Reshaping feasibility research process chain.

In order to verify the suitability of SPIF as Reshaping strategy, it is crucial to analyze to what extent the SPIF operations affect the highly thinned areas (with possibly limited formability) of the DD part. In order to analyze such interaction level, thinning distribution as well as major and minor strains were acquired both after DD and SPIF processes.

The obtained values were then compared to analyze the changes caused by the Reshaping process. To acquire the thickness distribution, the obtained samples were resin casted in an epoxy resin and afterwards cut along the diagonal, examined through a microscope and processed by ImageJ software. Concerning major and minor strains measurement, circles with diameter equal to 1.5 mm were laser incised across the starting blank and their change in shape was again acquired by microscope after both DD and SPIF process as illustrated in Figure 10.

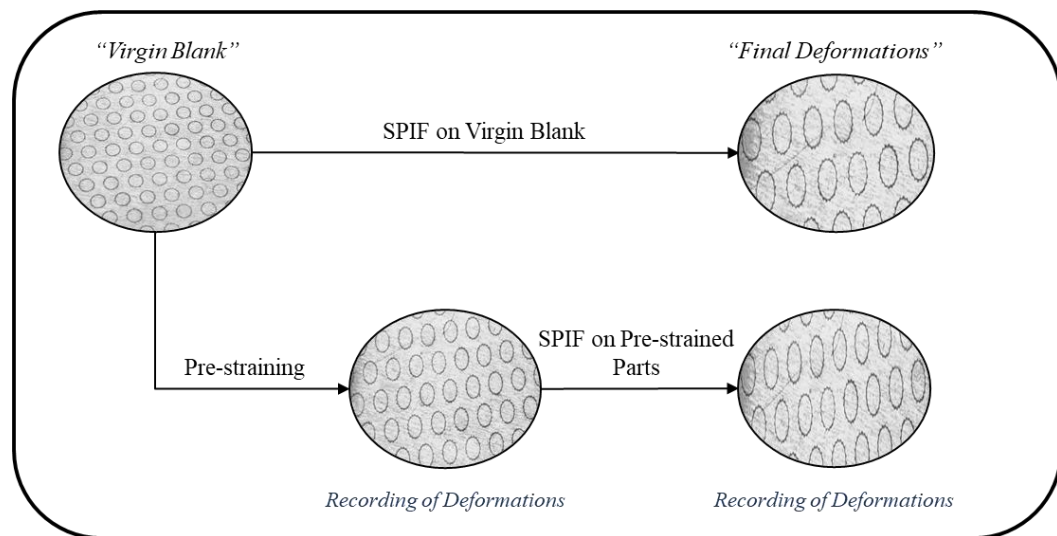


Fig. 10. Strain measurement methodology.

2.2.2 Case study 1: SPIF operations away from highly thinned areas

The first case study concerns the addition of a truncated cone by SPIF at the center of the base of the deep drawn part. The cone was selected with a major base diameter (34 mm) significantly smaller than the side of the square box. Meaning that the SPIF tool operates quite far from the bottom angle (highly thinned areas) of the DD part. The target

truncated cone is characterized by a wall angle equal to 45° as well as by a height of 10 mm. Both outwards (O-Cone) and inwards (I-Cone) approaches were successfully applied. In both cases sound samples were obtained (Figure 11 a), neither ductile fracture nor plastic instability occurred. In order to describe the results, three different zones were identified. Zone A is the bottom corner of the DD part, zone B is a transition zone between the DD and SPIF area, zone C is the wall of the geometry obtained by SPIF. In Figure 11 (b) It is possible to notice that in zone A, the local minimum corresponding to the thinning induced by DD process, and in zone B no change in thickness occurs. This first result is already significant as it means that SPIF process does not at all affect the thickness of the dangerous area of the DD part. In zone C, an expected thinning phenomenon is visible and it is due to the stretching mechanics typical of SPIF process. Regarding major and minor strains, the results of the measurements acquired after both DD and SPIF processes are reported in Figure 11 (c) along with the Forming Limit Diagram (FLD) of the used material.

As it can be observed no change in strain values occurs in zone A and B; while in zone C the strain induced by SPIF process is visible. Also under the strains perspectives, SPIF process does not affect the zone A. In conclusion, for this specific case study, SPIF enables a large deformation in areas barely deformed by the DD process without affecting the dangerous zones of the DD component.

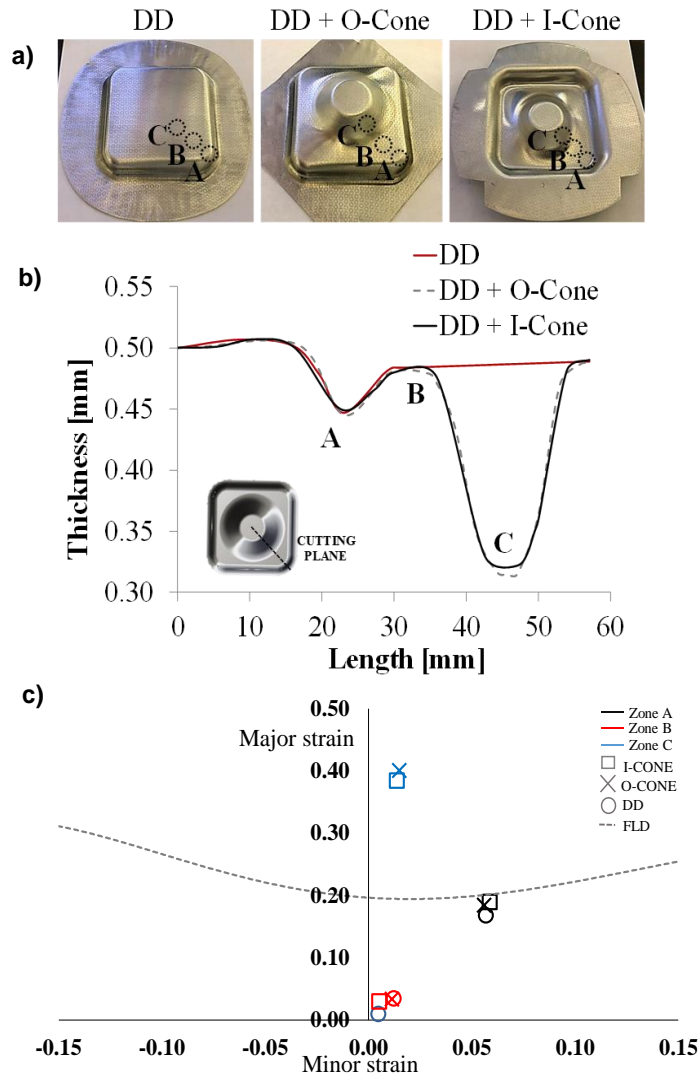


Fig. 11. a) Obtained samples, b) related thickness distribution along half of the diagonal for the O-Cone and I-Cone case studies, c) Major and Minor strains values over three different zones.

2.2.3 Case study 2: SPIF operations close to highly thinned areas

The addition of a truncated Pyramid with a major base side of 41 mm was considered to operate SPIF as close as possible to the bottom corner of the DD part. In order to further challenge, the Reshaping process, a pyramid with a wall angle as high as 60° was added. This choice was driven by the intent to reach higher strains level as well

as higher SPIF forming loads [85, 67]. The obtained samples along with thickness distribution are reported in Figure 12. Only Outwards case studies were reported as no significant difference were observed in the results of the Inwards versions. As it is possible to notice, the transition zone disappears as the SPIF process affects the corner itself. Part of the sheet already thinned by the DD process are, in fact, further deformed by SPIF.

In order to further explore such sheet portion, a numerical model was set up to carry out the thickness and strain histories of this area. Ls-Dyna commercial code was used with a four steps approach; two explicit steps for DD and SPIF, one implicit approach after the explicit simulation of each of the forming step, for the spring-back analysis, was also performed, the accuracy of numerical simulation was verified by comparing numerical end experimental thickness values. The results of the numerical model validation is illustrated in Figure 13.

Referring a research study performed on the spring-back prediction, a full integrated quadrilateral shell element with seven integration points along thickness was used [86]. The starting element size was set as 7 mm and a three levels geometric remeshing strategy was applied for the DD simulation process. For the SPIF, starting from the final mesh of the DD part, only one remeshing level was activated.

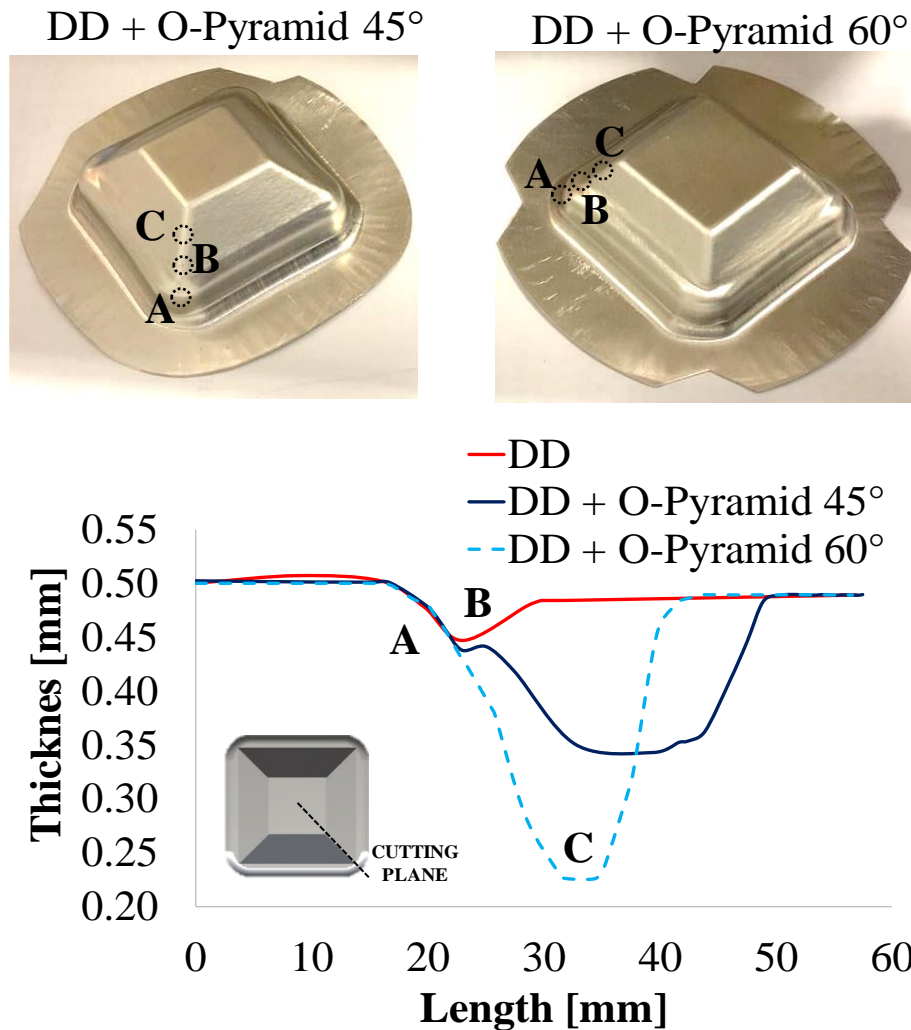


Figure 12. O-Pyramid obtained samples and related thickness distribution along half of the diagonal.

In Figure 14 (a) the numerical simulation output for the O-Pyramid 45° case study is reported; the elements selected for strains history analysis are highlighted. Figure 14 (b) depicts the thickness versus process time (artificial time due to explicit formulation constraints) trend of the selected elements for both 45° and 60° O-pyramid case studies. These trends were carried out exclusively by the SPIF step of the numerical simulation.

In two out of the three selected elements, an extra thinning caused by SPIF is visible, this effect is more evident for the trend of element 3 of O-Pyramid 60°.

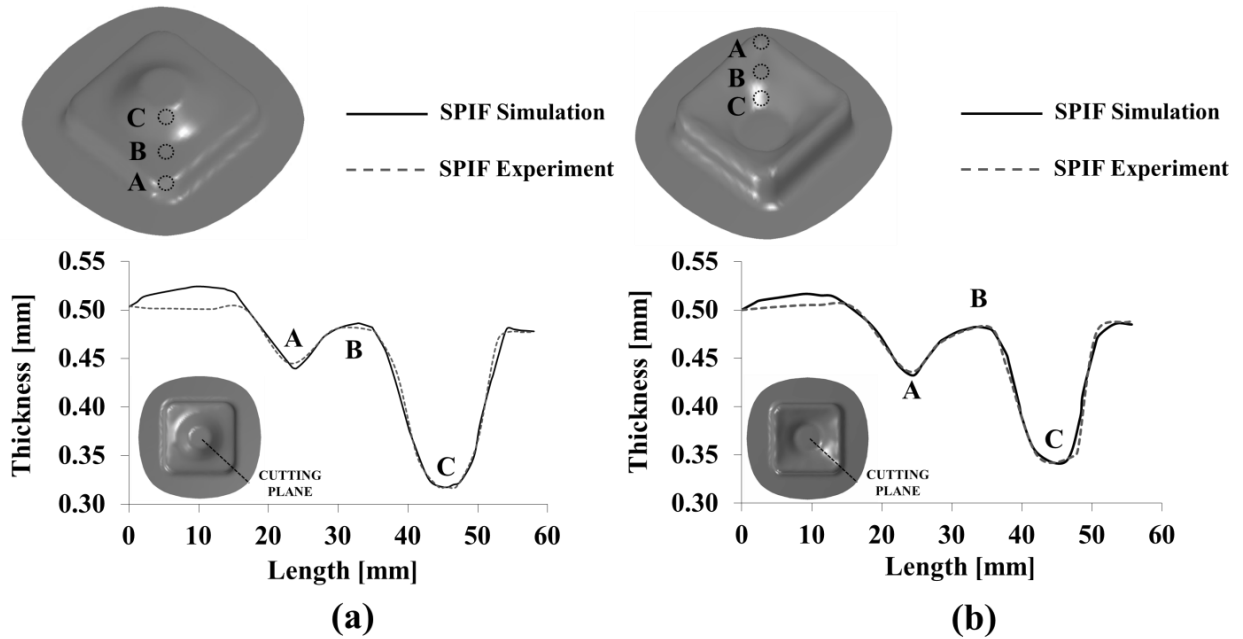


Figure 13. Thickness distribution comparison between experimental and simulation results along half the diagonal; (a) Outwards Direction, (b) Inwards Direction.

In fact, element 3 is the most interesting one as it is significantly affected by SPIF although it still belongs to the corner area. For this element the Major and Minor strain trends, as computed by the SPIF step numerical simulation, are reported in Figure 14 (c). Again, a substantial change in strain values is visible, actually extra strain is superimposed to the strain level of the DD step. The increase is more relevant for the major strain of the O-Pyramid 60°.

It is worth remarking that here presented approach can be applied to any other metallic materials. Regarding the extent of the complexity of the shape obtainable during the

Reshaping, it depends on SPIF formability performance of the material being formed [87, 88].

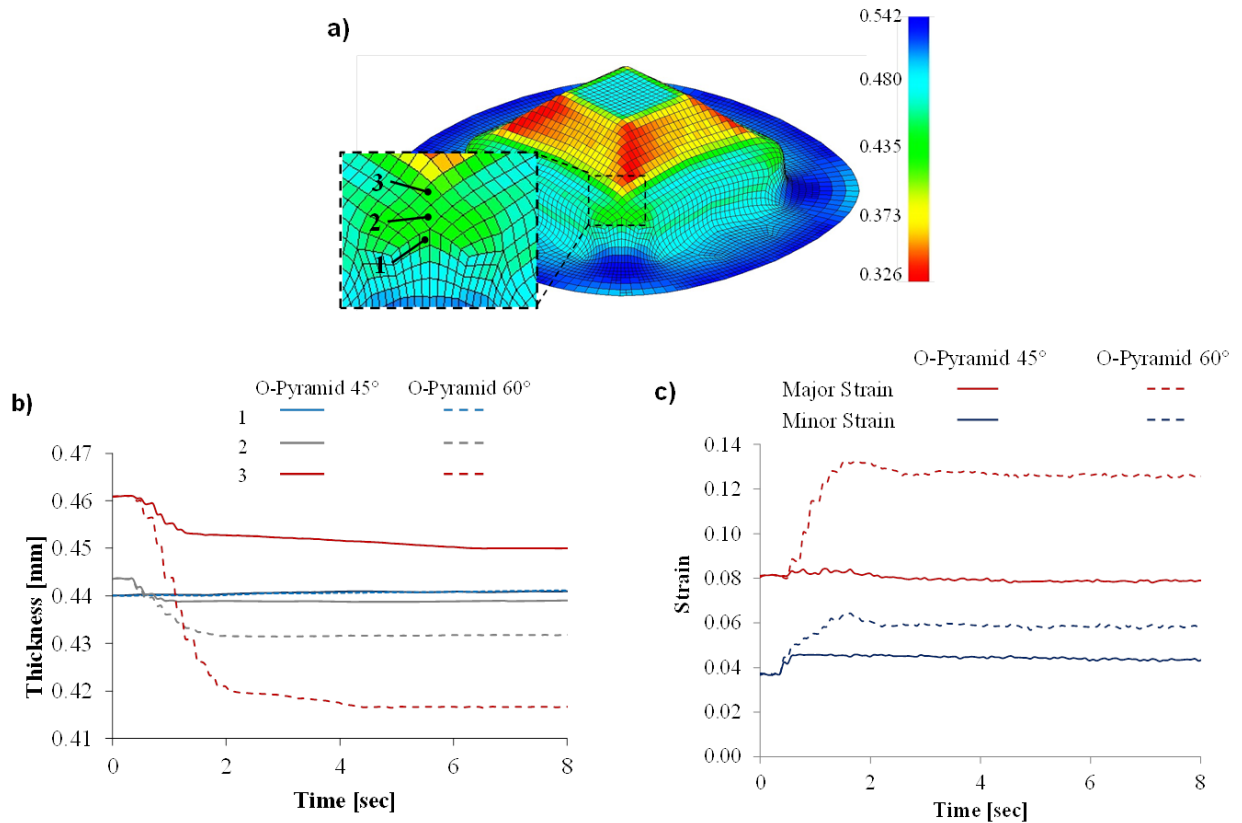


Fig. 14. a) Numerical simulation thickness map for O-Pyramid 45°, b) thickness history of the selected elements, c) Major and Minor strain histories for element 3 for O-Pyramid cases studies.

These results moved the research direction towards the exploration of the possibility of Reshaping solution using conventional forming processes.

2.3 Effectiveness of Reshaping Using Conventional Forming Process

2.3.1 The Adapted Approach

In this section a numerical approach was taken following the similar approach, with a difference being the performance of Reshaping using the DD process as illustrated in Figure 15.

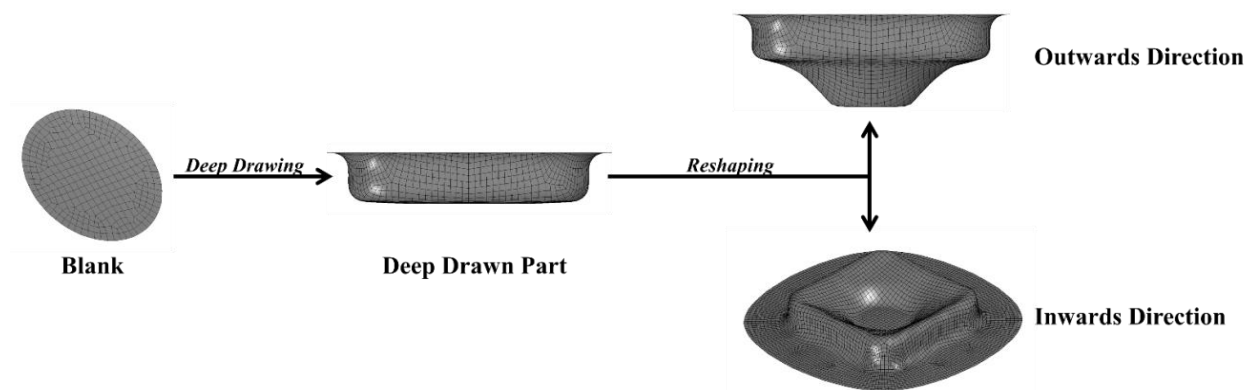


Fig. 15. Adapted Research Approach.

In order to prove the advantage of SPIF as a feasible Reshaping approach in comparison to conventional forming processes, a numerical campaign was developed in order to simulate alternative Reshaping processes based on conventional processes. The entire process chain was numerically simulated using the explicit code LS-DYNA, and spring-back analysis were carried out with its implicit solver after each forming simulation. In other words, a two steps approach was undertaken, one explicit step for DD and one implicit approach after the explicit simulation. For this research a truncated cone was

formed on the base of the DD component in both inwards and outwards directions and two levels of the cone angles i.e., 45° and 60° were selected.

Having obtained a good overlapping of the thinning profile between the experimental and the simulation results in the previous research, the numerical model was validated. A node blocking strategy was applied to minimize numerical instability and replicate the blank holder function.

To achieve the objective of this research, different approaches based on conventional stamping processes were applied in order to obtain the same reshaped components. In this respect, several numerical simulations were run in such a way that the punch used in the stamping process was given the form of a cone so as to attain the desired final shape.

Two case studies were analyzed, i.e. Reshaping with a cone angle of 45° in the first case study and 60° in the second. For each of the case studies, Reshaping was performed in both inwards as well as outwards directions. Three different strategies were undertaken, in the first strategy Reshaping without any counter die, in the second case a ring was used to simulate a counter die having an inner radius of 35 mm and a fillet radius of 3mm, for the third strategy a second ring was used to completely limit material flow during the stamping process. This third choice was driven by the will to overcome the wrinkling phenomenon occurring during the first two applied strategies. The resulting parts along with their forming limit maps have been illustrated in the following subsections.

2.3.2 Analysis of Alternative Reshaping Solutions

45° Cone Case Study. In the first case study a cone with a wall angle of 45° was selected to be formed on the base of the previously deep drawn part. The three strategies yielded results as presented in Figures 16 and 17.

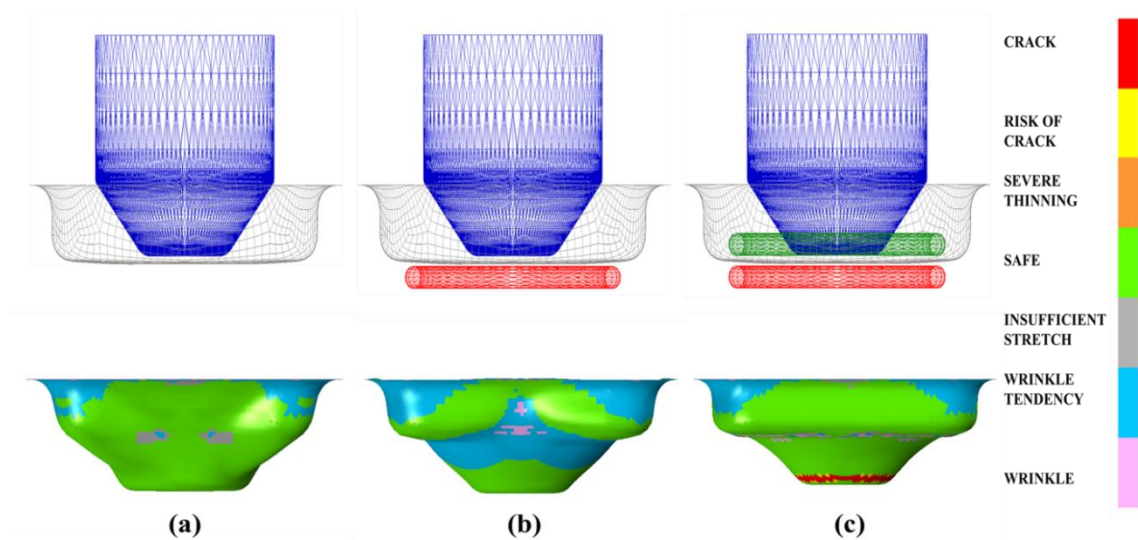


Fig. 16. Numerical simulation setup and the resulting forming limit map at 45° cone angle in outwards direction; (a) without counter die, (b) with counter die, (c) with blocked material flow.

As it can be seen from the results presented in Figure 16, without the use of a counter die the obtained result has a final form very different from the one projected. In fact the lack of material flow control allows the lateral walls to get pushed inwards whereas the entire base of the initial square cup is deformed due to the absence of a counter stamp. On the usage of a counter die (ring) the desired form is obtained but at the same the lateral wall experiences a push in as seen in Figure 16 (b). Such push in is also proved by the wrinkling tendency pointed out by the forming limits map.

Lastly, the limiting of total material flow using a counter die and a binder (second ring), causes the part to fracture proving the strategy as non-feasible. In fact, in this case the Reshaping strategy would be put in place exclusively by stretching mechanics, such a strategy is unfeasible for the present case study due to early ductile fracture occurrence, though. Similar results were obtained in the inwards direction (See Figure 17), confirming the non-feasibility of the undertaken strategies.

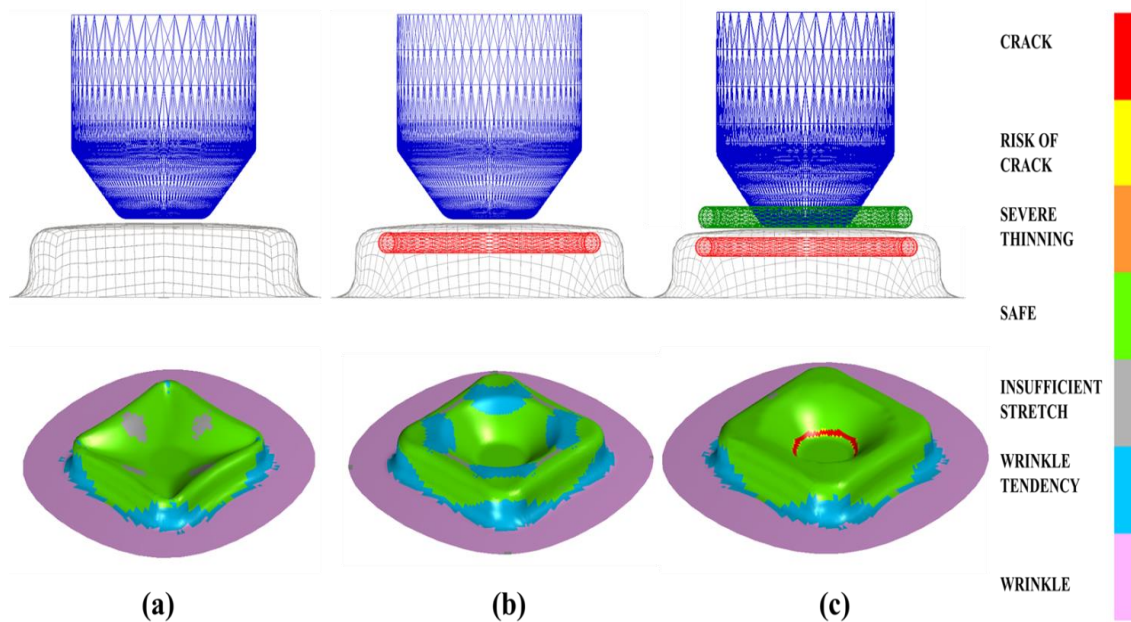


Fig. 17. Numerical simulation setup and the resulting forming limit map at 45° cone angle in inwards direction ; (a) without counter die, (b) with counter die, (c) with blocked material flow.

Again, in Figure 17 (a) it is possible to see that, without any material flow control, the obtained shape has a final form very different from the one projected. Another peculiar defect was noted in the case where a counter die was utilized, that is the occurrence of small depressions near the angles on the base of the square cup as seen in Figure 17 (b).

In Figure 17 (c) it is possible to notice that an excessive stretching mechanics occurs causing fracture.

60° Cone Case Study. The second case study was performed to further highlight the obtained results in the previous case study. That is, performing the addition of a cone with a higher wall angle (60°) in order to verify the occurrence of the defect types, thus, confirming the impracticality of Reshaping by deep drawing. Figure 18 illustrates an experimental results and a thickness distribution result of a cone of 60° wall angle Reshaped onto a square cup through the SPIF process.

The experimental result verified the possibility of Reshaping at a higher angle and obtaining a sound and defect free component. The scale in the figure denotes the numerical thickness distribution (mm) of the part. Being a local action process, SPIF enables the Reshaping of an EoL part subjected to a significantly high degree of deformation. As it is evident from the illustrated figure, the part reaches a wall thickness of 0.259 mm without the occurrence of any cracks.

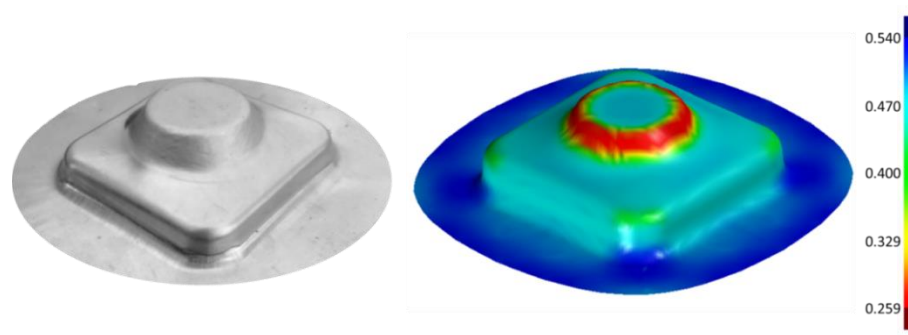


Fig. 18. Obtained sample and Numerical thickness distribution of a part Reshaped through SPIF process with a cone angle α (60°), outwards direction.

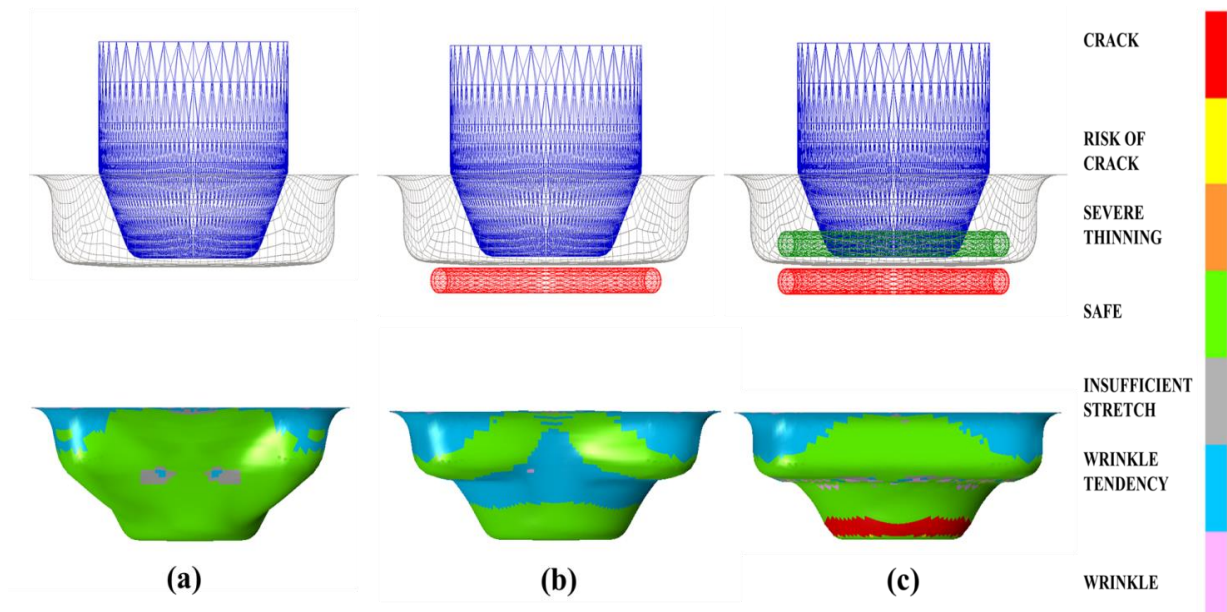


Fig. 19. Numerical simulation setup and the resulting forming limit map at 60° cone angle in outwards direction; (a) without counter die, (b) with counter die, (c) with blocked material flow.

From Figure 19 the defects mentioned in the previous case study are more clearly visible, i.e. the draw-in of the lateral walls of the square cup on the usage of a counter die, as well as part fracture on blocking of the material flow. These results confirm the fact that Reshaping utilizing conventional stamping, stretching based, processes is rather difficult as compared to Reshaping carried out by SPIF. Further analysis was also carried out in the inwards direction so as to get a final confirmation on the ascertained idea.

Similarly, in the case of Reshaping in the inwards directions, the same defect occurs and is just relatively more evident as in the case of Figure 20 (b) the depressions on the base of the square cup as well as the part fracture as seen in Figure 20 (c). These occurring defects hinder the possibility of allocating a new function to a Reshaped component due to poor final product quality. Thus, negating the feasibility of using a conventional

forming technique for a successful Reshaping of an EoL component. The attempts aimed at improving the part quality are limited to the usage of a counter stamp as the use of an additional binder absolutely limits material flow on the base of the square cup leading to its eventual fracture.

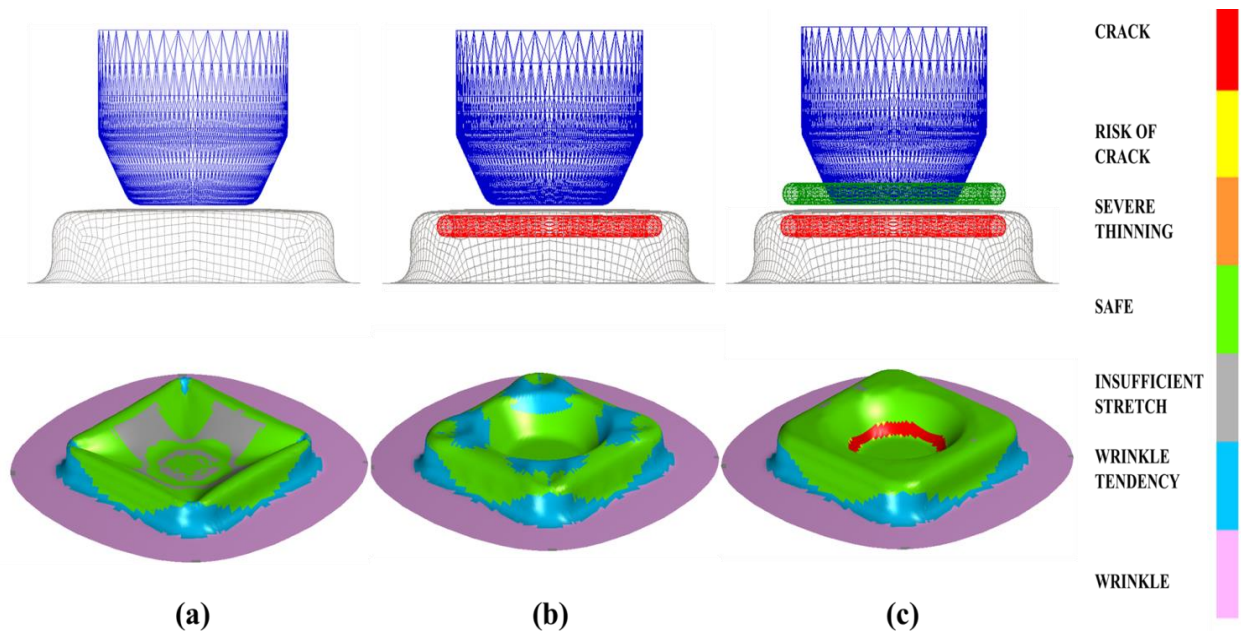


Fig. 20. Numerical simulation setup and the resulting forming limit map at 60° cone angle in inwards direction; (A) without counter die, (B) with counter die, (C) with blocked material flow.

2.4 Discussions

In this section SPIF was challenged as a process to Reshape sheet metal End-of-Life components. A process chain made of DD process followed by SPIF was experimentally performed at lab scale to simulate the entire metal reuse route. Different shapes and forming directions have been tested. Results revealed that SPIF is a proper candidate to success. Thickness and strain measurements showed two main advantages:

- The SPIF local action allows selectively reworking safe areas of the EoL components;
- The improved formability allows to superimpose further deformation even in already formed zones (such as the bottom corner of DD component).

After obtaining the above results, conventional sheet forming processes were studied in order to perform sheet metal EoL component Reshaping in comparison to SPIF process. A research scheme made of forming and re-forming of an aluminum alloy component was numerically simulated to replicate a sheet metal reuse strategy. Shapes with two geometrical variations and working directions had been simulated and analyzed by utilizing three different strategies for each of the two geometrical variations. The results showed an infeasibility of the selected approaches as opposed to the results obtained by the use of SPIF process to achieve the same. The Forming limit maps indicated that the desired result was in fact obtainable through the use of a single counter tool but, unfortunately, with an occurrence of a defect. As a matter of fact, plastic instability phenomenon were observed on the non-worked portions of the EoL component. The other attempted strategies failed either because they don't provide the desired final geometry or because of fracture occurrence due to excessive stretching mechanics activation.

In conclusion, the first research effort started to lay the groundwork for a successful SPIF based Reshaping approach development while, the second research highlighted the fact

that Reshaping, while can be performed using conventional forming processes but with the resulting parts of a compensated quality. Even though the results of this research show that SPIF is an advantageous method for Reshaping, it still presents some challenges like limited accuracy and long process time which still limits its implementation at an industrial scale.

Further analysis will concern the study of the formability performance of SPIF used as a Reshaping process, with particular focus on the necessity of providing process windows, showing to what extent this approach will allow a change in shape. To this aim, this approach will be tested with varying the manufacturing process to get the End of Life Part.

3 Formability And Geometrical Accuracy Performances

After having presented the technical feasibility of the SPIF process as a Reshaper for the metal reuse, the research progressed towards the exploration of the study of the geometrical accuracy of the Reshaping strategy as well as the changes in the part formability when subjected to different types of pre-straining.

Currently some researches on the accuracy of parts formed by SPIF have been focused on various different aspects, in general, researches on the effects of varying end effectors and controlling the forming forces by altering end-effector designs are limited in number [89] and may provide a better understanding of the achieved surface finish and dimensional accuracy of formed parts. Jeswiet et al. [90] in a study reported that, while most industrial parts required an accuracy of ± 0.5 mm, parts formed by SPIF had a significantly noticeable geometrical inaccuracies. Ham and Jeswiet [91] utilized The Box-Behnken design analysis, which allows for the determination of how material type, material thickness, formed shape, tool size, and incremental step size affect the dimensional accuracy. In two other research articles [92, 93], the authors found the dimensional inaccuracies in a two-slope pyramid formed by SPIF could be attributed to elastic strains caused by structural elastic bending in addition to the local spring-back. Subsequently, the research work in this field has expanded to take into consideration an

improvement in the failure and accuracy analysis [94] , as well as the improved dimensional accuracy in parts [95, 96, 97],

Essa and Hartley [98] proposed different strategies to improve the part accuracy in incremental forming such as, the use of a flexible support, counter pressure, multipoint and back-drawing incremental forming etc.

3.1 Geometrical Accuracy of EoL Component

3.1.1 The Adapted Approach

In order to cover a larger portion of production scenarios, two different SPIF approaches were implemented. That is, SPIF process was carried out on the base of the square cup imparting an additional truncated pyramid shape from both inwards as well as outwards directions with the geometrical attributes as illustrated in Figure 21.

In order to analyze the effect of geometrical parameters on the accuracy of the Reshaped component some of them had been varied, in particular, the height of the deep drawn part (H), the SPIF angle (α), and the SPIF base (B). Two levels for each parameter had been selected, and a full factorial design was performed for each SPIF direction; thus, a total of 16 configurations were analyzed, as reported in Table 1. Considering the selected levels for each parameter, the higher numerical value were selected very close to the part property limits, which in this case study was 60°, whereas the lower value was selected as 45°, significant for the scope of the paper.

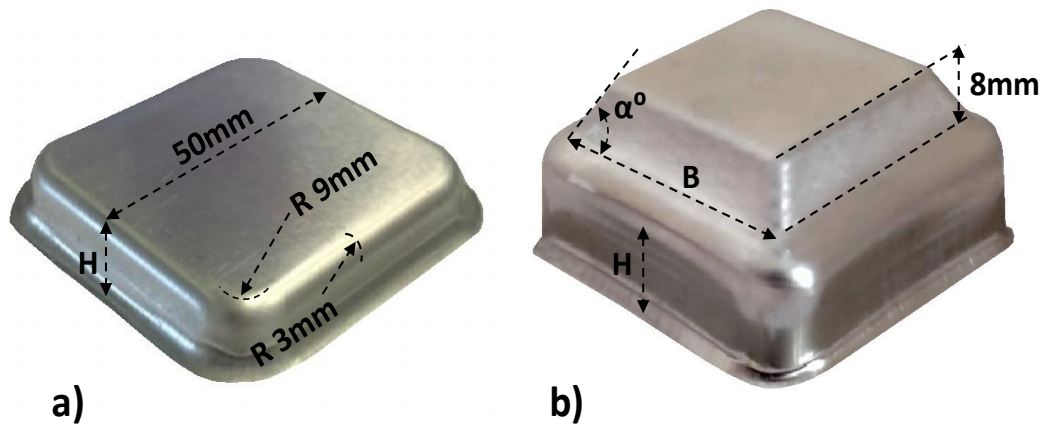


Fig. 21. Geometrical Parameters: a) End-of-Life component; b) New/Reshaped component.

Similarly, for the SPIF base the values were selected as close as possible to the square cup corners as well as decently far from the corners. As far as Deep drawing height (H) is concerned, the higher value was selected as a limit, in fact a value much higher than that selected caused fracture because of the process limit (too high local deep drawing ratio). Each process configuration was performed thrice for result consistency, since the difference in the obtained results was smaller than two order of magnitude with respect to the average value, only the average value has been reported in this study.

Although the SPIF process causes severe thinning in the cone walls [99], sound samples were obtained for all the experiments. In Figure 22 the Reshaped samples of four different parameters combinations are reported.

Table.1 Geometrical parameter notations and combinations for each experiment.

Case Study	Experiment Id.	Deep Drawing Height (H, mm)	SPIF Pyramid Base (B, mm)	SPIF Pyramid angle (α°)
SPIF in Outwards Direction.	1	8	34	45°
	2	8	34	60°
	3	8	41	45°
	4	8	41	60°
	5	16	34	45°
	6	16	34	60°
	7	16	41	45°
	8	16	41	60°
SPIF in Inwards Direction.	9	8	34	45°
	10	8	34	60°
	11	8	41	45°
	12	8	41	60°
	13	16	34	45°
	14	16	34	60°
	15	16	41	45°
	16	16	41	60°

The aim of the research was to evaluate the geometrical deviation caused by SPIF process, in this respect the shape of the Reshaped component had to be compared with

that of the EoL part. In order to do so, the outer surface of the component was acquired both after Deep Drawing and after SPIF, utilizing a photo acquisition system, ‘Steinbichler COMET’ Laser Scanner.

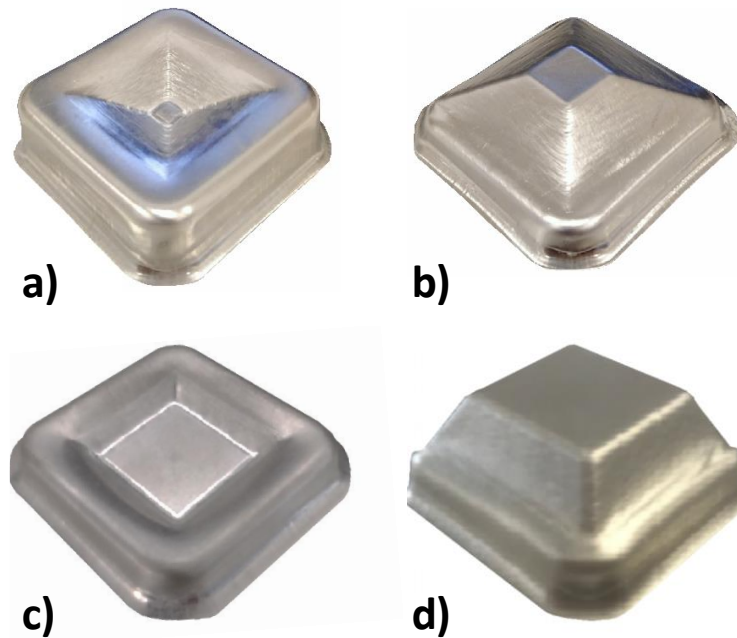


Fig. 22. Obtained parts with experiment ID: a) 13; b) 3; c) 2; d) 16.

The acquired geometries were then analyzed through GeoMagic Control X software, which through the function of auto alignment between EoL and Reshaped part geometries, yielded the Maximum deviation and the Root Mean Squared error between the non-worked zones, i.e. the lateral walls of the square cup. The overall workflow of this research work is presented in Figure 23. The observations and results are detailed in following sub-sections.

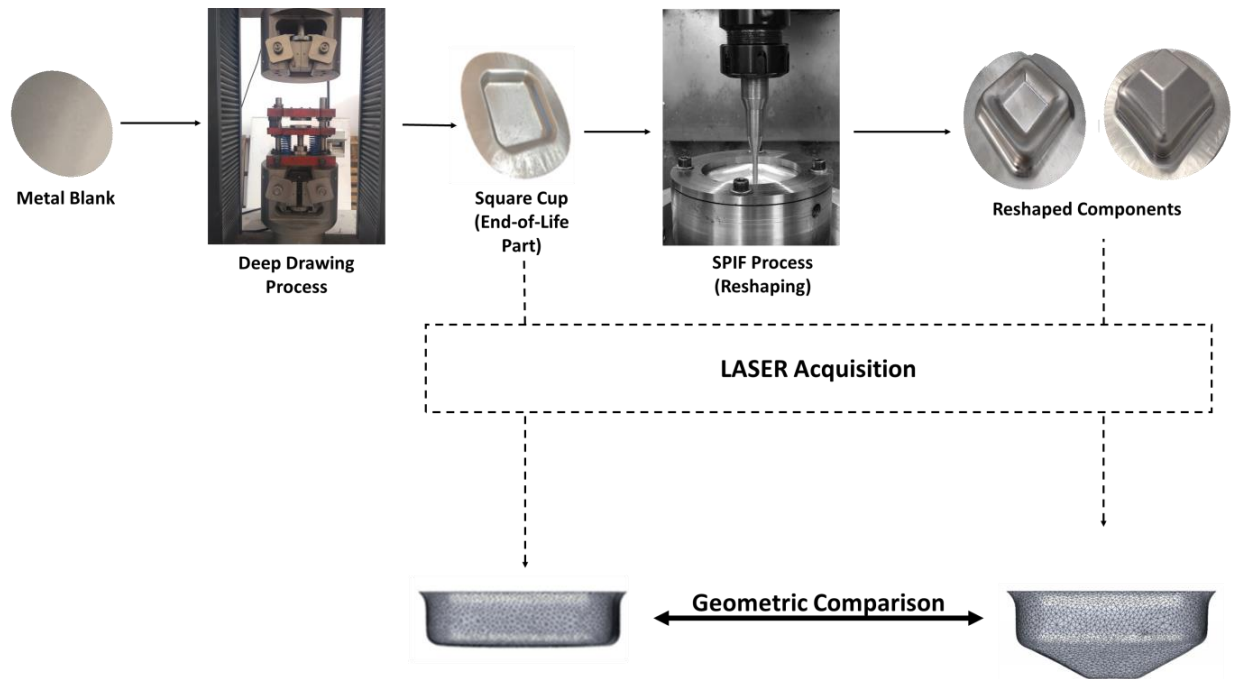


Fig. 23. Experimental workflow

3.1.2 Results Analysis

SPIF Operation in Outward Direction. The first case study involved the addition of a truncated pyramid by SPIF at the center of the base of the deep drawn parts in the outwards direction. All the results have been reported in Table 2, where the Maximum Deviation and the Root Mean Squared error have been indicated.

As seen from the results, the maximum deviation was observed in experiment ID 7, the analysis result of which is illustrated in Figure 24. In this figure the 2D profiles of a selected cutting plane are compared. As it can be seen, the forming load required by the SPIF operation draw in the lateral walls inwards.

Table.2 Maximum Deviations and RMS values recorded and from analysis in Outwards Direction.

Experiment Id.	Deep Drawing Height (H, mm)	SPIF Pyramid Base (B, mm)	SPIF Pyramid angle (α°)	Maximum Deviation (mm)	Root Mean Squared (RMS) value
1	8	34	45°	0.178	0.071
2	8	34	60°	0.308	0.129
3	8	41	45°	0.322	0.132
4	8	41	60°	0.116	0.061
5	16	34	45°	0.333	0.139
6	16	34	60°	0.319	0.131
7	16	41	45°	0.681	0.255
8	16	41	60°	0.541	0.197

To explore the influence of different parameter influences a Pareto analysis was conducted. A Pareto analysis is a statistical technique used in order to understand the relationship between parameters and effects indicating the most influential parameter producing the most significant overall effect. This analysis helps in root cause investigations by assisting the identification of the principal influencers of the obtained results [100]. The chart indicates a reference line to highlight the statistically significant parameters. To further understand the results a main effects plot was generated as well, in order to get an idea of the relation between the response and the selected parameters. The

analysis was performed utilizing MINITAB software, a statistical analysis tool. The Pareto Chart and the consequently derived main effect plots are presented in Figure 25. In this study a significance level of $\alpha = 0.1$, had been used as opposed to 0.05, as with a value of 0.05 no correlation had been found, and since 0.1 is used at early screening stage [100].

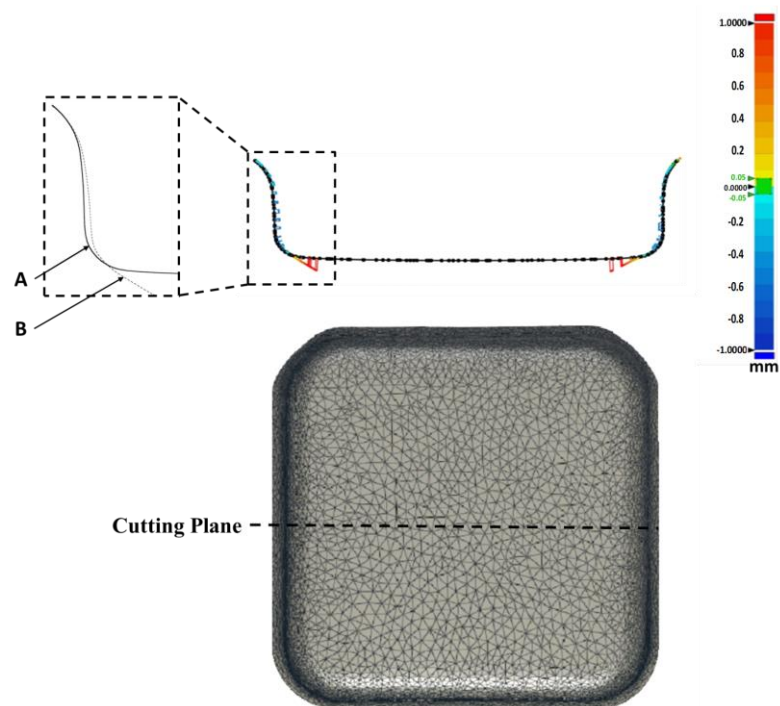


Fig. 24. Geometrical deviation for Pyramid in Outwards Direction (ID 7), (A) Deep Drawn Part; (B) Reshaped Part.

It can be noted that on carrying out the analysis taking into account all the parameters, none seems to have a significant influence on the results, with deep drawing height being a major but not sufficiently significant parameter of the three. Although a certain amount of geometrical deviation was observed, it is still limited.

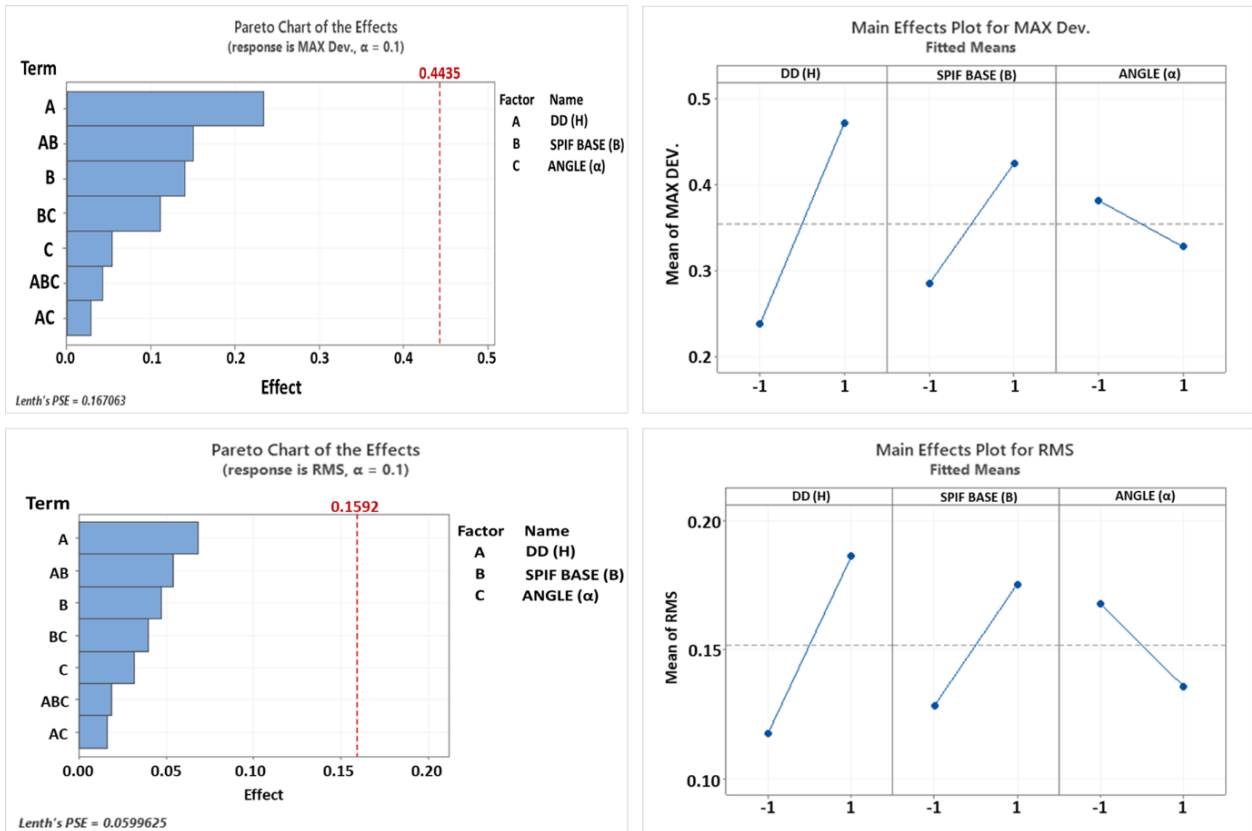


Fig. 25. Pareto chart and Main Effects plots for Pyramid in Outwards Direction.

SPIF Operation in Inward Direction. In order to further study, the effects of SPIF process on the part geometry, SPIF operations performed in the inward direction were also performed on the bottom of the DD part, and the same number of experiments were carried out as well.

Overall, the geometrical deviation is characterized by a different behavior. Actually, as reported in Figure 26 (b), a shortening of the lateral walls whilst experiencing an outward push, as opposed to the draw in as seen in the first case study. The obtained deviations and the geometric analysis are presented in the Table 3. It is possible to see that for ID 15

and 16 quite high geometrical deviations were observed, in fact the highest values of the entire experimental campaign. These values are characterized by maximum values of SPIF Pyramid base (B) and Deep Drawing Height (H). To be More specific, in this case scenario, the maximum geometrical deviation was seen in the case of the Experiment ID 15 where the parameters selected were 16mm deep drawing height and a pyramid of base 41 mm at an angle of 30°. Contrary to the results obtained in the first case scenario the maximum deviation occurs in the most extreme case scenario, indicating an influence of the SPIF base directly at the occurring maximum deviation. The results from the Pareto analysis of the above data are shown in Figure 27. From the graphs, it can be deduced that, two parameters, Deep Drawing height and the SPIF base, have a significant influence on the result with the SPIF base being a more relevant candidate. This can also be noted from the main effects plot which indicates that the occurring geometrical deviations increase with increasing both selected SPIF base and Deep Drawing Height values.

To visualize the effect of SPIF pyramid base on geometric deviation due to Reshaping, in Figure 26, a comparison of geometric deviation of part ID-14 and ID-16 is reported. These IDs differ only in the pyramid base parameter. Actually in the part with higher B value a higher deviation occurs and this is due to a slight buckling effect occurring in the inward case scenario under specific conditions.

Table.3 Maximum Deviations and RMS values recorded and from analysis in Inwards Direction.

Experiment Id.	DD Height (H, mm)	SPIF Pyramid Base (B, mm)	SPIF Pyramid angle (α°)	Maximum Deviation (mm)	Root Mean Squared value
9	8	34	30°	0.182	0.074
10	8	34	60°	0.272	0.109
11	8	41	30°	0.366	0.140
12	8	41	60°	0.652	0.251
13	16	34	30°	0.190	0.076
14	16	34	60°	0.343	0.128
15	16	41	30°	1.270	0.503
16	16	41	60°	1.188	0.504

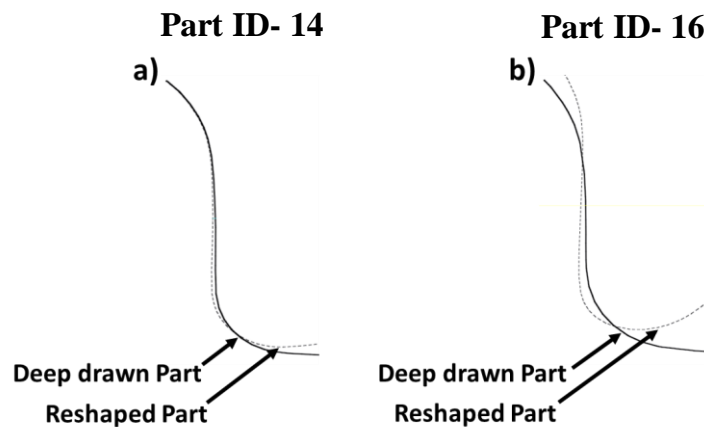


Fig. 26. Geometrical deviation for Pyramid in Inwards Direction for (a) Part-ID 14; (b) and for Part-ID 16.

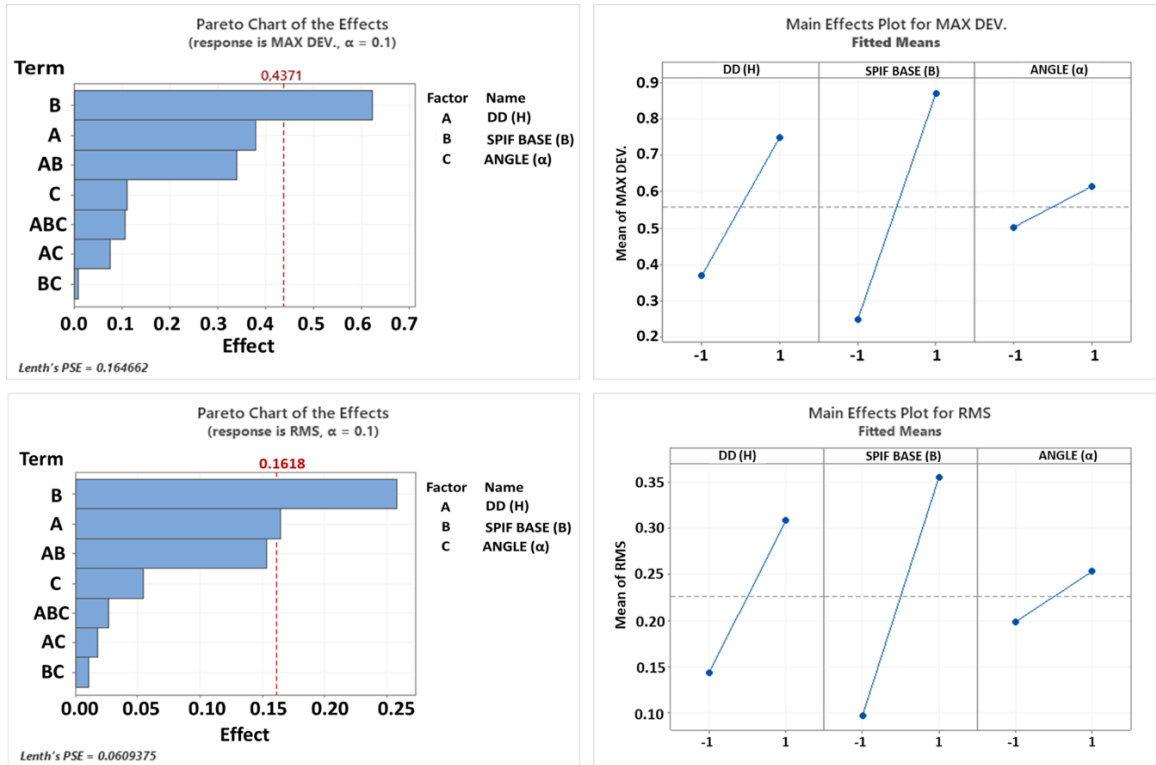


Fig. 27. Pareto chart and Main Effects plots for Pyramid in Outwards Direction.

To provide information on the buckling mechanism, it is necessary to analyze the force occurring during SPIF. Specifically, as reaction to deformation superimposed, tridimensional force is applied on the tool during SPIF. The force trends as well as its analytical formulation has been widely analyzed by researchers [68, 101]. Basically, forces trend along three main directions were analyzed in the past and it was observed that during the forming, spire based tool paths yields a stable trend for F_z and two sinusoidal signals for F_x and F_y [68]. The extent of the F_z component is significantly higher than F_x and F_y ones. The force changes with varying material properties and process parameters setting (wall angle, tool diameter, step down) [68,101]. In order to better understand the higher buckling effect when B increases, a linear buckling analysis

was developed on a simplified model to provide clarity concerning the mechanics perspective. To be more specific, a Finite Element (FE) model developed using the Structural Analysis Program (SAP2000) was set up, considering 1088 rectangular mesh elements. The simplified deep drawn part was modelled using shell elements, a sample vertical force equal to 1 kN was applied and three different analysis, varying the point force location, were launched. The details and the results of the developed analysis are reported in Figure 28. It is apparent that the closer the point force location is to the vertical walls the higher the buckling effect. Such an effect is shown by analyzing both the stress status and the resulting geometrical deviation (Figure 28 c). For the Reshaping case study analyzed in the present study, the results are consistent with the latter presented analysis. In fact, the larger the Pyramid base (the closer the application point of the SPIF force to the vertical walls) the higher the bucking risk/effect as proved by the Pareto analysis previously discussed.

In this research the geometrical deviation as a consequence of SPIF operations were studied on the non-worked zones of the EoL component. For this aim, two different SPIF directions (named inwards and outwards) were analyzed; the effect of some geometrical parameters was taken into account. The research, by a wide experimental campaign, revealed two different geometrical deviations as the direction of SPIF changes. In the Outward case, limited deviation occurred and basically a draw in of the lateral walls of the EoL part occurred. For this case study, the statistical analysis did not reveal any

significant correlation between the variation of geometrical parameters and the geometrical distortion indicators (Maximum deviation and RMS).

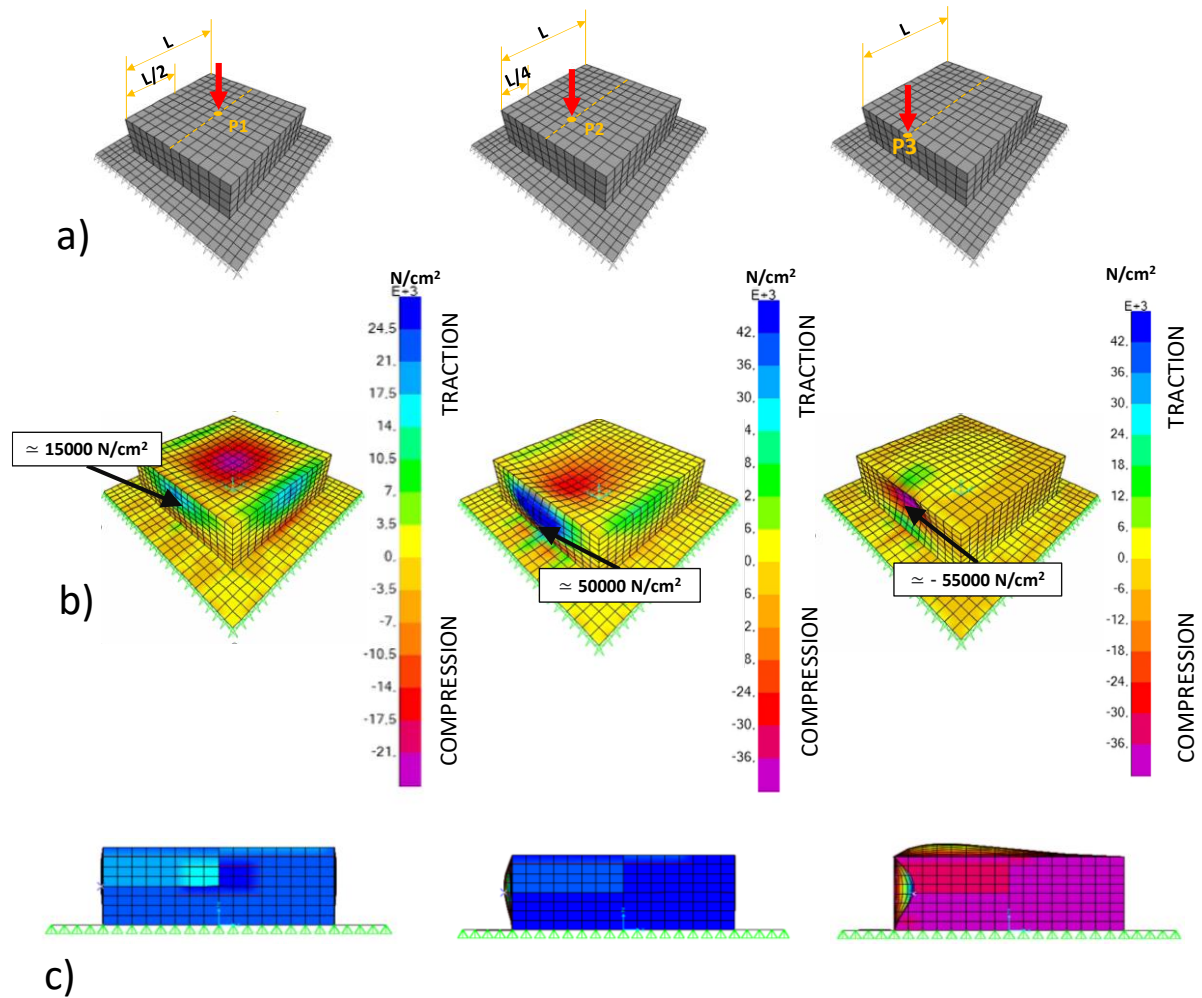


Fig. 28. Buckling linear analysis: a) three different point force locations; b) shell stress status; c) simulated geometrical deviation.

With regard the Inward case study, a different phenomenon was observed. In fact, SPIF Reshaping causes a shortening of the lateral walls as well as an outward displacement, actually a limited buckling phenomenon was observed. For the inward approach higher geometric deviation occurred, and Pareto chart analysis and main effect plot revealed a

correlation between geometrical deviation and SPIF base as well as deep drawing height. Actually, the SPIF base showed a higher influence as it affects both the Maximum deviation and the RMS. The deep drawing height slightly affects only the RMS performance. In the present research, it was assumed that no specific natural precipitation hardening phenomena have occurred during the part life. Moreover, it was assumed that no creep phenomena were induced in the material. Such assumption is quite plausible for the considered aluminum alloy as well as for the potential applications of the obtained Reshaped component. In order to explore the capability of SPIF to actually change the shape, this approach needs an analysis with varying the kind and extent of the first deformation step. Along with deep drawing mechanics, stretching, bending and more complex strain histories have to be used as processes to get the EoL component. For each case the performance of SPIF has to be analyzed both in terms of formability and accuracy. Even though the SPIF process comprises of forming loads of low magnitudes [102, 103], geometrical distortions actions during the Reshaping of EoL parts still do tend to occur [104, 105, 106]. The results of this research call for a need to explore the formability fluctuations with respect to changing primary process endured by the EoL component and the geometrical accuracy of the geometry formed by SPIF process onto the EoL part.

3.2 Formability Variation And Geometrical Accuracy of SPIF Process

3.2.1 The Adapted Approach

The authors formulated the present research in order to better understand the influence of different pre-straining levels on the formability as well as on the geometrical accuracy of SPIF as used as Reshaping process. So far the change in the formability of the SPIF, when used as a Reshaping tool, hasn't been studied in depth. Lora et.al. [107] in a research, explored the change in SPIF formability when used as a hybrid process, i.e. is being coupled along with stretch forming, i.e. SPIF was performed on the part, right after it's stretch forming while it was still held clamped on the stretch forming system. In their study the authors concluded that the pre-straining directly influenced the occurring deformations in the formed parts, i.e., higher deformations resulted in a high amount of residual hardening of the parts. The proposed study focuses on understanding the limits up to which SPIF as a Reshaping strategy of EoL components may be used, in light of the effects of pre-straining on the new part geometry.

In order to realize the research objectives, the authors turned a virgin blank into an EoL component by imparting it deformations. Two different levels of uniaxial pre-straining, and a biaxial pre-straining (deep drawing) were considered as primary processes to resemble an EoL component. For the Reshaping of the components truncated pyramid and cone were formed onto the deformed parts via the SPIF process. The EoL component

obtained after deep drawing was Reshaped by performing SPIF process on base of the component along the direction same as that of deep drawing. A simplified objective of the research approach is illustrated in Figure 29.

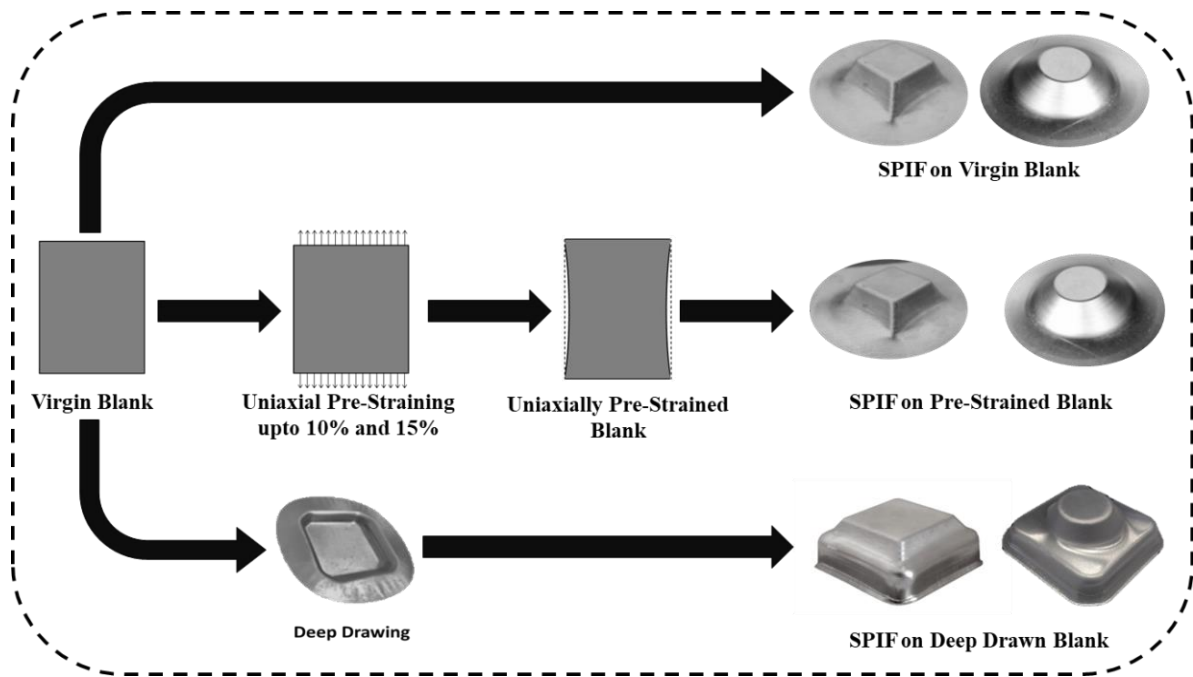


Fig. 29. The proposed processes chains for characterizing Reshaping

In order to proceed with the research objectives, an experimental campaign was designed where the pre-straining step of the experimental campaign was performed on the Galdabini Quasar 500 hydraulic press. The sheets were subjected to two different levels of uniaxial strain, i.e., stretching of the blank up to 10% and 15% of its original length. For the performance of biaxial straining, deep drawing process was performed to obtain a square cup 16mm deep.

The authors chose to take into account the maximum formable angle (α_{max}) via the SPIF process as an indicator of the variation in formability resulting from different types of pre-straining. The campaign was divided into 2 case studies, incremental forming of a truncated cone and pyramid, the dimensions of the deep drawn part and the SPIFed shapes are illustrated in Figure 30 (a, b and c).

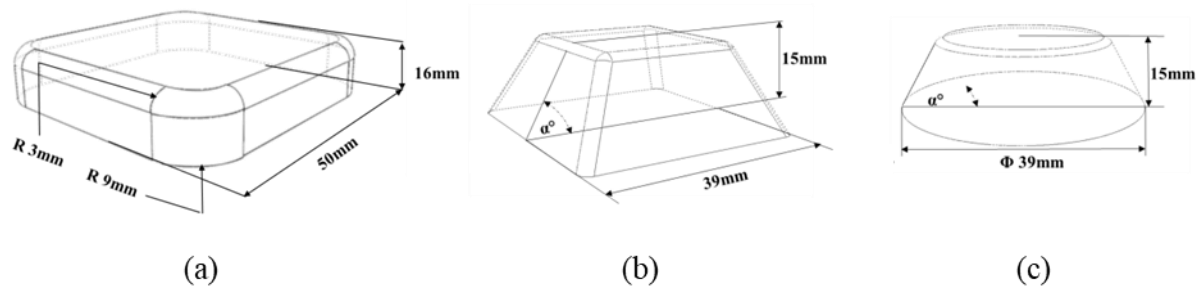


Fig. 30. Part dimensions; (a) Square Cup geometry; (b) Pyramid Geometry; (c) Cone geometry.

3.2.2 Methodology for α_{max} calculation

The primary objective of this research was to investigate the maximum formable angle (α_{max}) through the SPIF process, for the forming of truncated cone and pyramid. Consequently, SPIF was performed onto a virgin blank to form the selected shapes while increasing the forming angle by half a degree every time a non-fractured part was obtained. As soon as, a fractured part was obtained the preceding angle was ascertained as the α_{max} corresponding to the shape being formed. With the aim to have a decent consistency in the findings, the SPIF process at the obtained α_{max} was performed thrice. After the identification of α_{max} for both the case studies,

the research proceeded towards studying the influence of different types of pre-straining on the SPIF formability. The process for α max identification was performed again on the pre-strained blanks. After determining the α max corresponding to each pre-straining condition, the next step of the experimental campaign was the measurement of the occurring deformations in each of the parts when undergoing SPIF at α max + 0.5°. In order to do so, a pattern of circles 1.5mm in diameter, having a depth of 0.05mm, were laser incised on the sheets before they underwent the pre-straining and later SPIF.

For the correct identification of the pre-straining level in the case of DD, the process chain was numerically simulated. The numerical approach was adapted to track back the pre-straining level corresponding to the fractured zone, i.e. upon identifying the fracture zone in the deep drawn part, after its Reshaping, the exact pre-straining levels were also measured experimentally. The model was simulated on the commercial finite element software ABAQUS / CAE Explicit software, and spring-back analysis were carried out with its implicit solver between the pre-straining and forming simulation. In other words, a four steps approach was undertaken, two explicit steps for pre-straining and SPIF, followed by one implicit approach after the explicit simulation. Following the previously adapted methodology of simulating the process chains [29], a full integrated quadrilateral shell element with five integration points along thickness was used, the blank was simulated by assigning the material properties

pertaining to AA5754 alloy and the system default Hill yield surfaces with associated plastic flow was used.

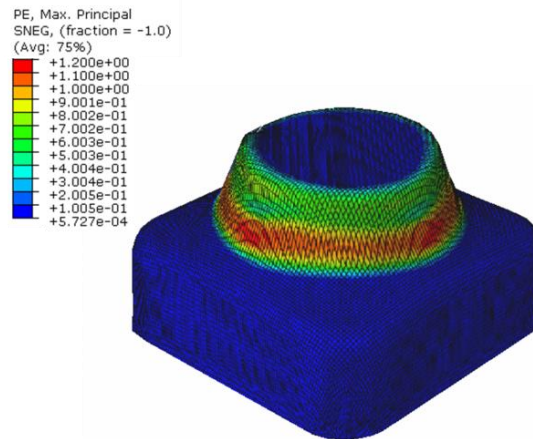


Fig. 31. Numerical model of the Reshaped part after deep drawing.

Once the strain values were obtained from the simulation, the numerical model was validated by verifying the experimentally obtained strain values and thickness distributions. The major and minor strains induced on the base of the deep drawn part (in the zone where the fracture occurs during Reshaping) were 0.00372 and 0.00383 respectively. Once the model validation was performed, the strain values corresponding to those of incrementally forming a deep drawn part were also obtained numerically Figure 31.

3.2.3 Methodology for the geometrical accuracy analysis

In order to study the variation in the geometrical accuracy of parts Reshaped through SPIF, corresponding to different types of pre-straining levels, comparisons of geometries after Reshaping were developed. In particular, the geometries obtained after

the SPIF process were compared to a reference CAD model of a truncated cone and pyramid designed having the same geometrical attributes. In order to analyze if the extent of deformation of SPIF affects the accuracy of the Reshaping process, the two angles selected for the shapes to be formed were: a lower value ($\alpha = 45^\circ$); and higher value ($\alpha = 65^\circ$) for both the truncated cone and the pyramid. In Table 4 the developed Design of Experiment is reported.

In order to have a consistency in the results, three replications of each experiment ID were performed. Throughout the experimental campaign, SPIF was performed following a helical tool path with a 0.3 mm descent applied for each spire. The Maximum Deviation and the Root Mean Squared (RMS) error, generated by the software, were recorded as metric for geometric accuracy quantification. The recorded data were then analyzed through the ANOVA (Analysis of variance) statistical tool. ANOVA is a statistical tool which allows the detection of differences between the means of different experimental group. ANOVA is formulated in experimental designs with a parametric numerical outcome which is a variable dependent on one or multiple experimental groups (independent variables) [100]. The analysis was performed utilizing MINITAB statistical analysis software considering a significance level of $\alpha = 0.05$. Figure 32 shows some of the results obtained corresponding to IDs 6, 3, 8, 13, 10 and 16.

Table 4. Experimental Campaign.

Case Study	Part ID	Angle	Pre-straining Level
CONE	1	45°	Virgin Blank
	2	45°	Uniaxial Pre-strained 10% Blank
	3	45°	Uniaxial Pre-strained 15% Blank
	4	45°	Deep Drawn Blank
	5	65°	Virgin Blank
	6	65°	Uniaxial Pre-strained 10% Blank
	7	65°	Uniaxial Pre-strained 15% Blank
	8	65°	Deep Drawn Blank
PYRAMID	9	45°	Virgin Blank
	10	45°	Uniaxial Pre-strained 10% Blank
	11	45°	Uniaxial Pre-strained 15% Blank
	12	45°	Deep Drawn Blank
	13	65°	Virgin Blank
	14	65°	Uniaxial Pre-strained 10% Blank
	15	65°	Uniaxial Pre-strained 15% Blank
	16	65°	Deep Drawn Blank

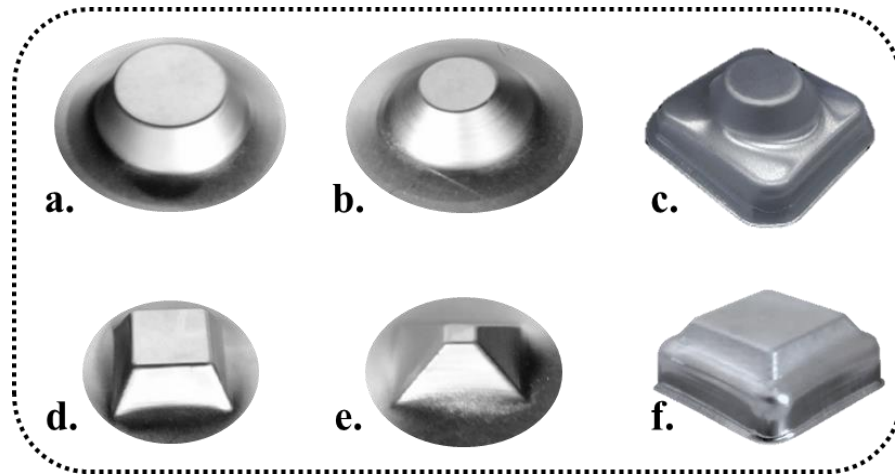


Fig. 32. Obtained parts with the part IDs: a) 6; b) 3; c) 8; d) 13; e) 10; f) 16.

3.2.4 Results

α max determination. The obtained values of α max corresponding to the different levels of pre-straining for both the case studies is reported in Figure 33. As far as the Reshaped samples for the cone case study are concerned, the maximum obtainable value was 68° for the virgin blank, with a decrease of 1° moving from the virgin blank conditions up to the uniaxial pre-straining of 15% and deep drawing. Whereas, in the pyramid case study the same trend was seen, with an α max of 67.5° for the virgin blank. The results show that, even though the SPIF formability decreases for EoL parts, the difference is minimal and the Reshaping through SPIF could still be performed successfully.

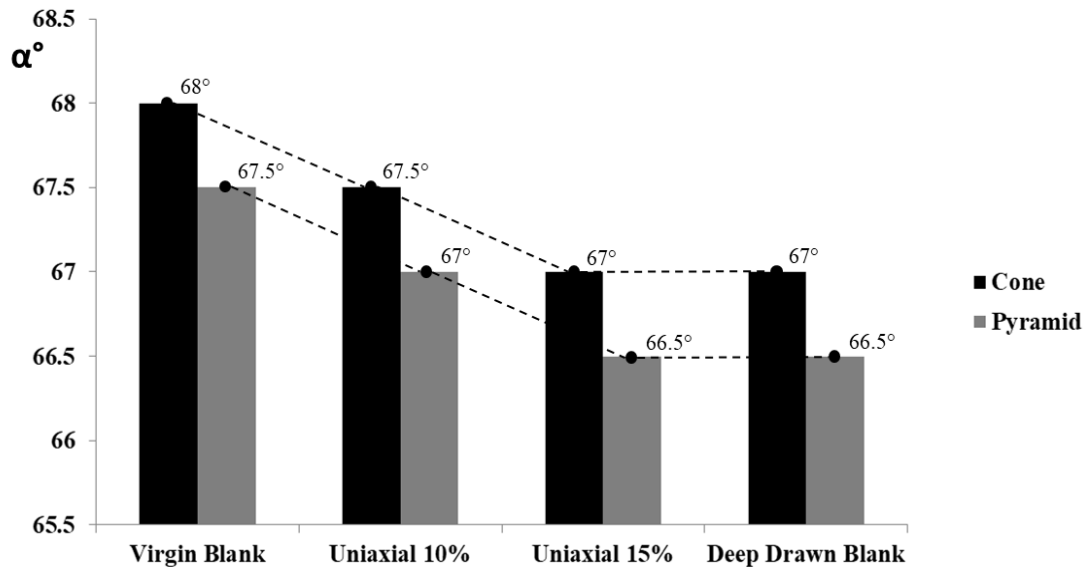


Fig. 33. Obtained α_{max} for different pre-straining levels for both the Cone and Pyramid case studies.

Furthermore, Figure 34 illustrates the right quadrant of the Fracture Forming Limit (FFL) for the two selected case studies under different pre-straining levels has been reported. Actually, the reported diagram is an adapted FFL as the strains were measured by performing the SPIF in all the case studies at their respective $\alpha_{max} + 0.5^\circ$. This approach does not allow to spot any fracture angle occurring between α_{max} and $\alpha_{max} + 0.5^\circ$, nevertheless for the purpose of this research, in the authors' opinion, such approximation does not affect the conclusions carried out in this section. Actually, such adapted FFL was performed so as to better understand the relation between formability limits in terms of part fracture, as failure by fracture in SPIF occurs without necking [108, 109, 110]. FFL allows a better visualization of the possible reduction in formability of SPIF because of the pre-straining characterizing the starting blank. Strain values measured on the edge

of the SPIFed truncated cones and pyramids are presented, strains were measured as close as possible to the identified fracture area. SPIF process applied on a flat sheet with 15% of uniaxial pre-straining and on the deep drawn part leads to the strain values being the same. As expected, the cone case study led to fracture strains conditions close to that of plane strain; in the pyramid case studies a certain amount of minor strain was observed, instead. Overall, it is possible to notice that in all the case studies pre-straining caused a very limited shifting downwards of the FFL. These results confirm the fact that, a good amount of available formability is still present in the parts after their pre-straining.

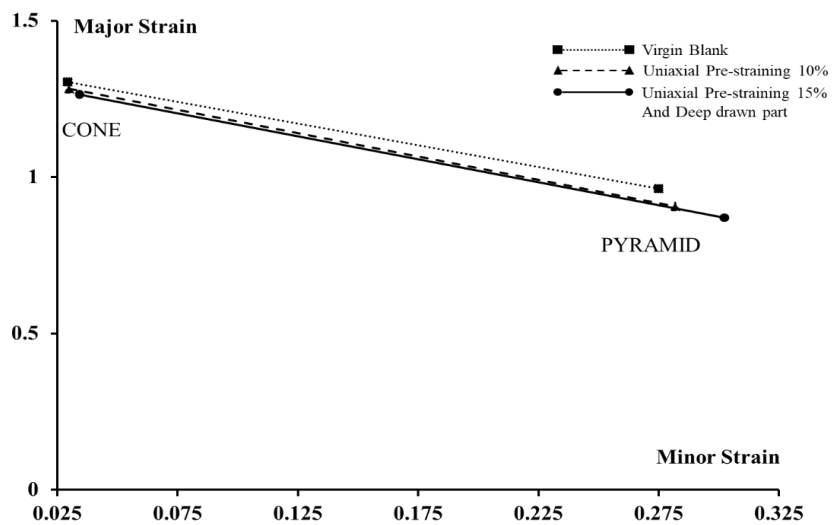


Fig. 34. Fracture Forming Limits for Virgin and Pre-Strained Blanks for Cone and Pyramid case studies at $\alpha_{max} + 0.5^\circ$.

Geometric Accuracy Analysis. All the photo acquired parts were compared to a CAD model corresponding to an ideal part with the same geometry. Some of the results from the geometric analysis are shown in Figure 35. The geometric deviation on the lateral sides of the SPIFed shapes has been illustrated for better clarity.

From the analysis, the maximum deviation and the RMS error values were obtained in correspondence to each part's geometrical accuracy. The values have been reported through an Average-Max-Min chart summarizing the results in the Figures 36 and 37 corresponding to the two case studies respectively. Since three tests were performed for each sample, the scattering indicated the maximum, minimum (indicated with small dots) and the average values (indicated with a big dot), as recorded from the geometric analysis.

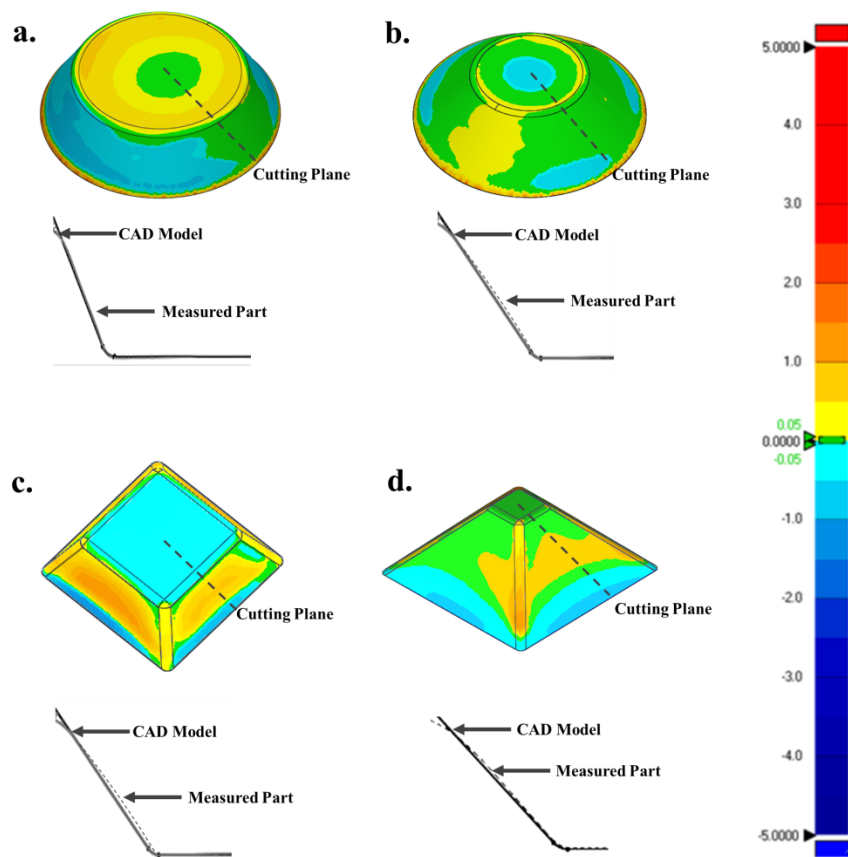


Fig. 35. Geometric Deviation (mm) of scanned parts with respect to CAD geometry corresponding to part IDs: a) 5; b) 3; c) 13; d) 11.

It can be seen that, in the cone case study, figure 36, no clear trend is visible from the obtained data. The geometrical accuracy seemed to worsen with the pre-straining of the parts but no exact correlation can be drawn from the graphs concerning the effect on the level of pre-straining on the accuracy obtained. However, in the pyramid case study, figure 37, even an improvement in the SPIF accuracy can be seen with the increase in the pre-straining degrees.

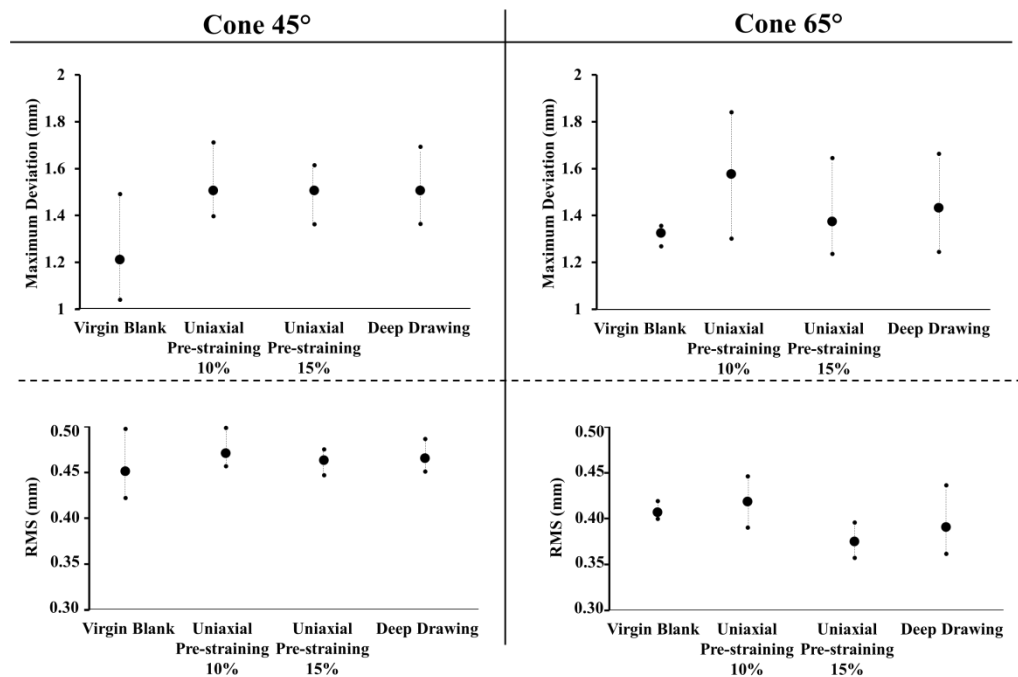


Fig. 36. Average-Max-Min chart for geometrical analysis of the Cone case study.

With the aim of better understanding the data presented in the graphs and eventually, derive meaningful interpretations, the ANOVA statistical tool was utilized to clearly identify the influence, if any, of the varying parameters on the geometrical accuracy of SPIF.

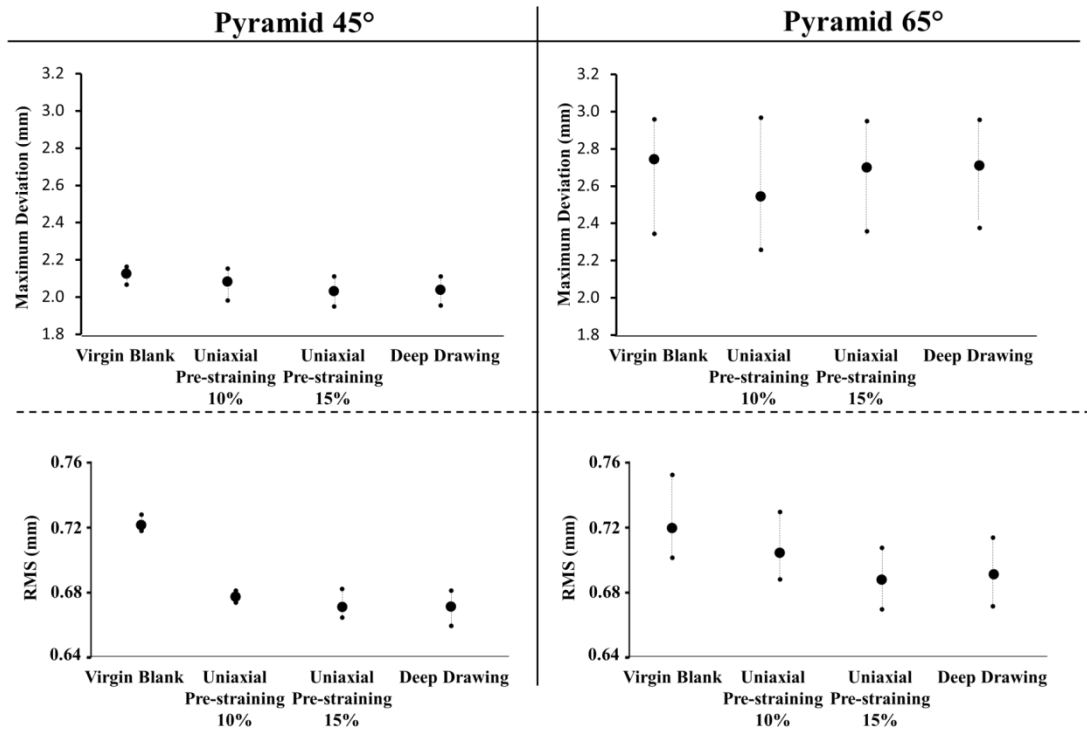


Fig. 37. Average-Max-Min chart for geometrical analysis of the Pyramid case study.

ANOVA analysis.

Cone Case Study: Figure 38 illustrates the ANOVA analysis results performed on the maximum deviation and the RMS values obtained from the geometric accuracy analysis. The analysis of the maximum deviation values deemed that none of the two factors, pre-straining levels or angles, resulted as significant ones. Since the obtained p value from the ANOVA analysis was a lot higher than the significance level used during the analysis ($p > 0.05$). On the other hand, the impact of the governing factors on the obtained RMS values of the geometric analysis showed that the selected angle had a significant influence on the RMS values obtained, a P-value of 0.004 paired with the obtained F-

value ($F > 3.35$) provides ground for rejecting the null hypothesis. It is worth noting that, for this case study, the effect of varying the pre-straining levels in either of the two analyzed data was statistically insignificant.

Maximum Deviation						RMS					
Analysis of Variance for Transformed Response						Analysis of Variance for Transformed Response					
Source	DF	Adj SS	Adj MS	F-Value	P-Value	Source	DF	Adj SS	Adj MS	F-Value	P-Value
Angle	1	0.000027	0.000027	0.03	0.875	Angle	1	0.004568	0.004568	62.58	0.004
PS	3	0.020690	0.006897	7.41	0.067	PS	3	0.000822	0.000274	3.75	0.153
Error	3	0.002792	0.000931			Error	3	0.000219	0.000073		
Total	7	0.023510				Total	7	0.005610			

Fig. 38. ANOVA analysis results for the Maximum Deviation and RMS values for Cone Case Study.

Pyramid Case Study: The results from analyzing the data corresponding to the geometrical accuracy of the truncated pyramid shape via SPIF, are presented in Figure 39. From the results it could be concluded that, in case of maximum deviation just the angle resulted as a significant factor influencing the obtained data ($P < 0.05$). Whereas, in the case of RMS data analysis both the factors were relatively significant with the angle having a higher influence on the result, as the corresponding F value was much higher compared to that of pre-straining.

Maximum Deviation						RMS					
Analysis of Variance for Transformed Response						Analysis of Variance for Transformed Response					
Source	DF	Adj SS	Adj MS	F-Value	P-Value	Source	DF	Adj SS	Adj MS	F-Value	P-Value
Angle	1	0.140566	0.140566	4690.13	0.000	Angle	1	0.005131	0.005131	162.40	0.001
PS	3	0.000192	0.000064	2.13	0.275	PS	3	0.001302	0.000434	13.74	0.029
Error	3	0.000090	0.000030			Error	3	0.000095	0.000032		
Total	7	0.140848				Total	7	0.006528			

Fig. 39. ANOVA analysis results for the Maximum Deviation and RMS values for Pyramid Case Study.

These results showed that the pre-straining of parts did not have a significant role in affecting the geometrical accuracy of the SPIF process. This deduction points towards the fact the SPIF indeed can be used for the Reshaping of components as the eventual accuracy of parts geometries is highly influenced by the process parameters rather than the pre-straining level the parts underwent prior to their Reshaping.

This research was aimed at understanding and exploring the use of SPIF process as metal Reuse enabler via the Reshaping approach. The changes in a part's formability and the variation in the achievable shape accuracy through SPIF used as Reshaping process had been analyzed. To achieve this aim, process chains consisting of different types and levels of pre-straining followed by their Reshaping through SPIF were projected, and the resulting α max and final shape accuracy have been determined. Results showed that SPIF though had a reduced formability with the increase in the pre-straining levels, performed decently well for both the analyzed aspects. As a matter of fact, even with a decrease in the formability of SPIF was seen, the difference was minimal and the Reshaping through SPIF could still be performed successfully on the analyzed EoL parts. With regards to the part's geometric accuracy, the ANOVA analysis of the obtained deviation values yielded the conclusion that the pre-straining of the parts, before their Reshaping, did not significantly influence the accuracy performance of SPIF. Rather in some cases increased pre-straining level actually yielded a part with better accuracy in comparison to SPIF performed on a virgin blank.

3.3 Discussions

In these researches the geometrical accuracies of EoL parts as well as the formability changes with respect to EoL part's original straining, has been studied. Results showed that SPIF affected the geometrical accuracy of the non-worked zones of the EoL component, depending on the Reshaping parameters adapted. Besides it was also observed that, though SPIF had a reduced formability with the increase in the pre-straining levels, it performed decently well for all the analyzed aspects

Overall, performances of the SPIF process as a Reshaper are promising, although this research field deserves to be further explored. It is worth mentioning that the extent of deformation applicable on an EoL component depends both on the formability performance of the selected processes for Reshaping (in the present case SPIF) as well as on the conditions (thickness distributions) of the recovered component. Besides thickness distribution, the overall material condition/properties of the EoL Material should be also assessed prior to Reshaping. Change in mechanical properties or creep occurrence could compromise the Reshaping approach by SPIF. Nevertheless, in an industrial environment the inspection step becomes crucial for a successful Reshaping strategy implementation. Thinning distribution of EoL and material properties/conditions are crucial pieces of information to properly design the Reshaping. This pieces of information will allow correct identification of the zones of EoL component to be Reshaped.

These findings pave the way for future researches which may include further exploration of the considered factors for the Reshaping of metal sheets. Moreover, to fully explore the potential of Reshaping, other flexible sheet metal forming processes should be analyzed. Other candidates could be: Hydroforming (possibly the assisted temperature versions) and Hot Gas Forming. These options deserve to be explored to identify the most suitable process with varying EoL properties. Finally, some innovative fixture to be used during SPIF experiments could be thought of, to prevent distortion in extreme case studies.

From the results obtained on the technical feasibility and the analysis of formability changes along with the geometrical accuracy of the SPIF based Reshaping approach, the research focus moved towards the analysis of the efficiency of the Reshaping strategy in comparison to conventional recycling techniques in terms of their cumulative energy demand as well as the equivalent CO₂ emission. This would help shed further light on the performance of SPIF as a Reshaper when applied on a practical scale and its applicability on a more universal level.

4. ENERGY EFFICIENCY ANALYSIS

Reprocessing EoL components raises new challenges for manufacturing processes scientist. As a matter of fact, returned core are characterized by a high variability of quality condition [111]; such high variability coupled with the increased product variety results in a need of high level of flexibility and re-configurability of de- and remanufacturing processes/systems [27].

As previously discussed in Chapter 1, materials production has been one of the greatest contributor to global anthropogenic CO₂ emissions, different strategies have been put forward to combat this. Allwood et al. [112] outlined the strategies to put in place effective emissions reduction approaches in the field of material production. The strategy consists of four points:

- energy efficiency;
- yield improvements: minimizing loss of material between its liquid form and use in a final product;
- increasing recycling rates;
- decarbonation of the global energy system.

In light of the above strategies, material recycling through conventional techniques has a considerable CO₂ emission due to various process steps such as remelting, hot rolling etc. making a comparative analysis of alternative metal recycling strategies a valuable study.

The making end-of-life scenarios able to recover as much “embodied energy” as possible from product/component is nowadays mandatory. The metric named “Embodied Energy” (which represents all the energy (MJ) committed to produce 1 kg of a given material), could help to give an idea about the obtainable savings.

This research aimed at outlining the environmental impact of the SPIF based Reshaping approach; in this respect a Cumulative Energy Demand (CED) and CO₂-eq comparative analysis is presented. Three different routes were analyzed and compared to one another: SPIF based Reshaping, conventional recycling and SSR routes.

4.1 The comparative CED and CO₂-eq analysis

In this section the comparative analysis about three different EoL strategies for aluminum based sheet metal components is presented. To be more specific, the performance of the proposed SPIF Reshaped approach is compared with those of two different recycling strategies: conventional and SSR based technique. For the latter approach the ECAP extrusion based process was selected as the most analyzed [113]. The aim of such comparison is to quantify the environment performances of a new, here proposed, novel reuse strategy. Also, the study aims at identifying the main factors influencing comparative analysis results. In this section, after describing the system boundary and the main Life Cycle Inventory (LCI) data, the discussion of the obtained results are reported.

4.2 System Boundary and Major Assumptions

The comparison was focused on the reuse strategy applied to one single component obtainment. For each strategy all the process steps to turn the EoL component into the Reshaped one are taken into due account. Concerning the metric for comparison, CED (MJ) and CO₂-eq emissions (Kg) were used. The adopted system boundary with all the steps included in the analysis is reported in Figure 40. Material yields for each proceeds were considered and both permanent losses and conventional process scraps are modeled in this study. It is worth mentioning that as the Reshaped component is a sheet based one thus, a sheet production step is to be considered for all the recycling routes, this step is mandatory to obtain a sheet metal part to be stamped. Overall, it is possible to see how the Reshaping process allows significant process steps reduction and less material is involved.

It is worth mentioning that for the SSR route both extrusion and sheet production (homogenization, hot-rolling, cold-rolling and annealing) process had to be included. In fact, studies showed that extrusion is still necessary for a better consolidation also in case of sheet production from scraps [3, 114]. Two different kinds of material losses have been considered: processes scraps and permanent losses (occurring during melting because of oxidation).

Concerning processes scraps, these are basically home scraps (high quality with a high level of purity), according to the definitions of the EAA [115] , therefore they can be easily recycled. It is, therefore, assumed that such scraps leave the system without any environmental cost.

Concerning the permanent material losses occurring during remelting , these are much more damaging scrap from the environmental impact point of view and the related impact was dealt with by adding the same amount of primary aluminum in the model. As it can be observed extra material was added at different level for compensating the material losses (both permanent and process scraps). In the remelting route extra material was added at melting level while in the SSR route it was assumed that extra material can be added in the compaction step.

4.3 Life Cycle Inventory

The life cycle inventory data was generated utilizing different approaches. Data found in scientific literature databases and technical report were used. Also, experimental measurements and modelling approaches were used to set up a reliable inventory data set. Overall, the EAA environment report as the primary reference as it provides reliable data for aluminum production and processing. Besides this, the CES Edupack [116] database and the comparative analysis provided by Duflou et al. [9] were also used as data source. In Table 5 all the data along the used references for the LCI are reported.

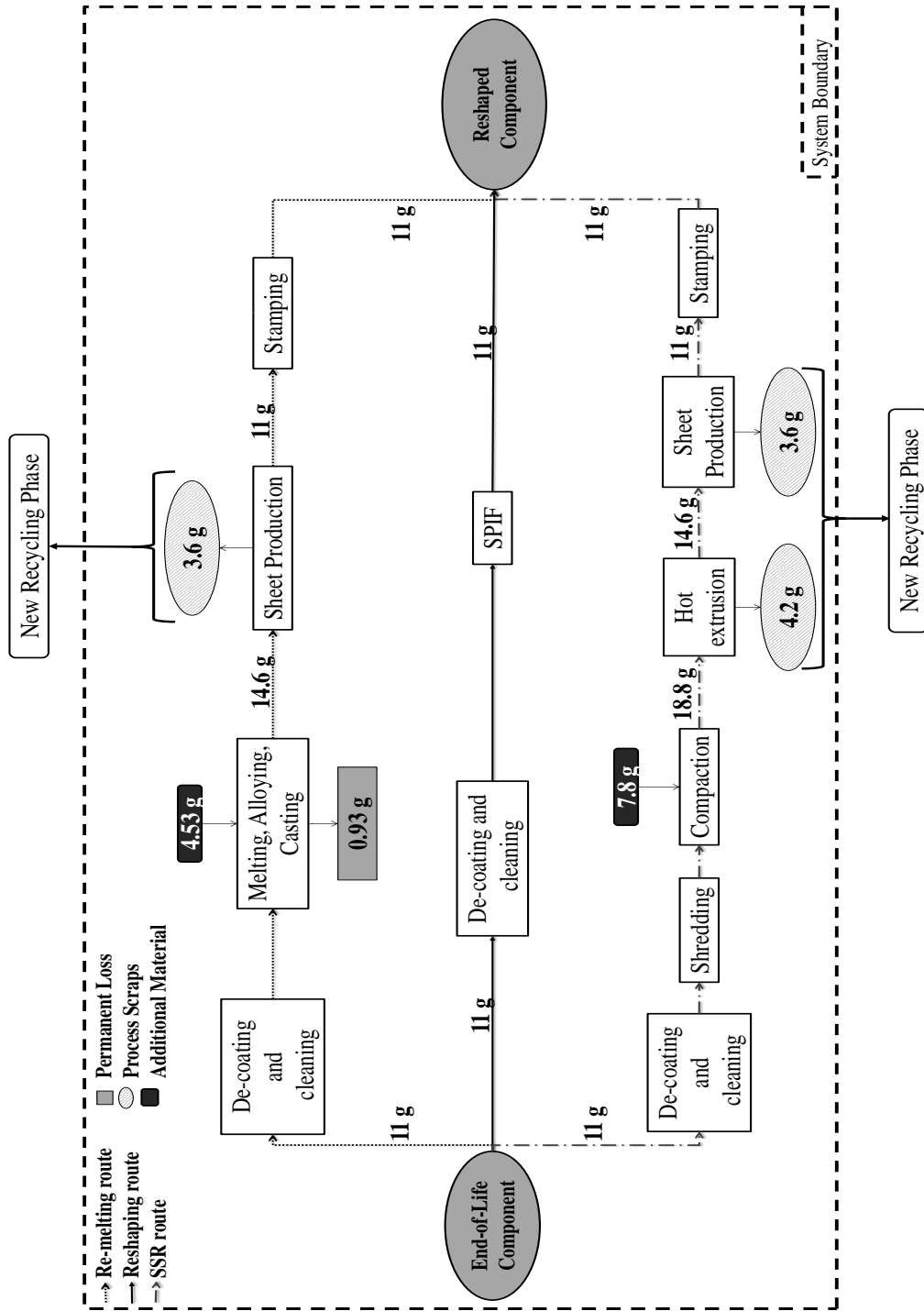


Fig. 40. System boundary with the process steps and the mass flow highlighted.

In the case of SPIF process, a research by Ingarao et al. [117] was referred, which, after comparing the efficiency of three different set-up able to perform SPIF processes, indicated that a robot assisted SPIF was the most efficient, and thus chosen for the intended study. In that study the authors provided a model able to link the Ultimate Tensile Stress (UTS) of a given material being formed to the robot power demand while forming. In this paper that model is used to quantify the electric energy demand of the SPIF based Reshaping approach. Also, in that study [117] the authors proved that forming time is the dominant factor for electric energy demand. Process parameters (feed rate and step down) are to be selected in order to get a forming time as little as possible. A high machine feed-rate coupled with a high step down value was considered as a best case scenario and a low feed-rate as a worst case scenario, these two variants were carried out with an intent to analyze the effects of wrong process parameters selection on the environmental performance of the Reshaping based reuse.

Since the stamping process wasn't carried out on an industrial press, a FEM code was used to simulate the stamping process and predict the punch load as a function of the distance travelled, thus the theoretical (plastic deformation energy plus the work needed to overcome the friction actions) forming work (W) was calculated by quantifying the area under the force - displacement graph. The obtained value on dividing by the press efficiency, assumed as 0.25, resulted in the electrical energy consumption. An idle

machine time of 20s was assumed for each working cycle during which an average power consumption of 5kW was considered (Ingarao et. al. 2016).

One of the main advantage of single point incremental forming is the lack of dedicated tools, such aspect make this process more energy efficient with respect conventional stamping when small batch size are to be manufactured. Such aspect has been discussed by Cooper and Gutowski [118]. In the present study the impact of the tooling for the stamping processes was taken into account. It assumed that the tooling is made of O1 steel according to the ASME guidelines [119], the energy and the CO₂-eq emission related to material production and processing were quantified by using Eco-properties found in CES Edupack [116].

Material impact for tooling is the dominant factor and therefore its modelling deserves particular attention. Specifically it is necessary accounting for the credits arising from recycling. Although there isn't one single criterion to account for recycling benefits, some useful guidelines are provided by Hammond and Jones [120]. Two principal methods exist: (1) the recycling content approach and (2) the substitution method. The first one ascribes the full benefit of material recycling to the start of its life, lowering the material impact by considering the fraction of recycled material in the input material (R). The substitution method, instead, allocates the environmental credit of recycling to the end-of-life stage. In this case only the technological losses (r) of the recycling processes in considered. Normally the r value is higher than R making the substitution method often

an optimistic estimation. Equation (1) and (2) can be used for accounting for material impact with the recycling content and the Substitution method, respectively.

$$E_{\text{Recycling content approach}} = E_V \cdot (1-R) + R \cdot E_R \quad (1)$$

$$E_{\text{Substitution method}} = E_V - r \cdot (E_V - E_R) \quad (2)$$

where:

R=recycled content (fraction of recycled material in the input material);

r=recyclability (fraction of material recycled at the end-of-life);

E_R =embodied primary energy, secondary production;

E_V =embodied primary energy, primary production.

For the present analysis we took R value as 55% [116] and r value as 90% [121].

Table 5. Life cycle inventory data

Process	Primary energy (MJ/kg)	CO₂ eq. emission (kg)	Yield	Reference
De-coating & Cleaning	2.30	0.100	1	Ashby 2009 [122]
AA-5754 Primary production	210	13.3	--	Granta Design Limited 2017 [116]

O1 steel Primary production	41.45	2.76	--	Granta Design Limited 2017 [116]
O1 steel secondary production	10.3	0.81	--	Granta Design Limited 2017 [116]
Shredding	0.60	0.105	1	EAA, environmental report 2018 [115]
Compaction	8.79	0.370	1	Duflou et al. 2015 [9]
Hot Extrusion	16.0	0.680	0.77	EAA, environmental report 2018 [115]
Extra Pressing Energy	2.05	0.090	--	Duflou et al. 2015 [9]
Sheet Production	9.00	0.430	0.75	EAA, environmental report 2018 [115]
Melting & Casting	5.90	0.330	0.88	EAA, environmental report 2018

Stamping (Per Part (PPt))	0.025	0.001	1.00	Calculated
SPIF - Worst Case Scenario (PPt)	0.67	0.028	1.00	Calculated
SPIF - Best Case Scenario (PPt)	0.36	0.015	1.00	Calculated

4.4 Results

In this section the results of the developed analysis are reported for both Cumulative energy demand and CO₂-eq. emissions. The results are discussed with the aim to analyze the influence of the batch size, of the methods used for recycling credits accounting as well as of the used feed rate in SPIF on the comparative analysis. The results for CED with varying batch size are reported in Figure 41 a and b for the case of substitution method and recycled content, respectively. Overall as the tooling is the only factors varying with changing batch size, the decreasing trends is visible only for the conventional and the SSR based approaches. Whereas the Reshaping approach has a constant trend and its value significantly decreases when using high feed rate.

It can be seen that SPIF with High Feed Rate (HFR) has the lowest CED in considered scenario, even when very high batch size are considered, the SPIF based approach is always the best solution. Whereas, when SPIF with Low Feed Rate (LFR) is considered, break-even points (BP), where two routes demand the same amount of CED/CO₂-eq occur, under the recycled content approach, BP occur only between remelting route and

SPIF LFR at a batch size of 319. When the Substitution Method approach is considered break-even points occur at much lower batch size values, i.e. 187 for the remelting route with SPIF LFR, and at 638 between SSR and SPIF LFR. This change in Energy value is due to the lower environmental impact ascribed to the material by the substitution method as discussed in the previous section.

Similarly for calculations regarding the CO₂-eq, break-even points occur just between the remelting and the SPIF LFR routes, at a batch size of 630 when calculations were done using the recycled content approach and at 397 on using the substitution approach.

The results prove that the here proposed Reshaping approach has the potential for putting in place energy efficient material reuse strategies. In fact when the proper SPIF process parameters are selected (High Feed rate) Reshaping proved to be the best option both in terms of CO₂-eq emission and CED regardless of the analyzed scenario.

Unlike what was reported in an earlier study, the SSR approach displays worse performance than remelting based route. This is mainly due to the higher number of process steps as both Extrusion and sheet production steps have been included. Also, because as suggested by Duflou et al [9], a small value of permanent value loss are considered. In order to provide a clearer picture the breakdown analysis for each analyzed route is reported in figure 42. In this figure the contribution of each factor towards the total CED and CO₂-eq emission for a batch size of 350 is illustrated.

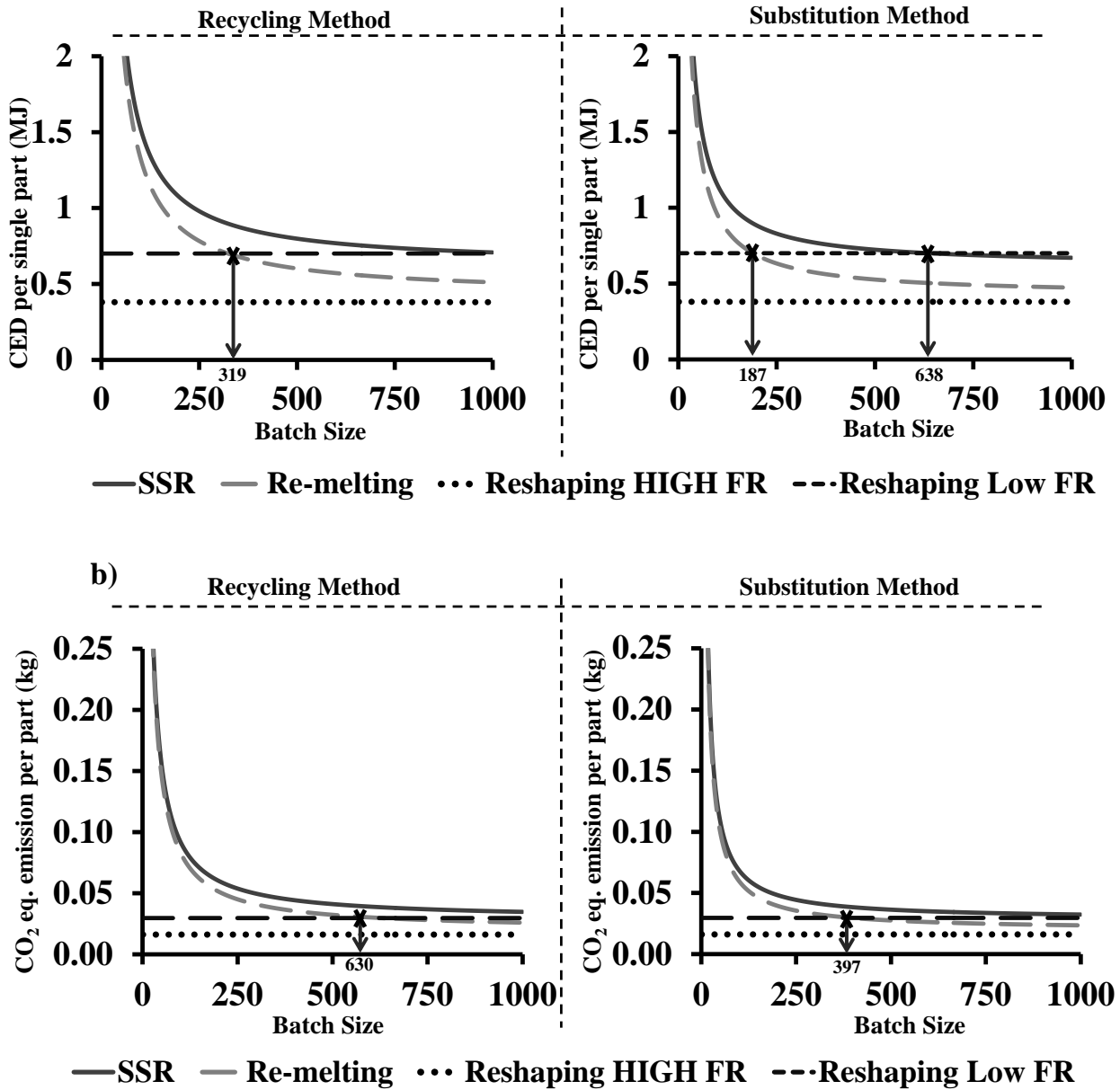


Fig. 41. Routes performance trends for recycled content and substitution approaches with varying batch size: (a) CED trend (b) CO₂-eq. emission trend.

As far as SSR is concerned, Besides tooling, it is badly affected by the larger number of high energy demanding processes steps (compacting, hot extrusion and sheet production). Concerning remelting, the high contribution of permanent loss is evident as it accounts

for 27% and 32% of the total for recycled content and substitution method scenario, respectively. Finally for SPIF it is possible to see that the electric energy demand while processing is the dominant factor and it is significantly affected by the process time. Proportional values with similar trends were obtained for CO₂-eq. emissions, results are reported in Figure 42.

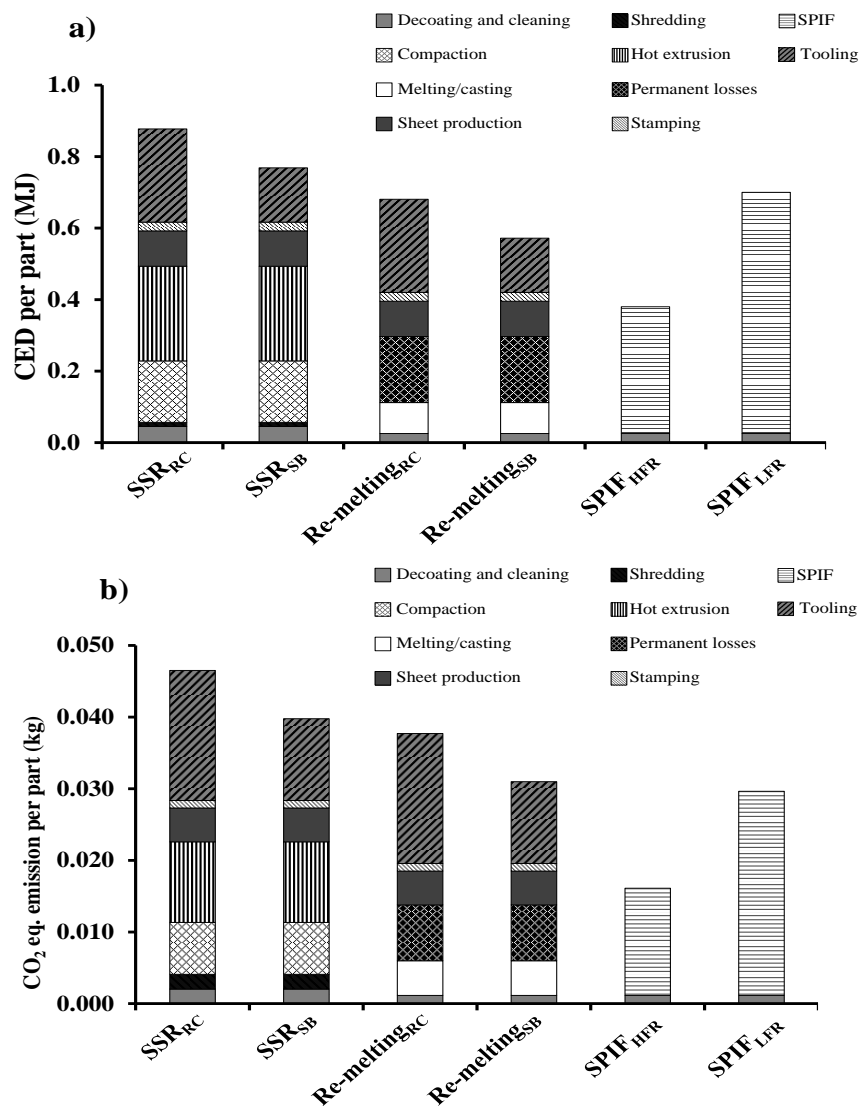


Fig. 42. Process steps contribution to the total route performance for both the selected approaches: (a) CED shares of routes; (b) CO₂-eq. emission.

4.5 Discussions

In this research the suitability of Single point Incremental Forming process in changing the shape of EoL components has been proved by the analysis of its environmental impact performance. In this respect, a comparative analysis with two other strategies, namely conventional recycling and ECAP based SSR approaches. Different scenario were considered with varying the production batch size and the method for accounting for credits arising from recycling.

The SPIF based approach, subjected to proper process parameter selection, proved to be the most environmentally friendly strategy regardless of the analyzed scenario. For instance for a batch size of 350 parts, the Reshaping approach allows and CO₂-eq emissions saving as high as 47% and 50% with respect conventional and SSR approached, when the substitution method is considered, respectively. When the analysis is developed with the Recycled content approach the saving increase up to 57% and 59%, respectively. The advantage is mainly due to the fewer steps as well as to the less material (less material scraps) involved in turning an end of life parts in a newR components. Besides the benefits just reported, some issues are still to be addressed to scale up such a new Reshaping processes; some of them are discussed below.

Similarly to what happens for remanufacturing processes, poor information about return products make the inspection step fundamental for making reuse strategies successfully

from technological, economic and environmental perspectives [123]. For sheet metal based EoL components the thinning distribution is a crucial piece of information to properly design the Reshaping process. Since the thinning distribution is caused by the first forming processes, this information can be easily accessed if the company who develops Reshaping is the original equipment manufacturer, otherwise a proper inspection step is to be envisaged. Possible candidates for the inspection step may be laser based or ultrasound, the suitability of the inspection technology is to be still identified and both technological and environmental performance have to be considered. In this paper no energy was ascribed to inspection step because of the lack of industrial practices. Another step deserving research attention is the de-coating. Normally, sheet metal based components have an outer layer, typically painting, to be removed. Such layer has to be removed without affecting the mechanical properties of the components. These processes normally take place at elevated temperatures, and the effect of the sheet heating on the mechanical properties it is mandatory to identify proper de-coating strategies.

Besides the above mentioned technical issues , other aspects have to be dealt for actually putting in place the here proposed Reshaping technology. Specifically, proper reverse logistics need to be identified as the recovery step is of crucial importance to get suitable cores to be remanufactured. Finally, proper business model making the SPIF Reshaping

approach both environmentally friendly and profitable for manufacturing companies is needed.

To further understand the potential of the SPIF approach, there is a need for the study of using other sheet metal forming processes such as hydroforming or super-plastic forming for Reshaping purposes as well.

5 Reshaping by Hydroforming: Feasibility Analysis

In this chapter, a different flexible sheet metal forming process is proposed as suitable for Reshaping purposes. Specifically, Hydroforming is applied to Reform sheet metal based components. To replicate the entire process chain, a deep drawing process is applied to impart a square feature, and subsequently, Hydroforming process is performed and the capability of nullifying the deep drawn feature is analyzed. A wide experimental campaign is proposed and a numerical/ experimental approach is developed to carry out design methodologies for Reshaping processes.

In order to realize the research objectives, the authors turned a virgin blank into an EoL component by imparting it deformations. Pre-straining by means of Deep Drawing (DD) was performed on a virgin blank, considering it as a primary processes to resemble an EoL component. The EoL component obtained after Deep Drawing was Reshaped by performing Hydroforming process on the component along the direction same as that of deep drawing.

The study of the feasibility of this Reshaping strategy was carried out in the light of the analysis of the effects of variations in the Hydroforming process parameters, as well as, the positioning of the deep drawn feature. Figure 43 presents a graphical synthesis of the proposed research along with the objectives for the same.

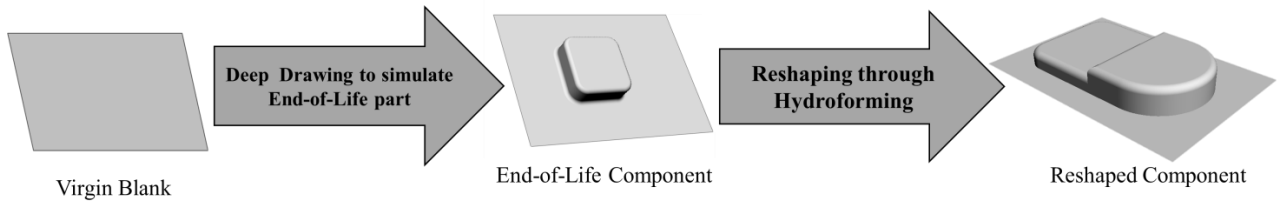


Fig. 43. Proposed Research Strategy

5.1 Experimental setup

5.1.1 Deep Drawing Setup

The Deep Drawing process was performed on a Galdabini Quasar 600 hydraulic press. The tools utilized comprised of a die, punch and a blank holder. The DD process was performed on rectangular blanks with a BHF increasing linearly from 2027N up to 4202N and a constant punch velocity of 1mm/s. Figure 44 illustrates the geometric parameters of the resulting component.

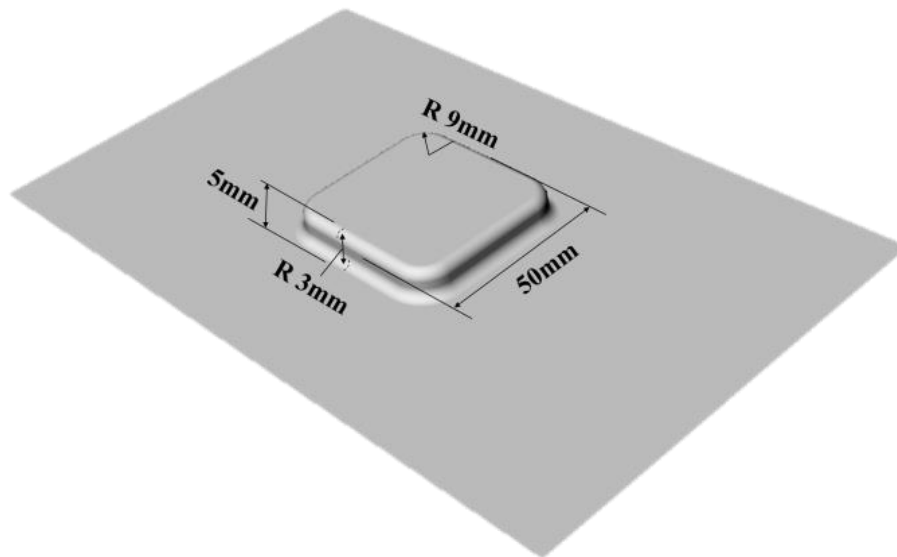


Fig. 44. Geometrical Parameters of DD Component.

5.1.2 Hydroforming Setup

Hydroforming (HF) tests were carried out using a prototype 2500 kN electro-hydraulic press machine, shown in Figure 45 (a). HF tools consist of an upper die and a blank holder. In Figure 45(b) the die used for manufacturing the investigated case study is shown: it is a stepped die characterized by a two depths cavity (12mm and 20mm, respectively).

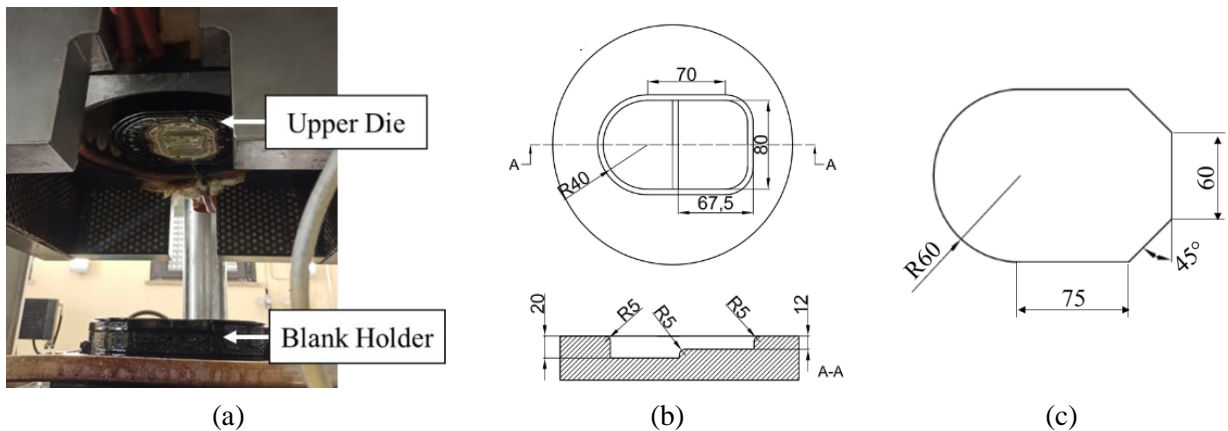


Fig. 45. (a) Equipment used for the experimental HF tests; (b) Geometrical features of the case study; (c) Optimized initial blank geometry

Before the HF test, the deep drawn part was cut in order to change its external profile as depicted in Figure 45(c). Such an external profile was designed by means of numerical simulations to optimize the material drawing. Depending on the position of the DD feature on the initial blank, four different conditions can be distinguished:

- *Top-DD* (Figure 46 a): the DD feature is located close to the circular part of the blank profile and, as a consequence, it is in front of the deepest part (20 mm) of the cavity during the HF process;

- *Bot-DD* (Figure 46 b): the DD feature is located opposite to the circular part of the blank profile and, as a consequence, it is in front of the shallowest part (12 mm) of the cavity during the HF process;
- *Mid-DD* (Figure 46 c): the DD feature is located in the middle of the initial blank and, as a consequence, it is the feature is placed between the two cavities during the HF process;
- *No-DD* (Figure 46 d): there is no DD feature on the initial blank; this condition was introduced as reference.

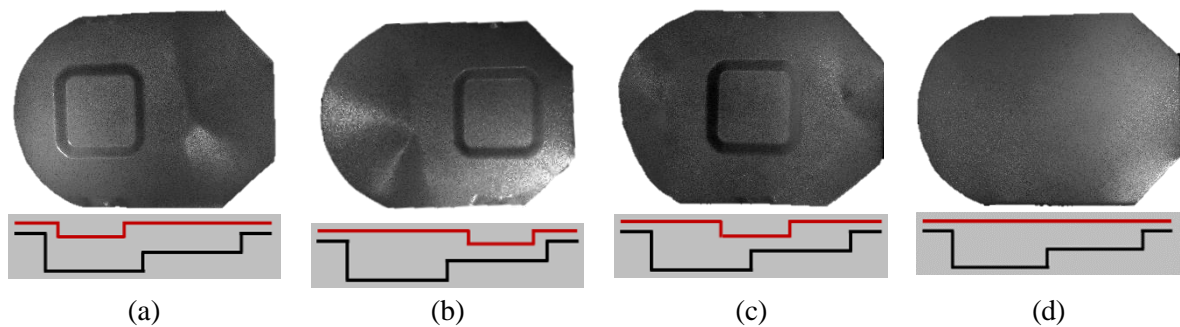


Fig. 46. (a) Top-DD, (b) Bot-DD (c) Mid-DD and (d) No-DD conditions in the case of HF tests; the red line indicates the starting blank for HF tests; the black line represents the die cavity.

The blank was then placed between the tools (between the upper die and the Blank Holder). The BHF and the oil pressure were increased according to linear profiles (as shown in Figure 47) using a Programmable Logic Control (PLC) managed by the press machine control system; in particular, the oil pressure profile started to increase when the minimum value of the BHF was reached.

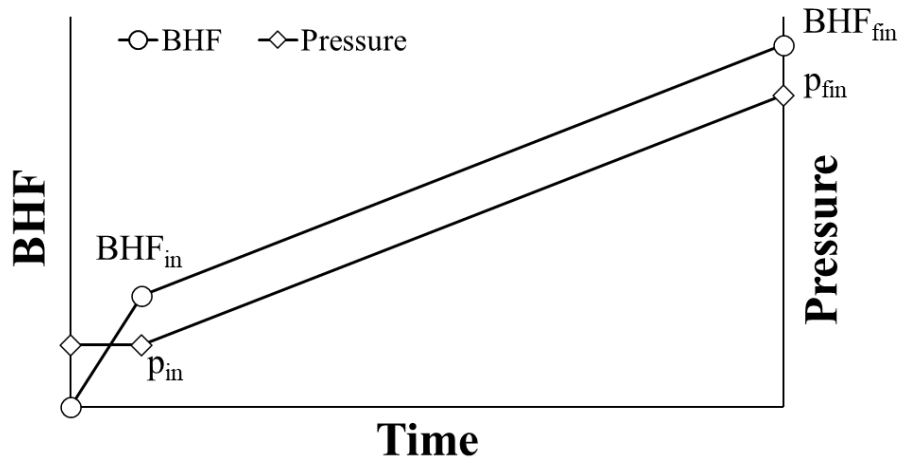


Fig. 47. BHF and pressure profiles adopted during the HF step

For the Hydroforming tests, the initial and final Blank Holder force (BHF_{in} and BHF_{fin} , respectively) as well as the position of the drawn feature were chosen as input variables. In particular, two levels both for BHF_{in} (13 kN – 33 kN) and BHF_{fin} (57 kN – 77 kN) were considered and four levels of the position of the drawn feature (Top-DD, Mid-DD, Bot-DD, No-DD as described previously) were investigated. The pressure law was the same for all the tests, being a linear law starting from 1 bar to 52 bar, with an oil pressure rate of 1 bar per second.

5.1.3 Geometric Acquisition Setup

After performing the two forming processes were carried out, the resulting components were then scanned using the 3DPhoto Acquisition system, ‘Steinbichler Comet’ in order to obtain a three dimensional model of the parts. These three dimensional models of the experimental specimens were then analyzed for the geometric deviations occurring in the Reshaped components when compared to Hydroformed virgin

Blanks. The comparison was performed using a 3D quality control and dimensional inspection software, ‘Geomagic Control X’ with the observations reported in the Results section. Table 6 shows an overview of the experimental results after the Hydroforming step.

Table 6. Experimental campaign for HF after DD tests

Experiment Id.	BHF _{in} [kN]	BHF _{fin} [kN]	Position of the feature
1	13	57	TOP
2	13	57	MIDDLE
3	13	57	BOTTOM
4	13	77	TOP
5	13	77	MIDDLE
6	13	77	BOTTOM
7	33	57	TOP
8	33	57	MIDDLE
9	33	57	BOTTOM
10	33	57	NO FEATURE
11	13	77	NO FEATURE
12	13	57	NO FEATURE

For each condition, the values of the input parameters (BHF_{in} and BHF_{fin}) as well as the initial position of the feature have been specified.

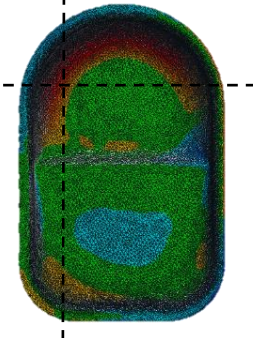
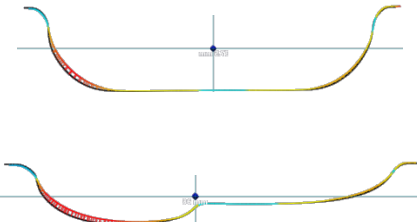
5.2 Results and Discussions


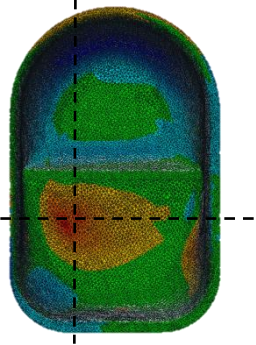
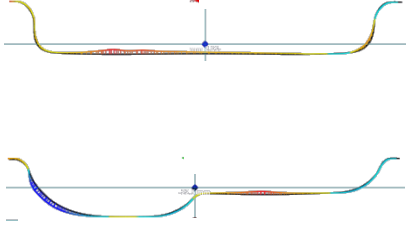

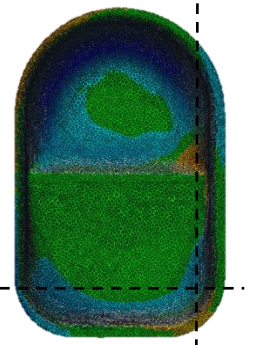
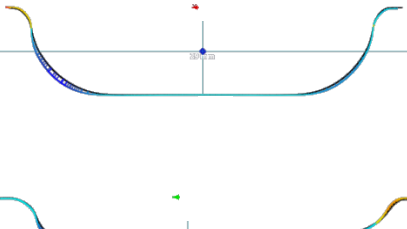
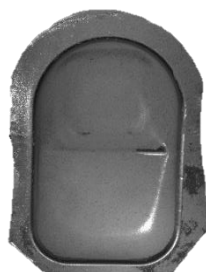
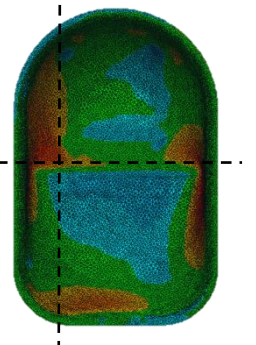
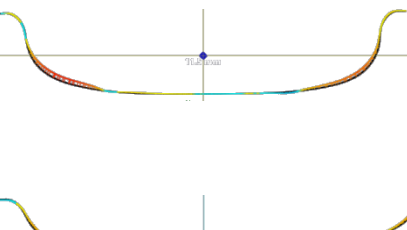
For the geometric accuracy two different analyses were developed namely a Global and a Local one. The Global analysis was performed on the entire surface while the local one was developed on a narrowed area to better quantify the presence of the DD feature in the Reshaped component.


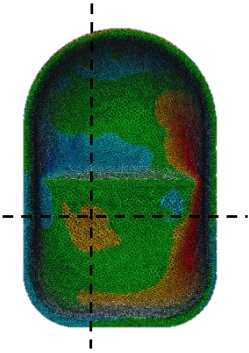
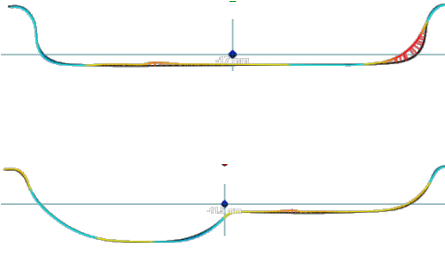

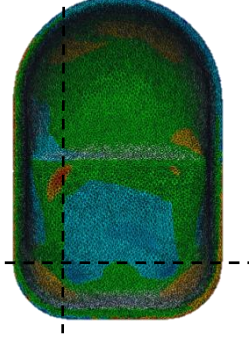
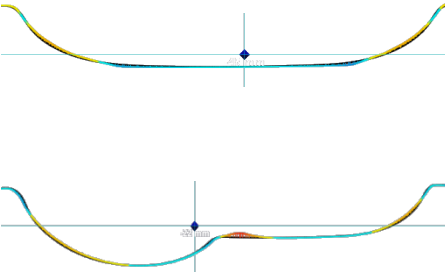

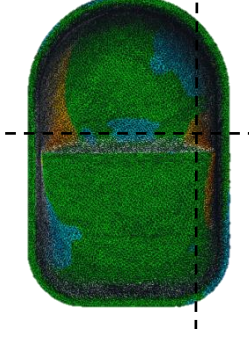
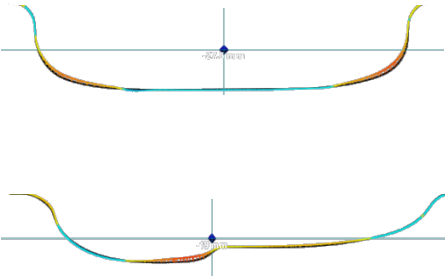
Concerning the Global analysis, for each ID the final Reshaped surface was compared with the relative parts obtained on the Hydroforming of a virgin blank with the same parameters.


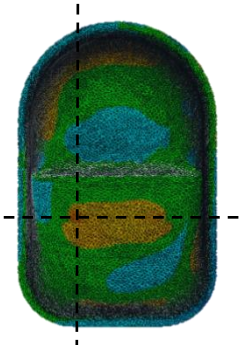
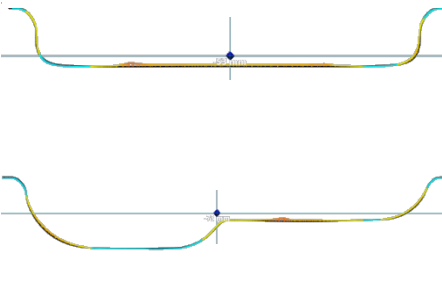

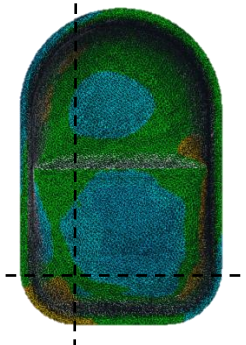
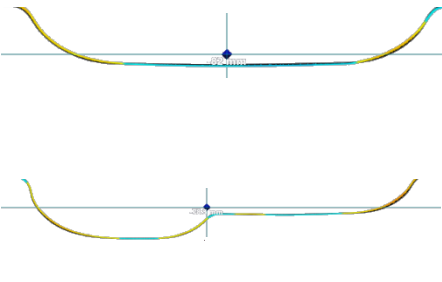
For each ID the Maximum deviation and the standard deviation values were recorded as metrics to quantify the geometrical accuracy. Results are reported in Table 7. For each ID, the error map along with significant (where the maximum deviation were observed) sections views analyses are reported.

Table 7. Geometric accuracy results for the Reshaping by HF tests

ID	Geometric Analysis	Section View	Maximum Deviation (mm)	Standard Deviation (mm)
ID 1			1.5238	0.3969

<p>ID 2</p> 			<p>1.1282</p>	<p>0.3513</p>
<p>ID 3</p> 			<p>1.4026</p>	<p>0.3984</p>
<p>ID 4</p> 			<p>1.1729</p>	<p>0.2341</p>

<p>ID 5</p> 			<p>1.7514</p>	<p>0.3316</p>
<p>ID 6</p> 			<p>1.5957</p>	<p>0.24</p>
<p>ID 7</p> 			<p>0.9263</p>	<p>0.1617</p>

<p>ID 8</p> 			<p>0.7047</p>	<p>0.1705</p>
<p>ID 9</p> 			<p>0.6302</p>	<p>0.1544</p>

Overall it is possible to state that the difference in geometry is limited, actually as the starting blanks (Virgin/flat vs Deep Drawn) are characterised by different hardening levels the material flows during Hydroforming is different although the same process parameters are used. In order to have a clearer picture of the influence of the process parameters on the global geometric inaccuracies, Main effect plot analyses were carried out, Figure 48 illustrates the results of this analysis.

It is possible to notice that with increasing the BHF values, the shape accuracy improves. This is due to the higher deformation imparted which helps in reducing the geometrical error

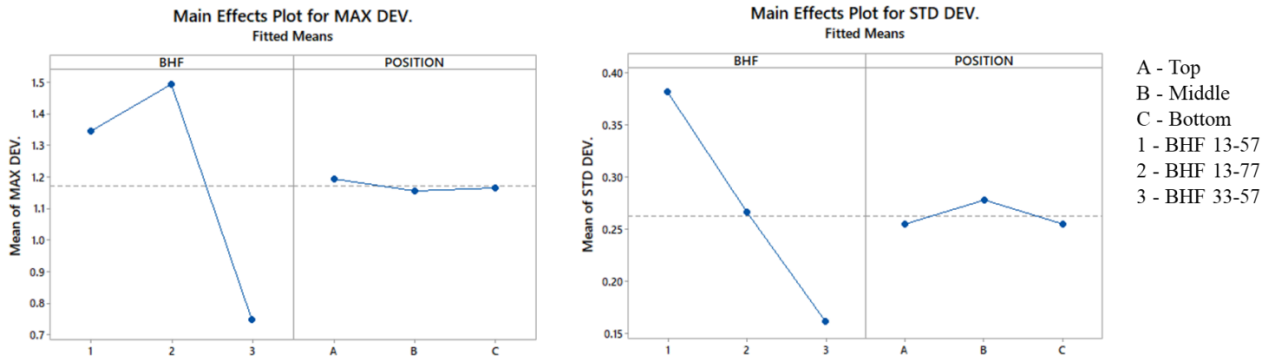


Fig. 48. Main Effects plots for the Maximum and Standard deviations recorded from the geometrical accuracy analysis of the components.

With the aim to better quantify to what extent the feature is still present on the Hydroformed component, a local analysis was developed. The most difficult area of the feature to nullify by Reshaping are the bottom corners of the DD feature; in consequence, the local analyses was narrowed on corners area and the maximum deviation at the bottom corners was quantified for each ID. The recorded maximum deviation values are reported in Figure 49.

The related Main Effects plot analysis is reported in Figure 50. It can be noticed that while BHF has not a clear impact on the feature presence, the position of the feature plays a significant impact, instead. In fact, the middle position configuration is characterized by the worst values. In Figure 51 the ID corresponding to the highest (ID 2-middle position) and lowest (ID 9-bottom Position) recorded values are reported. For

each ID Two section cut analyses are reported, while the feature was still visible in ID2, concerning ID 9 no shape defect was observed.

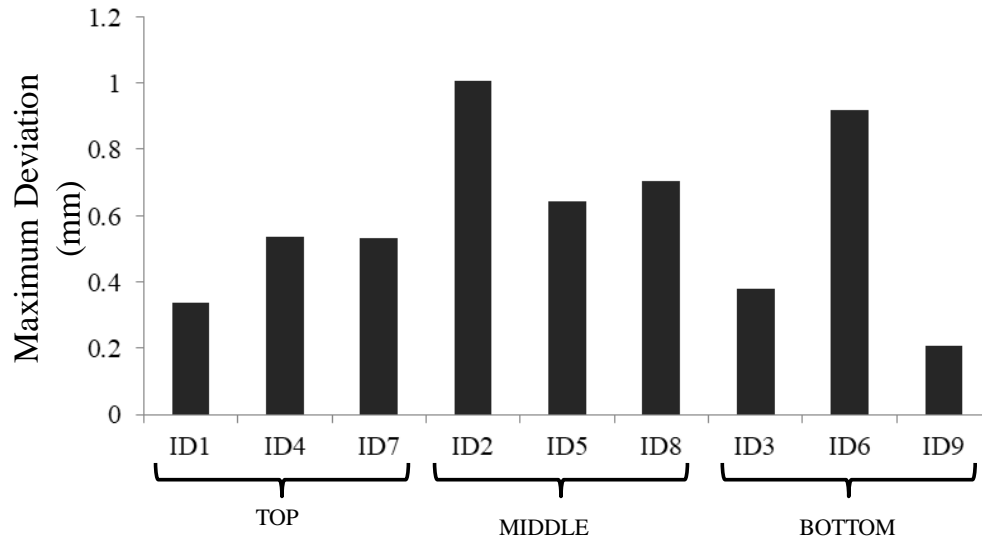


Fig. 49. Maximum Deviation values recorded on the local analysis of the components.

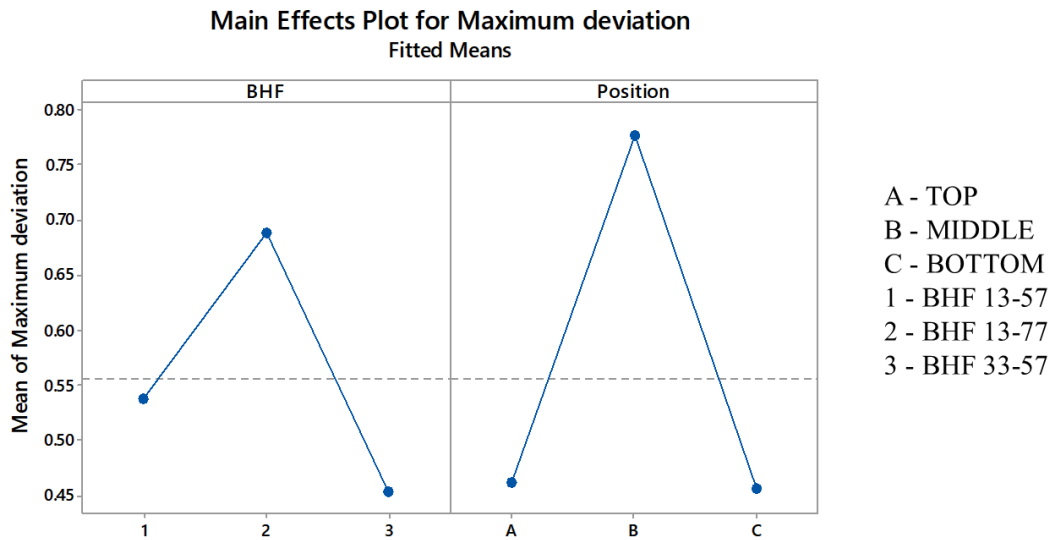


Fig. 50. Main Effects plots for the Maximum Deviation values recorded on the local analysis of the components.

Overall results revealed that the feature is more visible in the bottom region. It is worth mentioning that the bottom region is characterized by a lower values of strains imparted during Reshaping by hydroforming. As a consequence, it is evident that smaller the strain level occurring during Reshaping the more difficult it results to remove the feature.

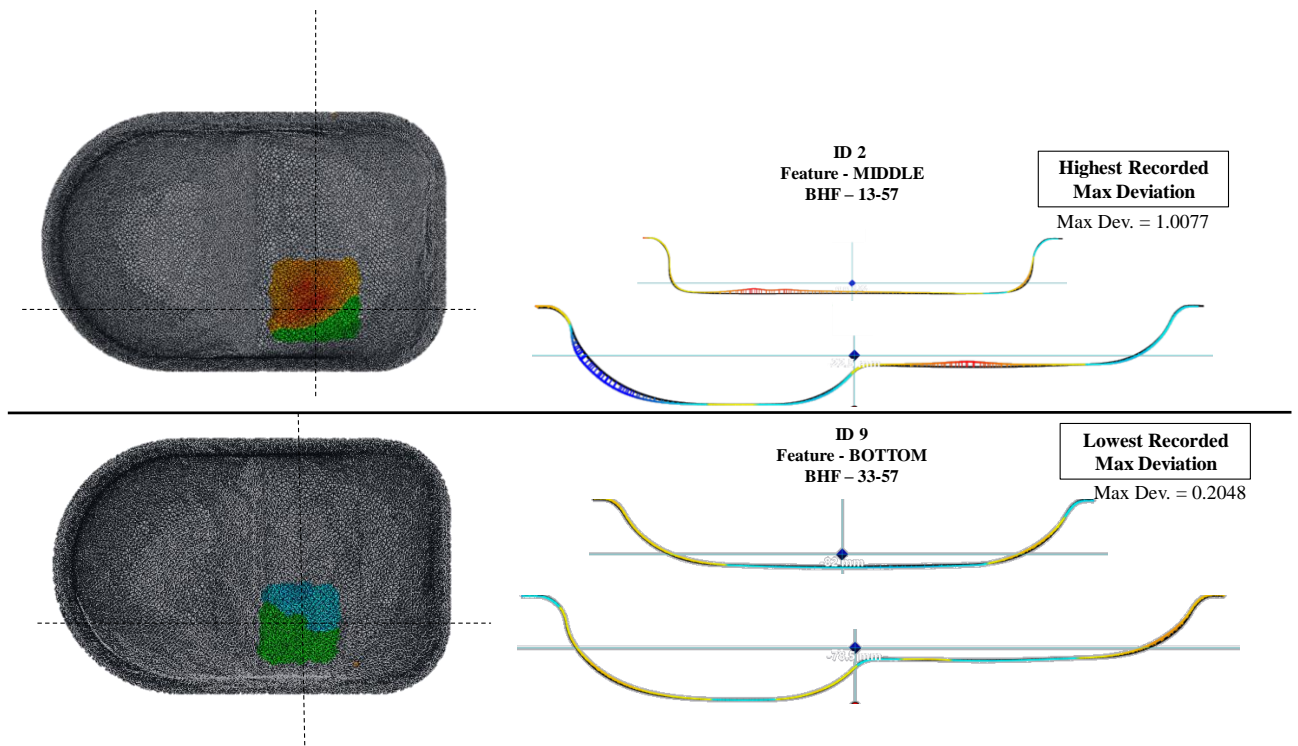


Fig. 51. Local analysis and section cut view of IDs 2 and 9.

6. Conclusions

6.1 Summary

In this dissertation, the concept of Reshaping as a novel circular economy strategy has been presented. Particularly the capabilities of Reshaping through the use of a flexible forming process for lightweight End-of-Life sheet metal components have been investigated under different aspects. The effectiveness of this peculiar metal reuse by Reshaping strategy has been assessed through the evaluation of the technical aspects pertaining to the forming process utilized and the environmental impact of the entire Reshaping process chain when compared to conventional methodologies. Summing up the obtained results the following conclusions can be drawn:

- ❖ Successful testing of the SPIF process capability on working with deformed parts without any detrimental effects was performed. SPIF was challenged as a process to Reshape sheet metal End-of-Life components. A process chain made of DD process followed by SPIF was experimentally performed at lab scale to simulate the entire metal reuse route. Different shapes and forming directions had been tested. Results revealed that SPIF was a proper candidate to success. Thickness and strain measurements showed two main advantages: 1/the SPIF local action allows selectively reworking safe areas of the EoL components; 2/the improved

formability allowed one to superimpose further deformation even in already formed zones (such as the bottom corner of DD component). This first research effort started to lay the groundwork for a successful SPIF based Reshaping approach development.

- ❖ The higher flexibility of the SPIF process as compared to conventional forming processes for the purpose of Reshaping components was demonstrated. Shapes with two geometrical variations and working directions had been simulated and analyzed by utilizing three different strategies for each of the two geometrical variations. The results showed an infeasibility of the selected approaches as opposed to the results obtained by the use of SPIF process to achieve the same. The Forming limit maps indicate that the desired result was in fact obtainable through the use of a single counter tool but, unfortunately, plastic instability phenomenon were observed on the non-worked portions of the EoL component. This highlighted the fact that Reshaping, while could be performed using conventional forming processes but with the resulting parts of a compensated quality.
- ❖ The geometrical deviation as a consequence of SPIF operations were studied on the non-worked zones of the EoL component. For this aim, two different SPIF directions (named inwards and outwards) were analyzed; the effect of some geometrical parameters were taken into account. The results, from a wide

experimental campaign, revealed two different geometrical deviations as the direction of SPIF action changed. In the Outward case, limited deviation occurred and basically a draw in of the lateral walls of the EoL part occurred. With regards to the Inward case study, a different phenomenon was observed. In fact, SPIF Reshaping caused a shortening of the lateral walls as well as an outward displacement, actually a limited buckling phenomenon was observed. For the inward approach higher geometric deviation occurred, and Pareto chart analyses and main effect plot revealed a correlation between geometrical deviation and SPIF base as well as deep drawing height.

It could also be ascertained that the extent of deformation applicable on an EoL component depended both on the formability performance of the selected processes for Reshaping (in the present case SPIF) as well as on the conditions (thickness distributions) of the recovered component.

The accuracy and formability variation of the SPIF process when used as a Reshaping with varying Pre-straining conditions were analyzed. Process chains consisting of different types and levels of pre-straining followed by their Reshaping through SPIF were projected, and the resulting α max and final shape accuracy had been determined. Results showed that SPIF though had a reduced formability with the increase in the pre-straining levels, performed decently well for both the analyzed aspects. As a matter of fact, even with a decrease in the

formability of SPIF was seen, the difference was minimal and the Reshaping through SPIF could still be performed successfully on the analyzed EoL parts. With regards to the part's geometric accuracy, the ANOVA analysis of the obtained deviation values yielded the conclusion that the pre-straining of the parts, before their Reshaping, did not significantly influence the accuracy performance of SPIF. Rather in some cases increased pre-straining level actually yielded a part with better accuracy in comparison to SPIF performed on a virgin blank.

- ❖ Analyzing the feasibility of SPIF, as a Reshaping alternate, in terms of Primary Energy consumption and CO₂ equivalent emissions with respect to conventional metal reuse strategies. An analysis of the Reshaping by SPIF strategy was performed in light of its environmental impact performance. In this respect, a comparative analyses with two other strategies, namely conventional recycling and ECAP based SSR approaches. Different scenario were considered with varying the production batch size and the method for accounting for credits arising from recycling. The SPIF based approach, subjected to proper process parameter selection, proved to be the most environmentally friendly strategy regardless of the analyzed scenario. The advantage was mainly due to the fewer steps as well as to the less material (less material scraps) involved in turning an end of life parts in a new/Reshaped components.

- ❖ The potential of employing an alternate Hydroforming technique as a Reshaping tool in terms of the part quality obtained and the influence of the process parameters selected was explored.

6.2 Future Developments

The results obtained by the investigations presented in this dissertation and summarized in the previous section shed light on the various aspects involved in the realization of Reshaping as a novel circular economy strategy and provide an in depth knowledge on different aspects involved in the realization of the same.

Furthermore, research effort is still needed for both designing an adaptive and effective clamping system, not relying on flat sheet availability, and for identifying proper EoL inspection strategy. The inspection strategy should provide the thickness distribution of the EoL part for supporting SPIF process designer.

Nevertheless, in an industrial environment the inspection step becomes crucial for a successful Reshaping strategy implementation. Thinning distribution of EoL and material properties/conditions are crucial pieces of information to properly design the Reshaping. These pieces of information will allow correct identification of the zones of EoL component to be Reshaped. Due to the limited use of the FLD of the sheet material due to the nonlinear strain path which it undergoes, the local strain paths and overall on residual ductility of the material is an major requisite in the implementation of the Reshaping strategy. As more complex sheet metal parts are considered for remanufacturing the

already imparted deformation plays a relevant role in the residual ductility of the material and on the possible additional deformation which can be conferred in the new forming process (such as SPIF or Hydroforming). This is a totally further issue which needs addressing, and is strongly related to the limited use of the FLD which can be done due to their intrinsic limits.

Possible candidates for the inspection step may be laser based or ultrasound, the suitability of the inspection technology is to be still identified and both technological and environmental performance have to be considered. In this paper no energy was ascribed to inspection step because of the lack of industrial practices.

Another step deserving research attention is the de-coating. Normally, sheet metal based components have an outer layer, typically painting, to be removed. Such layer has to be removed without affecting the mechanical properties of the components. These processes normally take place at elevated temperatures, and the effect of the sheet heating on the mechanical properties it is mandatory to identify proper de-coating strategies.

A research effort is still needed for designing an adaptive and effective clamping system. As a matter of fact, the clamping system should be easily adaptable to changeable workpieces (both in shape and dimensions). As the flange is not normally available in EoL life components and, therefore, innovative clamping system for SPIF should be provided not relying on flat sheet availability.

Besides the above-mentioned technical issues, other aspects have to be dealt for actually putting in place the here proposed Reshaping technology. Specifically, proper reverse logistics have to be identified as the recovery step is of crucial importance to get suitable cores to be remanufactured. Finally, proper business model making the SPIF Reshaping approach both environmentally friendly and profitable for manufacturing companies.

To fully explore the potential of Reshaping, other flexible sheet metal forming processes should be analyzed. Other candidates could be Hydroforming (possibly the assisted temperature versions) and Hot Gas Forming. These options deserve to be explored to identify the most suitable process with varying EoL properties.

Bibliography

1. Worrell E, Allwood J, Gutowski T (2016) The Role of Material Efficiency in Environmental Stewardship. *Annual Review of Environment and Resources* 41:575–98.
2. Olivetti EA, Cullen JM (2019) Toward a sustainable materials system. *Science*, 360/6396:1396-1398.
3. Allwood JM, Cullen J (2012) Sustainable materials: with both eyes open. UIT Cambridge.
4. Material efficiency in clean energy transitions (2019) IEA, Paris.
5. Atherton J (2007) Declaration by the metals industry on recycling principles. *International Journal of Life Cycle Assessment*, 12 (1): 59-60.
6. Kleiner M, Chatti S, Klaus A (2006) Metal forming techniques for lightweight construction. *Journal of Material Processing Technology*, 177:2-7.
7. Ingarao G (2017) Manufacturing strategies for efficiency in energy and resources use: The role of metal shaping processes. *Journal of Cleaner Production*, 142:2872–86. doi:10.1016/j.jclepro.2016.10.182
8. Ashby MF (2013) *Materials and the Environment*. Butterworth Heinemann/Elsevier, ISBN 978-0-12-385971-6.
9. Duflou JR, Tekkaya AE, Haase M, Welo T, Vanmeensel K, Kellens K, Dewulf W, Paraskevas D (2015) Environmental assessment of solid state recycling routes for aluminium alloys: Can solid state processes significantly reduce the environmental impact of aluminium recycling?. *CIRP Annals Manufacturing Technology*, 64:37–40. doi.org/10.1016/j.cirp.2015.04.051.

10. Wan B, Chen W, Lu T, Liu F, Jiang Z, Mao M (2017) Review of solid state recycling of aluminum chips. *Resources, Conservation and Recycling*, 125:37–47. doi.org/10.1016/j.resconrec.2017.06.004.
11. Haase M, Khalifa BN, Tekkaya EA, Misiolek WZ (2012) Improving mechanical properties of chip-based aluminum extrudates by integrated extrusion and equal channel angular pressing. *Material Science and Engineering A*, 539:194-204.
12. Widerøe F, Welo T, Vestøl H (2012) A new testing machine to determine the behavior of aluminum granulate under combined pressure and shear. *International Journal of Material Forming*, 6:199–208.
13. Kamilah Yusuf N, Amri Lajis M, Ahmad A (2017) Hot Press as a Sustainable Direct Recycling Technique of Aluminium: Mechanical Properties and Surface Integrity Materials, 10:902.
14. Tang W, Reynolds AP (2010) Production of wire via friction extrusion of aluminum alloy machining chips. *Journal of Materials Processing Technology*, 210:2231–2237.
15. Li X, Baffari D, Reynolds AP (2018) Friction stir consolidation of aluminum machining chips. *The International Journal of Advanced Manufacturing Technology* 94(5-8):2031-2042.
16. Baffari D, Reynolds AP, Masnata A, Fratini L, Ingarao G (2019) Friction stir extrusion to recycle aluminum alloys scraps: Energy efficiency characterization. *Journal of Manufacturing Processes*, 43:63-69.
17. Buffa G, Baffari D, Ingarao G, Fratini L (2020) Uncovering Technological and Environmental Potentials of Aluminum Alloy Scraps Recycling Through Friction

- Stir Consolidation. *International Journal of Precision Engineering and Manufacturing-Green Technology*, 7(955–964):1-10.
18. Jawahir IS, Bradley R (2016) Technological Elements of Circular Economy and the Principles of 6R-Based Closed-loop Material Flow in Sustainable Manufacturing. *Procedia CIRP*, 40:103-108.
 19. Lyle JT (1996) *Regenerative Design for Sustainable Development*, Wiley Ed.
 20. European Commission, 2015. Communication from the Commission to the European Parliament, the Council, the European Economic and Social Committee and the Committee of the Regions Closing the Loop - an EU Action Plan for the Circular Economy.
 21. Stahel W, Reday G (1981) *Jobs for Tomorrow, the Potential for Substituting Manpower for Energy*, Vantage Press, New York.
 22. McDonough W, Braungart M (2002) *Cradle to Cradle: Remaking the Way We Make Things*, North Point Press, New York.
 23. Frosch R, Gallopoulos N (1989) Strategies for Manufacturing. *Scientific American*, 261:144–152.
 24. Plastic Waste and Recycling Environmental Impact, Societal Issues, Prevention, and Solutions 2020, Pages 481-512
 25. MacArthur Foundation (2013) *Towards the Circular Economy: Opportunities for the Consumer Goods Sector*.
 26. Huisman S, Debaveyea S, Schaubroecka T, De Meestera S, Ardente F, Mathieux F, Dewulf J (2015) The Recyclability Benefit Rate of Closed-loop and Open-loop Systems: A Case Study on Plastic Recycling in Flanders. *Resource Conservation and Recycling*, 101:53–60.

27. Tolio T, Bernard A, Colledani M, Kara S, Seliger G, Duflou JR, Battaia O, Takata S (2017) Design, management and control of demanufacturing and remanufacturing systems. *CIRP Annals - Manufacturing Technology*, 66:585–609.
28. Cooper DR, Allwood JM (2012) Reusing Steel and Aluminum Components at End of Product Life. *Environmental Science and Technology*, 46:10334-10340.
29. Apra — Automotive Part Remanufacturers Association (2012) Remanufacturing Terminology, Remanufacturing Term Guideline.
30. Parkinson HJ, Thompson G (2003) Analysis and Taxonomy of Remanufacturing Industry Practice. *Proceedings of the Institution of Mechanical Engineers*, 217:243–256.
31. D’Adamo I, Rosa P (2016) Remanufacturing in industry: advices from the field. *The International Journal of Advanced Manufacturing Technology*, 86(9-12):2575-2584.
32. Chen C, Wang Y, Ou H, He Y, Tang X (2014) A review on remanufacture of dies and moulds. *Journal of Cleaner Production*, 64:13-23.
<https://doi.org/10.1016/j.jclepro.2013.09.014>
33. Esposito L, Bertocco A, Cricrì G, Rosiello V (2019) Welding-repair effect on F357-T6 aluminum castings: analysis of fatigue life. *International Journal of Advanced Manufacturing Technology*, 102:3699-3706.
<https://doi.org/10.1007/s00170.019.03436.4>
34. Wilson JM, Piya C, Shin YC, Zhao F, Ramani K (2014) Remanufacturing of turbine blades by laser direct deposition with its energy and environmental impact analysis. *Journal of Cleaner Production*, 80:170-178.
<https://doi.org/10.1016/j.jclepro.2014.05.084>

35. Ahn DG (2016) Direct Metal Additive Manufacturing Processes and Their Sustainable Applications for Green Technology: A Review. *International journal of precision engineering and manufacturing-green technology*, 3:381-395. <https://doi.org/10.1007/s40684-016-0048-9>
36. Kellens K, Baumers M, Gutowski TG, Flanagan W, Lifset R, Duflou JR (2017) Environmental Dimensions of Additive Manufacturing Mapping Application Domains and Their Environmental Implications. *Journal of Industrial Ecology*, 21:s49-s68. <https://doi.org/10.1111/jiec.12629>
37. Caiazza F, Alfieri V, Argenio P, Sergi V (2017) Additive manufacturing by means of laser-aided directed metal deposition of 2024 aluminium powder: Investigation and optimization. *Advances in Mechanical Engineering*, 9(8):1–12. DOI: 10.1177/1687814017714982.
38. Liu Q, Janardhana M, Hinton B, Brandt M, Sharp K (2011) Laser cladding as a potential repair technology for damaged aircraft components. *International Journal of Structural Integrity*, 2:314-331. DOI: 10.1108/17579861111162914.
39. Guepner M, Drawert T, Bliedtner J (2019) Process characterization in laser metal deposition of EN AC-43000. *Journal of Laser Applications*, 31:022315. DOI: 10.2351/1.5096114
40. Hascoët JY, Touzé S, Rauch M (2018) Automated identification of defect geometry for metallic part repair by an additive manufacturing process. *Welding in the World*, 62:229–241. DOI: 10.1007/s40194-017-0523-0
41. Yin S, Cavaliere P, Aldwell B, Jenkins R, Liao H, Li W, Lupoi R (2018) Cold spray additive manufacturing and repair: Fundamentals and applications. *Additive Manufacturing*, 21:628–650. DOI: 10.1016/j.addma.2018.04.017

42. Li W, Yang K, Yin S, Yang X, Xu Y, Lupoi R (2018) Solid-state additive manufacturing and repairing by cold spraying: A review. *Journal of Materials Science & Technology*, 34:440–457. DOI: 10.1016/j.jmst.2017.09.015
43. Zhang K, Li D, Gui H, Li Z (2019) An adaptive slicing algorithm for laser cladding remanufacturing of complex components. *The International Journal of Advanced Manufacturing Technology*, 101(9-12):2873-2887.
44. Zhang X, Cui W, Li W, Liou F (2019) Effects of tool path in remanufacturing cylindrical components by laser metal deposition. *The International Journal of Advanced Manufacturing Technology*, 100(5-8):1607-1617.
45. Baker A (1999) Bonded composite repair of fatigue-cracked primary aircraft structure. *Composite Structures*, 47:431-443. DOI: 10.1016/S0263-8223(00)00011-8.
46. Maleki A, Saeedifar M, Najafabadi MA, Zarouchas D (2019) The fatigue failure study of repaired aluminum plates by composite patches using acoustic emission. *Engineering Fracture Mechanics*, 210:300–311. DOI: 10.1016/j.engfracmech.2017.12.034
47. Khan SMA, Es-Saheb M, Mohsin MEA (2017) Fatigue life enhancement of cracked aerospace grade aluminium repaired with bonded composite patch: experimental study. *Chemical Engineering Transactions*, 56:1873-1878. DOI:10.3303/CET1756313.
48. Maleki HN, Chakherlou TN (2017) Investigation of the effect of bonded composite patch on the mixed-mode fracture strength and stress intensity factors for an edge crack in aluminum alloy 2024-T3 plates. *Journal of Reinforced Plastics and Composites*, 36(15):1074-1091. DOI: 10.1177/0731684417702001.
49. Rezgani L, Madani K, Feaugas X, Touzain S, Cohendoz S, Valette J (2016) Influence of water ingress onto the crack propagation rate in a AA2024-T3 plate

- repaired by a carbon/epoxy patch. *Aerospace Science and Technology*, 55:359-365. DOI: 10.1016/j.ast.2016.06.010.
50. Talebi B, Abedian A (2017) Optimization of composite patch repair for maximum stability of crack growth in an aluminum plate. *Proceedings of the Institution of Mechanical Engineers, Part C: Journal of Mechanical Engineering Science*, 231(20):3690-3701. DOI: 10.1177/0954406216653776.
 51. Bachir Bouiadjra B, Benyahia F, Albedah A, Bachir Bouiadjra BA, Khan SMA (2015) Comparison between composite and metallic patches for repairing aircraft structures of aluminum alloy 7075-T6. *International Journal of Fatigue*, 80:128-135. DOI: 10.1016/j.ijfatigue.2015.05.018.
 52. Kale SS, Raja VS, Bakare AK (2018) Enhancing the Environmentally Assisted Cracking Resistance of Aircraft Quality Al Alloy of Type AA7075 Stiffened with Polymer Matrix Composite Using Cerium Chloride Inhibitor. *Transactions of the Indian Institute of Metals*, 71:3021–3027. DOI: 10.1007/s12666-018-1403-z.
 53. Albedah A, Khan SMA, Benyahia F, Bachir B (2015) Experimental analysis of the fatigue life of repaired cracked plate in aluminum alloy 7075 with bonded composite patch. *Engineering Fracture Mechanics*, 145:210–220. DOI: 10.1016/j.engfracmech.2015.04.008.
 54. Benyahia F, Aminallah L, Albedah A, Bachir Bouiadjra B, Achour T (2015) Experimental and numerical analysis of bonded composite patch repair in aluminum alloy 7075 T6. *Materials and Design*, 73:67-73. DOI: 10.1016/j.matdes.2015.02.009
 55. He Y, Liu X, Yu Z (2019) Mechanical properties of UV-curable carbon fiber-reinforced polymer composite patch: Repair evaluation of damaged aluminum alloy. *Polymers for Advanced Technologies*, 30(8):2034-2044. DOI: 10.1002/pat.4636

56. Kim M, Kim H, Lee W (2015) Repair of aircraft structures using composite patches bonded through induction heating. *Advanced Composite Materials*, 24:307-323. DOI: 10.1080/09243046.2014.899553
57. Schubbe JJ, Bolstad SH, Reyes S (2016) Fatigue crack growth behavior of aerospace and ship-grade aluminum repaired with composite patches in a corrosive environment. *Composite Structures*, 144:44-56. DOI: 10.1016/j.compstruct.2016.01.107
58. Tilwankar AK, Mahindrakar AB, Asolekar SR (2008) Steel Recycling Resulting from Ship Dismantling in India: Implications for Green House Gas Emissions. *Dismantling of Obsolete Vessels*, 1-10.
59. Takano H, Kitazawa K, Goto T (2008) Incremental forming of nonuniform sheet metal: Possibility of cold recycling process of sheet metal waste. *International Journal of Machine Tool Manufacturing*, 48:477-482.
60. Brosius A, Hermes M, Ben Khalif N, Trompeter M, Tekkaya AE (2009) Innovation by forming technology: motivation for research. *International Journal of Material Forming*, 2:29-38.
61. Abu-Farha FK, Khraisheh MK (2008) An integrated approach to the Superplastic Forming of lightweight alloys: towards sustainable manufacturing. *International Journal of Sustainable Manufacturing*, 1:18-40.
62. Verbert J, Behera AK, Lauwers B, Duflou JR (2011) Multivariate adaptive regressionsplines as a tool to improve the accuracy of parts produced by FSPIF. *Key Engineering Materials*, 473:841-6.
63. Behera AK, De Sousa RA, Ingarao G, Oleksik V (2017) Single point incremental forming: An assessment of the progress and technology trends from 2005 to 2015, 27:37-62.

64. Jeswiet J, Young D (2005) Forming limit diagrams for single-point incremental forming of aluminium sheet. *Proceedings of the Institution of Mechanical Engineers, Part B, Journal of Engineering Manufacture*, 219:359–64.
65. Verbert J [PhD thesis] Computer aided process planning for rapid prototyping with incremental sheet forming techniques. Leuven: Katholieke Universiteit Leuven; 2010.
66. Hussain G, Gao L, Hayat N, Qijian L (2007) The effect of variation in the curvature of part on the formability in incremental forming: an experimental investigation. *International Journal of Machine Tools Manufacturing*, 47:2177-81.
67. Filice L, Ambrogio G, Micari F (2006) Online control of single point incremental forming operations through punch force monitoring. *CIRP Annals Manufacturing Technology*, 55:245-8.
68. Aereens R, Eyckens P, Van Bael A, Duflou J (2010) Force prediction for single point incremental forming deduced from experimental and FEM observations. *International Journal of Advanced Manufacturing Technology*, 46:969-82.
69. Szekeres A, Ham M, Jeswiet J (2007) Force measurement in pyramid shaped parts with a spindle mounted force sensor. *Key Engineering Materials*, 344:551-8.
70. Hussain G, Gao L, Hayat N, Ziran X (2009) A new formability indicator in single point incremental forming. *Journal of Material Processing Technology*, 209:4237-42.
71. Eyckens P [PhD thesis] Formability in incremental sheet forming: generalization of the Marciniak–Kuczynski model. Leuven: KU Leuven; 2010.

72. Centeno G, Bagudanch I, Martínez-Donaire AJ, Garcia-Romeu ML, Vallellano C (2014) Critical analysis of necking and fracture limit strains and forming forces in single point incremental forming. *Materials Design*, 63:20-9.
73. Emmens WC, Van den Boogaard A (2007) Strain in shear, and material behaviour in incremental forming. *Key Engineering Materials Trans Tech Publications*, 344:519-26.
74. Emmens W, Van den Boogaard A (2009) An overview of stabilizing deformation mechanisms in incremental sheet forming. *Journal of Materials Processing Technology*, 209:3688-95.
75. Martins P, Bay N, Skjødt M, Silva M (2008) Theory of single point incremental forming. *CIRP Annals Manufacturing Technology*, 57:247-52.
76. Trzepieciński T (2020) Recent Developments and Trends in Sheet Metal Forming. *Metals* 2020. <https://doi.org/10.3390/met10060779>
77. McAnulty T, Jeswiet J, Doolan M (2017) Formability in single point incremental forming: A comparative analysis of the state of the art. *CIRP Journal of Manufacturing Science and Technology*. <https://doi.org/10.1016/j.cirpj.2016.07.003>
78. Silva MB, Nielsen PS, Bay N, Martins PAF (2011) Failure mechanisms in single-point incremental forming of metals. *The International Journal of Advanced Manufacturing Technology*, 56(9-12):893-903.
79. Cui Z, Cedric XZ, Ren F, Kiridena V, Gao L (2013) Modeling and validation of deformation process for incremental sheet forming. *Journal of Manufacturing Processes*, 15(2):236-241.

80. Duflou JR, Habraken AM, Cao J, Malhotra R, Bambach M, Adams D, Vanhove H, Mohammadi A, Jeswiet J (2018) Single point incremental forming: state-of-the-art and prospects. *International Journal of Material Forming*, 11:743-773.
81. Silva MB, Skjoedt M, Martins PAF, Bay N (2008) Revisiting the fundamentals of single point incremental forming by means of membrane analysis. *International Journal of Machine Tools Manufacturing*, 48:3-83.
82. Malhotra R, Xue L, Belytschko T, Cao J (2012) Mechanics of fracture in single point incremental forming. *Journal of Materials Processing Technology*, 212:1573-90.
83. ShankerDixit U (2020) *Mechanics of Materials in Modern Manufacturing Methods and Processing Techniques*. Elsevier Series in Mechanics of Advanced Materials 2020, Pages 1-30.
84. Lazarescu L, Nicodim I, Comsa DS, Banabic D (2015) Effect of the Blank-Holding Load on the Drawing Force in the Deep-Drawing Process of Cylindrical and Square Cups. *Applied Mechanics and Materials*, 760:379-384.
85. Chang Z, Li M, Chen J (2019) Analytical modeling and experimental validation of the forming force in several typical incremental sheet forming processes. *International Journal of Machine Tools Manufacture*, 140:62-76.
86. Fratini L, Ingarao G, Micari F (2008) On the springback prediction in 3d sheet metal forming processes. *Steel Research International*, 79:77-83.
87. Ham M, Jeswiet J (2007) Forming limit curves in single point incremental forming. *CIRP Annals*, 56(1):277-80.

88. Fratini L, Ambrogio G, Di Lorenzo R, Filice L, Micari F (2004) Influence of mechanical properties of the sheet material on formability in single point incremental forming. *CIRP Annals*, 53(1):207-10.
89. Brüninghaus J, Volfson Y, Bickendorf J, Brell-Cokcan S (2016) Design of a novel end-effector for kinematic support in incremental sheet forming. *Key Engineering Materials*, 716:395-401.
90. Jeswiet J, Micari F, Hirt G, Bramley A, Duflou J, Allwood J (2005) Asymmetric single point incremental forming of sheet metal. *CIRP Annals Manufacturing Technology*, 54:623-49.
91. Ham M, Jeswiet J (2008) Dimensional Accuracy of Single Point Incremental Forming. *International Journal of Material Forming*, 1:1171-1174. DOI 10.1007/s12289-008-0189-7
92. Guzmán CF, Gu J, Duflou J, Vanhove H, Flores P, Habraken AM (2012) Study of the geometrical inaccuracy on a SPIF two-slope pyramid by finite element simulations. *International Journal of Solid Structures*, 49:3594-604.
93. Dabwan A, Ragab AE, Saleh MA, Anwar S, Ghaleb AM, Ur Rehman A (2020) Study of the Effect of Process Parameters on Surface Profile Accuracy in Single-Point Incremental Sheet Forming of AA1050-H14 Aluminum Alloy. *Advances in Materials Science and Engineering*. <https://doi.org/10.1155/2020/7265941>
94. Duchêne L, Guzmán CF, Behera AK, Duflou JR, Habraken AM (2013) Numerical simulation of a pyramid steel sheet formed by single point incremental forming using solid-shell finite elements. *Key Engineering Materials Trans Tech Publication*, 549:180-8.
95. Behera AK, Lauwers B, Duflou JR (2014) Tool path generation framework for accurate manufacture of complex 3D sheet metal parts using single point incremental forming. *Computers and Industrial Engineering*, 65:563-84.

96. Behera AK, Lauwers B, Duflou JR (2013) Tool path generation for single point incremental forming using intelligent sequencing and multi-step mesh morphing techniques. *Key Engineering Materials*, 554-557:1408-18, <http://dx.doi.org/10.4028/www.scientific.net/KEM.554-557.1408>
97. Behera AK, Verbert J, Lauwers B, Duflou JR (2013) Tool path compensation strategies for single point incremental sheet forming using multivariate adaptive regression splines. *Computer Aided Design*, 45:575-90.
98. Essa K, Hartley P (2011) An assessment of various process strategies for improving precision in single point incremental forming. *International Journal of Material Forming*, 4:401-12.
99. Ingarao G, Zaheer O, Campanella D, Fratini L (2020) Re-forming end-of-life components through single point incremental forming. *Manufacturing Letters*. <https://doi.org/10.1016/j.mfglet.2020.05.001>
100. Evans M (2009) *Minitab manual*. W H Freeman
101. Li Y, Daniel WJT, Liu Z, Lu H, Meehan PA (2015) Deformation mechanics and efficient force prediction in single point incremental forming. *Journal of Materials Processing Technology*, 221:100-111.
102. Li Y, Liu Z, Lu H, Daniel WB, Liu S, Meehan PA (2014) Efficient force prediction for incremental sheet forming and experimental validation. *The International Journal of Advanced Manufacturing Technology*, 73(1-4):571-587.
103. Bansal A, Lingam R, Yadav SK, Venkata RN (2017) Prediction of forming forces in single point incremental forming. *Journal of Manufacturing Processes*, 28:486-493.
104. Micari F, Ambrogio G, Filice L (2007) Shape and dimensional accuracy in single point incremental forming: state of the art and future trends. *Journal of Materials Processing Technology*, 191(1-3):390-395.

105. Ambrogio G, Cozza V, Filice L, Micari F (2007). An analytical model for improving precision in single point incremental forming. *Journal of Materials Processing Technology*, 191(1-3):92-951.
106. Wang C, He A, Weegink KJ, Liu S, Meehan PA (2020) 3D surface representation and trajectory optimization with a learning-based adaptive model predictive controller in incremental forming. *Journal of Manufacturing Processes*, 58:796-810.
107. Lora FA, Fritzen D, Alves De Sousa RJ (2021) Studying Formability Limits By Combining Conventional and Incremental Sheet Forming Process. *Chinese Journal of Mechanical Engineering*. DOI: 10.1186/s10033-021-00562-7.
108. Isik K, Silva MB, Tekkaya AE, Martins PAF (2014) Formability limits by fracture in sheet metal forming. *Journal of Materials Processing Technology*, 214(8):1557-1565.
109. Jawale K, Duarte JF, Reisa A, Silva MB (2018) Characterizing fracture forming limit and shear fracture forming limit for sheet metals. *Journal of Materials Processing Technology*, 255:886-897.
110. Soeiro JMC, Silva CMA, Silva MB, Martins PAF (2015) Revisiting the formability limits by fracture in sheet metal forming. *Journal of Materials Processing Technology*, 217:184-192.
111. Munot MA, Ibrahim RN (2013) Remanufacturing Process And Its Challenges. *Journal of Mechanical Engineering and Sciences*, 4:488-495. <http://dx.doi.org/10.15282/jmes.4.2013.13.0046488>
112. Allwood JM, Ashby MF, Gutowski TG, Worrell E (2011) Material efficiency: a white paper Resources. Conservation and Recycling, 55:362-381.

113. Tekkaya AE, Schikorra M, Becker D, Biermann D, Hammer N, Pantke K (2009) Hot profile extrusion of AA-6060 aluminum chips. *Journal of Materials Processing Technology*, 209(7):3343-3350. doi: 10.1016/j.jmatprotec.2008.07.047
114. Chiba R, Nakamura T, Kuroda M (2011) Solid-state recycling of aluminium alloy swarf through cold profile extrusion and cold rolling. *Journal of Materials Processing Technology*, 211:1878-1887.
115. EAA, Environmental profile report for the European aluminium industry, 2018.
116. Granta Design Limited. CES selector. 2017.
117. Ingarao G, Vanhove H, Kellens K, Duflou JR (2014) A comprehensive analysis of electric energy consumption of single point incremental forming processes. *Journal of Cleaner Production*, 67:173-186.
118. Cooper DR, Gutowski TG (2018) Prospective Environmental Analyses of Emerging Technology A Critique, a Proposed Methodology, and a Case Study on Incremental Sheet Forming. *Journal of Industrial Ecology* DOI: 10.1111/jiec.12748 article in press.
119. Semiatin SL (1993) *ASM handbook forming and forging*. 1993. ASM International, 14.
120. Hammond G, Jones C (2010) *Inventory of Carbon and Energy (ICE), Annex B: How to Account for Recycling; a Methodology for Recycling*. The University of Bath, Bath, UK.
121. Mayyas TA, Qattawi A, Mayyas AR, Omar MA (2012) Life cycle assessment based selection for a sustainable lightweight body-in-white design. *Energy*, 39:412-425.
122. Ashby MF (2009) *Materials and the environment: eco-informed material choice*. Burlington, MA, USA: Butterworth-Heinemann.

123. Errington M, Childe SJ (2013) A Business Process Model of Inspection on Remanufacturing. *Journal of Remanufacturing* 3(7):1-22.

Publications List

Ingarao G, Zaheer O, Campanella D, Fratini L (2020) Re-forming end-of-life components through single point incremental forming. *Manufacturing Letters*, 24:132-135.

Ingarao G, Zaheer O, Campanella D, Di Lorenzo R, Fratini L (2020) An energy efficiency analysis of single point incremental forming as an approach for sheet metal based component reuse. *Procedia CIRP*, 90:540-545.

Ingarao G, Zaheer O, Fratini L (2021) Manufacturing processes as material and energy efficiency strategies enablers: The case of Single Point Incremental Forming to reshape end-of-life metal components. *CIRP Journal of Manufacturing Science and Technology*, 32:145-153.

Zaheer O, Ingarao G, Pirrotta A, Fratini L (2021) Geometrical deviation of end-of-life parts as a consequence of reshaping by single point incremental forming. *International Journal of Advanced Manufacturing Technology*, 115:1579-1588.

Zaheer O, Ingarao G, Di Lorenzo R, Fratini L (2021) On the effectiveness of SPIF process to re-form End-of-Life components as compared to conventional forming approach. *SHEMET* 2021.

Zaheer O, Ingarao G, Di Lorenzo R, Fratini L (2021) Understanding formability and geometrical accuracy of SPIF process used as Reshaping approach. *ESAFORM* 2021.